Improving Stem Cell-Based Therapy and Developing a Novel Gene Therapy Approach for Treating Duchenne Muscular Dystrophy (DMD)

Improving stem cell-based therapy and developing a novel gene therapy approach for treating Duchenne Muscular Dystrophy (DMD)

A dissertation presented

By

Mohammadsharif Tabebordbar

to

The Division of Medical Sciences

in partial fulfillment of the requirements

for the degree of

Doctor of Philosophy

In the subject of

Developmental and Regenerative Biology

Harvard University

Cambridge, Massachusetts

December 2015

Dissertation advisor: Dr. Amy Wagers Mohammadsharif Tabebordbar

Improving stem cell-based therapy and developing a novel gene therapy approach for treating Duchenne Muscular Dystrophy (DMD)

Abstract

Genetic mutations in muscle structural genes can compromise myofiber integrity, causing repeated muscle damage that ultimately exhausts muscle regenerative capacity and results in devastating degenerative conditions such as Duchenne Muscular Dystrophy (DMD), Congenital Muscular Dystrophy (CMD) and different forms of Limb Girdle Muscular Dystrophy (LGMD). Gene supplementation and autologous stem cell transplant have been put forward as promising, though still unproven, therapeutic avenues for combatting these genetic muscle diseases. Both strategies aim to compensate expression of the missing or mutated protein. For cell therapy, autologous muscle stem cells (satellite cells) from dystrophic muscles undergo *in vitro* expansion and gene correction and then are transplanted into diseased tissue, where they fuse with resident myofibers to deliver a functional copy of the gene. One of the major obstacles for the autologous adult stem cell transplantation is that adult satellite cells account for a very rare population in muscle and they need to be expanded in culture, while retaining their engraftment potential, to generate sufficient number of cells for gene correction and transplantation. I tackled this problem by developing a culture condition that allows engraftable mouse satellite cells to expand in culture. This study also provides evidence for the feasibility of *in vitro* expansion, gene correction and transplantation of dystrophic satellite cells to restore DYSTROPHIN expression in dystrophic muscle.

In gene therapy, engineered gene products are delivered directly to muscle fibers as transgenes carried by viral vectors, such as Adeno Associated Viruses (AAVs). Viral-mediated delivery of a normal copy of the mutated genes into dystrophic muscle fibers holds big promise as a therapeutic avenue for Muscular Dystrophies. However, considering the indispensible role of satellite cells in muscle regeneration, an effective and long-term therapy for genetic muscle diseases requires restoration of gene expression in both dystrophic muscle fibers and satellite cells. Conventional gene therapy approaches lack the potential for long-term restoration of the mutated gene expression in satellite cells. In order to address this limitation, this study provides the proof of concept evidence for the use of a novel gene editing approach, which allows irreversible correction of the mutations in both dystrophic skeletal muscle fibers and satellite cells.

Table of contents

To my lovely Mom and Dad for your wholehearted support over the years.

Acknowledgements

I'm deeply grateful to Dr. Amy Wagers, who provided me with the opportunity of perusing my dream scientific projects as my dissertation research. I couldn't ask for a better environment to learn basics of muscle biology, to have constructive scientific discussions withy my colleagues and to contribute to the advancement of treatment options for Muscular Dystrophies. I'm also thankful to the members of my Dissertation Advisory Committee (DAC), Dr. Andrew Lassar, Dr. Alan Beggs and Dr. Kiran Musunuru, who provided me with insightful feedback and guidance throughout my dissertation research. Special thanks to Dr. Alan Beggs, who kindly agreed to also be the chair of my dissertation defense committee. I'd like to thank Dr. Rudolf Jaenisch, Dr. Lou Kunkel and Dr. Kevin Eggan for accepting to be a part of my dissertation defense committee.

I'd like to express my gratitude to the members of the Wagers lab for their support and technical guidance over the years. Thanks to Dr. Kah Yong Tan for his tremendous help in my initial settlement in the lab and to Dr. Albert Almada for great discussions and for cheering me up during the difficult times of graduate school. I'm greatly thankful to Kexian Zhu, Jason Cheng and Elizabeth Wu for their intellectual and technical help in different stages of my graduate career. Dr. Eric Wang has always been a great role model for me, whose constant support has had a great role in my research career and I can't thank him enough.

My great friends have always been there for me during the ups and downs of my PhD research and their presence and support enormously helped me deal with the stressful life as a graduate student. Thanks especially to Hamid Hezari, Ali Hakimian, Mohammad Fallahi, Darya Amin-Shahidi, Sophiya Shahla, Samira Salari and Masoud Akbarzade for the love and support.

Last but not least, I'd like to thank my parents and my brother who provided me with the most pleasant environment to achieve my goals, helped with make the right decisions in difficult times and supported my unconditionally. And I couldn't have done this without my most understanding, lovely and warm-hearted partner-in-crime, Sara, who selflessly provided me with all the love and support that I could possibly have.

List of Figures and Tables

List of Abbreviations

ECM	Extracellular matrix
ER	endoplasmic reticulum
SR	sarcoplasmic reticulum
T-tubules	Transverse tubules
DGC	dystrophin-glycoprotein complex
PLA2s	phospholipases A2
EC	Excitation-Contraction
IM	Inflammatory myopathies
DM	dermatomyositis
PM	polymyositis
sIBM	sporadic inclusion body myositis
NAM	necrotizing autoimmune myositis
MAC	membranolytic attack complexes
MHC-1	Major Histocompatibility Complex-1
SRP	signal recognition peptide
ADCC	Antibody-Dependent Cell-mediated Cytotoxicity
CK	Creatine Kinase
MG53	Mitsugumin 53
TRIM72	tripartite motif family protein
HGF	hepatocyte growth factor
EGF	epidermal growth factor
PDGF-BB	platelet derived growth factor-BB
IGF	insulin-like growth factor
FGF	fibroblast growth factor
bFGF	basic fibroblast growth factor

MRF	myogenic regulatory factors
FAPs	fibro-adipogenic precursors
DMD	Duchenne muscular dystrophy
ROS	reactive oxygen species
BMD	Becker Muscular Dystrophy
nNOS	Neuronal nitric oxide synthase
SCID	severe combined immunodeficiency
ESCs	embryonic stem cells
iPSCs	induced pluripotent stem cells
AAVs	adeno-associated viruses
ZFN	Zinc-finger nucleases
NHEJ	non-homologous end joining
TALENs	Transcription-activator like effector nucleases
CRISPR	clustered regularly interspaced short palindromic repeats
Sp	*Streptococcus pyogenes*
gRNA	guide RNA
PAM	protospacer adjacent motif
crRNA	CRISPR-derived RNAs
tracrRNA	trans-activating CRISPR RNA
DSB	double strand break
AON	antisense oligonucleotide
PMO	phosphorodiamidate morpholino oligomer
PDE	phosphodiesterase
mylz2	*myosin light polypeptide 2*
hpf	hours post fertilization
zESC	zebrafish ESC
cAMP	cyclic AMP
CREB	cAMP response element binding protein

FACS	fluorescence-activated cell sorting
HLA	juman leukocyte antigen
Sa	*Streptococcus aureus*
EFS	elongation factor 1a short
tcDNA	tricyclo-DNA
TA	tibialis anterior
PCR	polymerase chain reaction
RT-PCR	Reverse transcription polymerase chain reaction
RNP	Ribonucleoprotein
MRI	Magnetic resonance imaging
6MWT	6 minute walking distance test
GRMD	Golden retriever muscular dystrophy

Chapter 1.

Introduction

Skeletal Muscle: Composition, Structure, And Function

Skeletal muscle is composed of thousands of muscle fibers, which are bundled together and attached to the skeleton by tendons (Figure 1). Skeletal muscle fibers (myofibers) are multi- nucleated and form during development by the fusion of mononucleated myoblasts. Myofibers are surrounded by a specialized plasma membrane, the sarcolemma, which transduces signals from motor neurons and other external stimuli into muscle fibers. Myofibers are surrounded by a layer of extracellular matrix (ECM) known as the basement membrane, which is composed of both an internal basal lamina and an external reticular lamina [2]. The basal lamina associates closely with the sarcolemma, providing a protective niche in which muscle regenerative cells (known as satellite cells) reside. Satellite cells are unipotent adult stem cells that are activated in response to severe muscle damage to proliferate and differentiate, thereby forming myoblasts that can rebuild the muscle through fusion with one another or with residual myofibers. Satellite cells also possess self-renewal capacity, which ensures their persistence within the muscle and thereby preserves the muscle's ability to repair after injury.

The calcium-dependent contraction of muscle fibers requires a specialized cytoplasm (sarcoplasm) and modified endoplasmic reticulum (ER), called the sarcoplasmic reticulum (SR). Transverse tubules (T-tubules) invaginate the sarcolemma to properly transduce action potentials and activate the SR (Figure 1). Myofibers contain abundant myofibrils, which act as contraction units and are surrounded by SR. Myofibrils are composed of thin myofilaments (actin) and thick

myofilaments (myosin) whose calcium-dependent movement relative to one another produces muscle contraction. The organization of myofilaments into myofibrils underlies the normally striated appearance of skeletal muscle under light microscopy; thin filaments make up the light band (I-band), and thick filaments make up the dark band (A-band) (Figure 1). The Z-line defines the borders of each sarcomere, which is the structural unit of the myofibril [3].

Muscle contraction is induced by depolarization of the sarcolemma via action potential. This depolarization opens sarcoplasmic calcium release channels, increasing intracellular calcium concentrations and triggering actin-myosin mediated contraction of sarcomeres. Protein assemblies called costameres, which consist mainly of proteins contained within the dystrophin-glycoprotein complex (DGC) [4] and integrin-vinculin-talin complex [5], transmit contraction forces from muscle fibers to the ECM, and eventually to neighboring myofibers. Costameres align with the Z-line of peripheral myofibrils and physically link myofibrils to the sarcolemma.

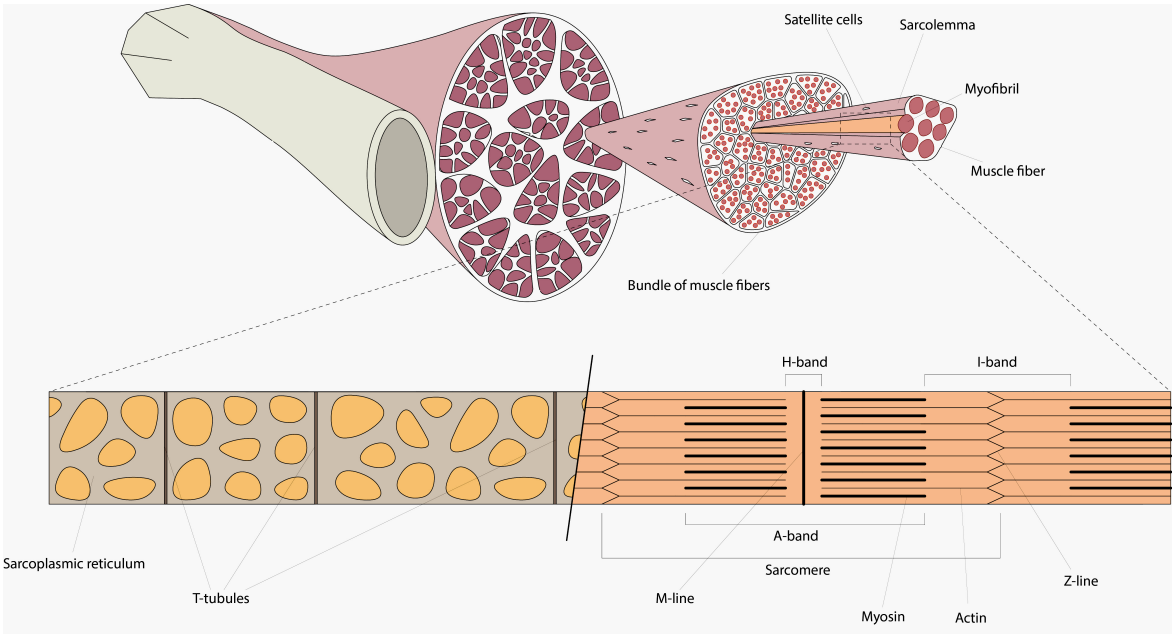

Figure 1. Skeletal muscle structure and composition. Skeletal muscle is composed of numerous bundles of muscle fibers. Each bundle consists of multiple fibers, and individual fibers encompass many myofibrils. Sarcomeres are the structural units of myofibrils and are made up of actin and myosin filaments. Abbreviation: T-tubule, transverse tubule. Adapted from [1].

Muscle Satellite Cells

Satellite cells are mononuclear cells with high nuclear to cytoplasmic ratio that were first identified in electron micrographs based on their distinct anatomical position between the sarcolemma and basal lamina of muscle fibers [6]. Satellite cells represent the primary endogenous source of muscle progenitor cells and are responsible for the regenerative potential of adult muscle [7]. Satellite cells remain mitotically and metabolically quiescent throughout most of life, consistent with the relatively infrequent turnover of myonuclei in uninjured adult muscle. However, satellite cells are activated in response to muscle injury and in the context of

chronic degenerative diseases (discussed below) [8-10]. Damage to skeletal muscle results in the release of growth factors and cytokines, such as hepatocyte growth factor (HGF), epidermal growth factor (EGF), platelet derived growth factor-BB (PDGF-BB), and members of insulin-like growth factor (IGF) and fibroblast growth factor (FGF) family [11,12] from the ECM [13], myofibers, endothelial cells, interstitial cells [14] and leukocytes [15]. Interaction of these GFs with their receptors on quiescent satellite cells triggers satellite cell proliferation. Quiescent satellite cells express a variety of proteins including Pax7, CD34, c-met, M-cadherin, syndecan-3 and syndecan-4 [16-18], that are important for their activation and proliferation [19]. Activated satellite cells downregulate Pax7 expression and increase synthesis of the early myogenic regulatory factors (MRFs) MyoD and Myf5 [20]. Activated satellite cells undergo a rapid proliferation stage, regulated in part by Notch signaling [21]. Notch inhibition and activation of Wnt signaling can induce progression of muscle satellite cells along the myogenic lineage to promote production of fusion-competent myoblasts [22] and trigger expression of late MRFs including myogenin. Fusion of terminally differentiated myoblasts into myofibers marks the final stage of muscle regeneration.

Efficient repair of skeletal muscle after repeated injuries indicates that satellite cells are replenished after muscle regeneration. Genetic fate-mapping studies strongly implicate satellite cells themselves as the endogenous source of this cell replacement; however, the mechanisms regulating satellite cell self-renewal are not fully understood. Some reports suggest that non-random segregation of DNA strands or asymmetric distribution of Numb, an inhibitor of

Notch signaling, into the daughter cells generated by satellite cells division [23,24] may drive asymmetric division of satellite cells and preservation of the satellite cell pool by generating satellite cells with self renewal capability. A recent study [25] provided evidence suggesting that asymmetric division in satellite cells expressing high levels of Pax7 results in segregation of template DNA to daughter cells with a more immature phenotype, whereas daughters inheriting newly synthesized DNA acquire a more differentiated phenotype. These authors also demonstrated that satellite cells harboring low levels of Pax7 exhibit random segregation of DNA strands during mitosis [25]. Myostatin, a member of the TGF-β superfamily, has also been proposed to promote satellite cell quiescence, based on the increased percentage of activated and proliferating satellite cells in myostatin-null mice [26] and involvement of the myostatin antagonist, follistatin, in myoblast fusion [27]. However, direct analysis of postnatal satellite cells in mice suggests that they lack expression of myostatin receptors and fail to respond to exogenous myostatin in in vitro proliferation assays [28].

In addition to soluble GFs and cytokines, satellite cell function is also regulated by infiltrating and interstitial cell populations, including recruited inflammatory cells [29] and resident fibro-adipogenic precursors (FAPs) [30,31] (Figure 2). The impact of inflammatory cells on muscle repair is quite complex. In the absence of any recruited immune cells, satellite cell regenerative activity appears to be blocked [29]; however, an over-exuberant or unbalanced immune response can lead to myopathic tissue destruction that is not recoverable through satellite cell-mediate repair processes. Neutrophils appear to be the first immune cells

recruited to damaged muscle [32]. Their recruitment signals subsequent infiltration by M1, and then M2, macrophages [33,34]. M1 macrophages are efficient inducers and effectors of inflammatory processes, whereas M2 macrophages are more often involved in tissue repair, remodeling and immunoregulation [35]. Both neutrophils and macrophages participate in the clearance of myofiber debris at the injury site, and production of inflammatory and immune regulatory cytokines, but macrophages (particularly M2 macrophages) appear to have an additional function in directly regulating muscle regeneration through induction of satellite cell activation and myoblast proliferation [36-38].

In addition to recruited immune cells, muscle-resident mesenchymal cells also appear to be critical for proper muscle repair. For example, skeletal muscle contains a unique population of Sca-1-expressing precursor cells, which can differentiate to form fibroblasts [39] and white or brown adipocytes [30,40]. While these fibro-adipogenic precursors (FAPs) possess no intrinsic myogenic activity, they are potent inducers of myogenesis by satellite cells [30,31] (Figure 2). Intriguingly, while undifferentiated FAPs promote myofiber formation, the presence of differentiated myofibers appears to inhibit FAP-mediated adipogenesis [31]. While the exact mechanisms by which this functional cross-antagonism is accomplished remain to be determined, studies have suggested a role for paracrine signaling, by soluble mediators such as IGF-1, Wnts and IL-6, between FAPs and muscle satellite cells in FAP-dependent promotion of myogenesis [30], whereas co-cultures of FAPs with differentiated myotubes implicate direct interaction in the inhibition of FAP-mediated adipogenesis by muscle fibers [31]. Thus, in addition to alterations in

satellite cell number and intrinsic signaling responses, a number of non-cell autonomous inputs clearly influence the extent and efficacy of satellite cell-mediated muscle repair.

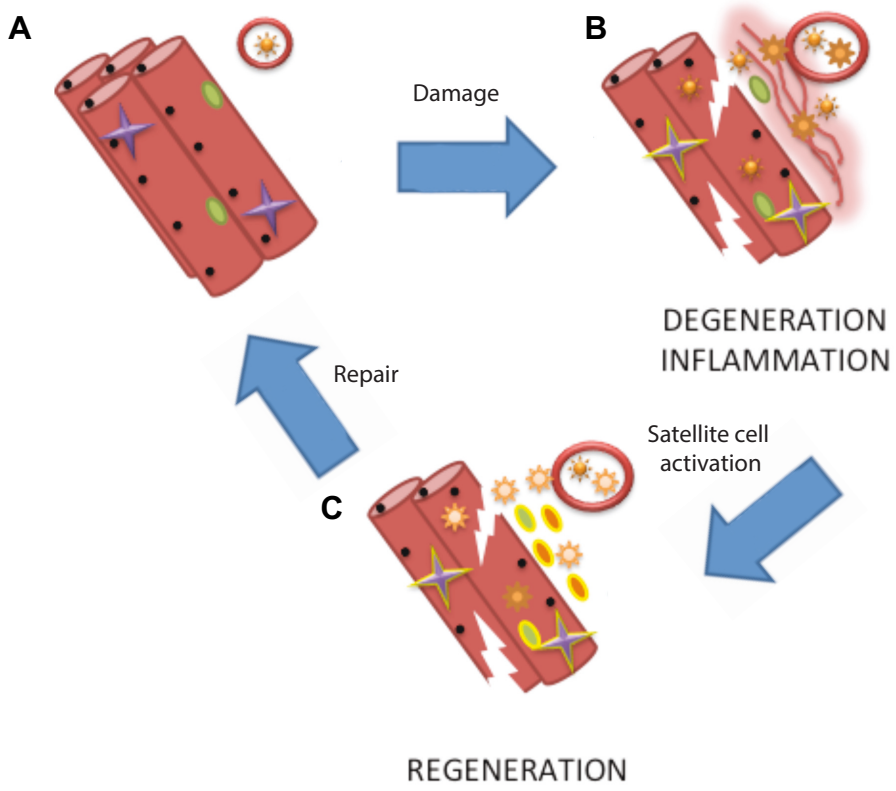

Figure 2. Mechanisms of Satellite Cell Activation and Regulation During Muscle Repair. (A) During homeostasis, satellite cells (*green*) reside in close association with muscle fibers (*red*). Resting muscle also contains resident fibro-adipogenic precursors [FAPs (*purple*)]. (B) Damage to muscle induces myofiber degeneration and inflammation, beginning with infiltration by neutrophils and M1 macrophages (*dark yellow*) from blood vessels (*red oval*). (C) During the regenerative phase, elaboration of growth factors and cytokines by muscle fibers, infiltrating M2 macrophages (*light yellow*) and activated FAPs (*purple with yellow border*) activate satellite cells (*green with yellow border*) to proliferate and differentiate to form myoblasts (*orange ovals with yellow border*) that exit the cell cycle and fuse with one another and with residual myofibers to replenish myofibers as well as the satellite cell pool. Adapted from [1].

Duchenne and Becker Muscular Dystrophies

Duchenne muscular dystrophy (DMD) is the most common X-linked genetic

disorder in humans, and affects one in 3500 males. Most boys with DMD manifest symptoms within the first years of life. Progressive muscle weakening delays walking and causes repeated falls, leaving patients wheelchair-bound, typically by ~12 years of age. Most patients experience premature death due to respiratory or cardiovascular failure in the second decade. Mutations in the *DYSTROPHIN* gene leading to genetic frame-shift or loss of expression and complete absence of protein function are causative for DMD[41,42]. *DYSTROPHIN* extends over 2.4 Mb of the X-chromosome and represents the largest gene in human genome. Point mutations in *DYSTROPHIN* are responsible for ~40% of DMD cases, with the remaining ~60% caused by large deletions or duplications in this gene [43].

The protein DYSTROPHIN is a structural protein in muscle, a component of the DGC [44] (Figure 3), and an essential part of the costamere. The protein was first described by Lou Kunkel's group in 1987 [45] and its primary function is to link the myofiber cytoskeleton to the ECM and thereby stabilize the sarcolemma [46]. DYSTROPHIN binds cytoplasmic actin through its amino terminal as well as its rod shaped domain, which is composed of 24 spectrin repeats and four hinge points [47]. The carboxy-terminal cysteine rich domain of DYSTROPHIN binds to transmembrane β-dystroglycan protein directly. β-dystroglycan is linked to highly glycosylated α-dystroglycan, which completes the connection between the myofiber cytoskeleton and ECM by interacting with laminin in the basal lamina [48]. Absence of functional DYSTROPHIN protein destabilizes the DGC, increasing the susceptibility of dystrophic muscle fibers to contraction-induced injury [49]. Increased cytosolic calcium following mechanical stress, activation of proteases (particularly

calpains), destruction of membrane constituents and ultimately myofiber necrosis occur frequently in dystrophic muscles. Thus, satellite cells in these patients must support repeated rounds of regeneration in an attempt to compensate for damage. As the disease advances, satellite cells show reduced capacity for muscle regeneration, possibly due to proliferation-induced reductions in telomere length [50] or damage-associated cell attrition [51]. A recent study by the Rudnicki group also provides evidence for the cell-intrinsic role of dystrophin in satellite cells. Dumont et al. reported that number of asymmetric divisions is diminished in dystrophic satellite cells and these cells show a defective cell division pattern. These defects result in a reduced number of myogenic progenitors capable of regenerating muscle and adversely affect muscle regeneration [52]. Absent an adequate muscle regenerative response, fat and fibrotic tissue replace muscle fibers, leading to further weakening and wasting [53].

In addition to mechanical stress, other secondary mechanisms also induce damage in dystrophic muscle. Loss of functional dystrophin leads to reduced expression and mislocalization of neuronal nitric oxide synthase (nNOS) from the sarcolemma [54] (Figure 3). Absence of nNOS signaling impairs blood supply to contracting muscles, exposing dystrophic muscles to continuous ischemic insult [55]. Various immune cells are also recruited to the dystrophic muscle as a result of persistent damage, and these can cause secondary damage through inflammatory responses and elaboration of reactive oxygen species (ROS) [56].

Like DMD, Becker Muscular Dystrophy (BMD) also is caused by mutations in *DYSTROPHIN*; however Becker mutations maintain the dystrophin reading

frame. The reading frame hypothesis for the difference between DMD and BMD was first proposed by Monaco et al. [57] and further established at the protein level by Hoffman et. al. in 1988 [58]. Thus, most BMD patients express a partially functional DYSTROPHIN protein, which lacks the internal spectrin repeats but contains the critical actin binding and carboxy-terminal domains [59]. BMD patients show a milder phenotype and more heterogeneous clinical manifestation of the disease. Some BMD patients remain ambulatory after their 40s, and some patients have a normal life-span[60] [61].

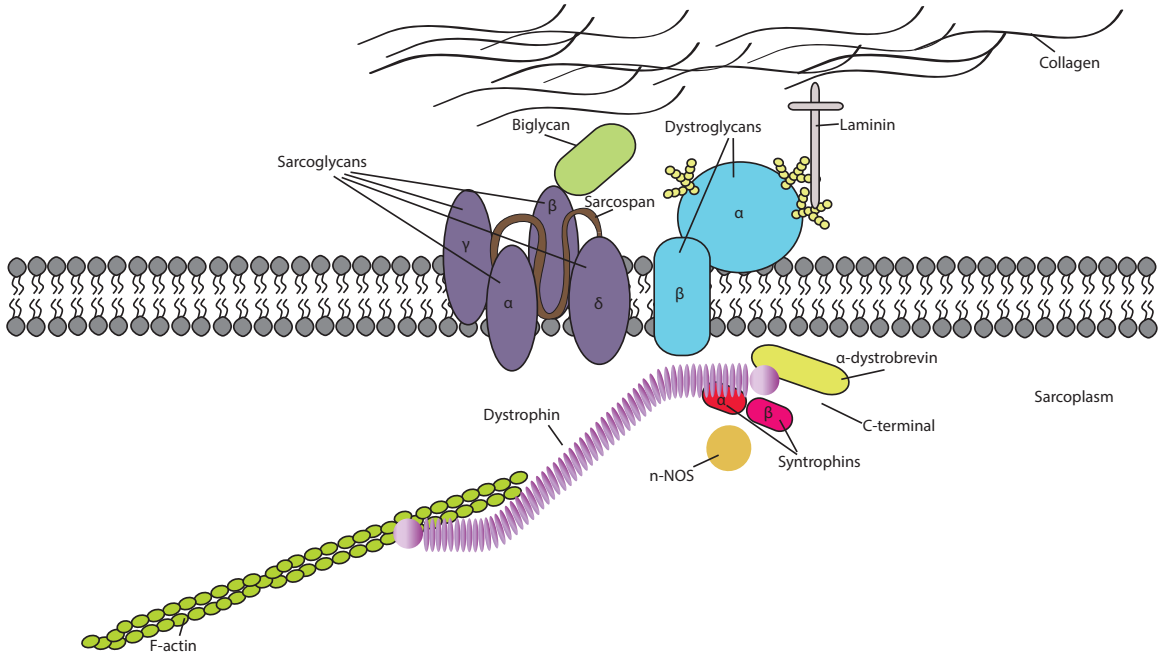

Figure 3. Dystrophin glycoprotein complex (DGC). Dystrophin connects the muscle fiber cytoskeleton to the extracellular matrix (ECM) via interaction with actin filaments in the sarcoplasm and β-dystroglycan in the sarcolemma. β-Dystroglycan interacts with α-dystroglycan, which is connected to laminin in the ECM through its glycan moieties. The sarcoglycan-sarcospan complex is also a part of DGC that includes α-, β-, γ-, and δ-sarcoglycans and sarcospan. This subcomplex is connected to the ECM through interaction with biglycan. Dystrophin also interacts with α-dystrobrevin and α- and β-syntrophins through its C-terminal domain. Neuronal nitric oxide synthase (nNOS) is localized to the DGC via its interaction with syntrophins. Adapted from [1].

Therapeutic Possibilities For Muscle Wasting Diseases

Current treatment options for muscular dystrophies are disappointingly limited, and focus mainly on managing symptoms and suppressing the immune and inflammatory response [62,63]. Therapeutic approaches that aim instead to cure these disorders have been a subject of research for many decades, and can be grouped broadly into two categories, based on strategic approach. The first category seeks to repair or replace the mutated gene, while the second strives to reduce the impact of the mutation by activating alternative pathways or intervening downstream to correct the pathological consequences. Each of these strategies presents its own unique advantages and challenges, and past experiences have helped to inform and focus the direction of future research and design of future clinical trials. Here I discuss several promising therapeutic avenues, including cell transplantation, gene supplementation or correction, and oligonucleotide and small molecule delivery, each of which has been considered as a basis for curative treatment of dystrophic disease.

Cell Transplantation

Because satellite cells represent a robust and exclusive source of new myofibers during normal muscle regeneration, these cells and their derivatives have long been considered as attractive targets for cell replacement therapy in muscle. In this approach, cells from an unaffected donor, or gene-corrected autologous cells (see below), could be infused into patients, where they

presumably would produce donor-engrafted muscle fibers carrying the normal allele of the affected gene, and thereby reconstituting gene function. Indeed, this strategy of precursor cell transplantation has been successful in the treatment of some hematopoietic disorders, where bone marrow transplantation now represents a relatively common (though certainly not risk-free) clinical intervention. However, limitations in the numbers of satellite cells that can be obtained from human muscle and the lack of viable methods to expand these cells in vitro, have thus far restricted clinical application of this approach and simultaneously spurred consideration of alternative sources of cells for transplantation. Early clinical trials evaluated the efficacy of transplanted myoblasts, generated by long-term culture from explants of donor muscle and injected directly into the muscle. However, these trials yielded largely disappointing results [64], perhaps due to a significant cell loss upon transplantation, which subsequently was shown to result in death of up to 90% of transferred cells within days of transplantation [65]. Progress in the ability to isolate and expand primitive satellite cells, which may show enhanced survival ability after transplantation [51], will likely be essential in reinvigorating this conceptually attractive therapeutic approach, and should be coupled with improvements in cell delivery strategies, as satellite cells cannot currently be delivered systemically and do not migrate far from the site of intramuscular injection, raising a daunting challenge for delivering donor cells to affected muscles throughout the body.

In addition to satellite cells, some groups have considered non-satellite cell populations residing in muscle as alternative potential cell therapy vehicles. In

particular, studies in dog models with cultured mesangioblasts, which may be related to blood vessel-associated pericytes [66] and exhibit broad differentiation potential in culture, including production of cells expressing markers of the skeletal muscle, smooth muscle, and vascular lineages [66-68], have been encouraging [69]. An attractive attribute of mesangioblasts, as well as the likely related population of $CD133^+$ [70] and muscle-derived "side-population" cells [71], for cell therapy is their apparent ability to home from the circulation into dystrophic muscle tissue [69,72], which enables their delivery via vascular, rather than intramuscular, injection. Similar promise for vascular delivery of muscle regenerative cells was excited by observations that transfusion of donor bone marrow cells could lead to detectable contributions in skeletal myofibers [73,74]; however, further evaluation of such approaches indicated that the rate of engraftment was far below that predicted to be necessary for therapeutic effect [39,75]. Indeed, in a DMD patient receiving a bone marrow transplant for co-incident severe combined immunodeficiency (SCID), although evidence of rare donor cell engraftment in muscle could be found, no improvement in dystrophic phenotype could be attributed to the transplanted cells [76].

In an effort to overcome the pervasive limitations of obtaining adequate numbers of immunologically matched donor cells when working with adult somatic cells for muscle regenerative medicine, a number of groups have focused their efforts on deriving engraftable muscle precursor cells from pluripotent stem cell sources. Such cells, including embryonic stem cells (ESCs), derived from human embryos, and induced pluripotent stem cells (iPSCs), derived by transcription

factor-dependent “reprogramming” of differentiated somatic cells, can be propagated indefinitely in culture and are in principle capable of differentiating into any cell type in the body [77,78]. Thus, a robust strategy for producing muscle precursors from these cells would provide an inexhaustible source of donor cells for transplant. Moreover, when coupled with gene correction strategies, iPS cells generated in a patient-specific manner have the potential to produce immunologically matched donor cells that could eliminate, or at least reduce, the threat of graft destruction due to recognition by the host immune system. Yet, a major challenge in realizing the potential of pluripotent stem cells for skeletal muscle therapy has been the difficulty in the field of deriving fully mature “adult” somatic cells from ESCs or iPSCs [79]. Nonetheless, important strides have been made, including the demonstration that transient induction of the satellite cell-associated transcription factors Pax3 or Pax7, or cell sorting with satellite cell-specific surface markers, in differentiating mouse ES or iPS cells can promote the recovery of myogenic precursors, which have been successfully engrafted in models of DMD and FSHD [80-84]. Furthermore, recent studies by our group [85] and other groups [86,87] have also demonstrated the feasibility of generating muscle progenitor cells and mature skeletal muscle fibers from ES or iPSCs without the need for transgene expression. However, the percentage of Pax7+ muscle progenitors generated by the current differentiation protocols is less than 25%. Development of culture conditions that allow for enrichment of Pax7+ muscle progenitors and identification of cell surface markers for isolation of Pax7+ cells from the pool of differentiated cells can help to move this approach towards clinical

application.

Gene Supplementation or Correction

Rather than relying on transplanted cells as vehicles for complementing defective alleles in MD patients, additional efforts in muscle regenerative medicine have focused on achieving direct gene therapy in affected muscle fibers, through exogenous delivery of a “normal” copy of the mutated gene, or more recently, by introduction of genome modifying nucleases that may enable in situ gene repair. Most gene delivery approaches have employed recombinant viral vectors, particularly adenoviruses due to their ability to carry very large inserts (a significant challenge when attempting genetic complementation of the largest gene in the human genome!) and adeno-associated viruses (AAVs) due to their relatively high efficiency of transduction in skeletal muscle and low immunogenicity [63]. However, even AAVs are susceptible to anti-viral host immune responses, which may require host immunosuppression and can prevent repeated gene delivery attempts [62]. Attempts have also been made to produce “pared down” versions of dystrophin (e.g. mini- and micro-dystrophin) that would provide at least partial restoration of gene function and enable packaging of target sequences into AAV, as well as retro- or lentiviral vectors [62]. Finally, strategies that may support transfer of entire regions of human chromosome, including those encompassing the human dystrophin gene and its regulatory elements, have been pursued using human artificial chromosomes, which can be introduced into target cells and maintained episomally to support tissue-specific expression of the exogenous gene [88].

A second and emerging approach in the gene therapy realm has been to attempt direct correction of the mutated allele(s) in the patient's own cells. This could in theory be accomplished *in situ*, or by genetic modification in autologous somatic cells or patient-specific iPSCs, which would be otherwise genetically matched to individual patients and could be transplanted therapeutically to restore gene function in patient muscles. Early efforts towards this goal employed site-specific Zinc-finger nucleases (ZFNs), which are experimentally engineered DNA-binding proteins, modified by fusion to the Fok1 nuclease domain. Site-specific nuclease activity, directed by the ZFN DNA-binding domain is used to induce a strand break in the target genomic sequence, which can then be repaired by non-homologous end joining (NHEJ) or, in the case of therapeutic gene correction, by homologous recombination with a "normal" donor sequence to generate a gene-corrected allele. However, despite more than 15 years of development and recent progress in the application of some of these technologies in clinical trials for suppression of HIV-1 in vivo, ZFNs remain cumbersome to design and employ, due in part to the context specificity of ZFN sequences, non-specific DNA binding that can lead to off-target gene cleavage, and a relative stranglehold on the technology by a single biotech company that limited its availability and greatly increased the cost of ZFNs for research and clinical studies [89]. Happily, the emergence of related technologies have largely circumvented these obstacles. Transcription-activator like effector nucleases (TALENs), based on DNA-binding virulence factors produced by plant pathogens, exhibit sequence-specific binding to target DNA sequences like ZFNs; yet unlike ZFNs, TALENs are considerably

more approachable in design and may show greater efficacy with less cellular toxicity [89]. But it was the, emergence of the clustered regularly interspaced short palindromic repeats (CRISPR)-Cas9 genome editing tool that truly revolutionized gene therapy approaches. The CRISPR-Cas9 system was originally coopted from the type II CRISPR-Cas bacterial adaptive immune system, which protects bacteria against foreign invading DNA. The first step in CRISPR-mediated immunity is integration of the foreign viral or plasmid DNA into the CRISPR locus [90]. Each CRISPR locus includes a series of repeats separated by unique spacer sequences obtained from foreign genetic elements (protospacers). Each protospacer is flanked by a short DNA sequence called the protospacer adjacent motif (PAM) present on the foreign DNA [91]. Bacterial type II CRISPR-Cas systems also include four cas genes and one of these genes encodes the Cas9 endonuclease [92]. Transcription of the CRISPR locus generates a long primary transcript that is subsequently processed into a library of short CRISPR-derived RNAs (crRNAs), each containing a spacer sequence complementary to a previously integrated foreign nucleic acid. Pre-crRNA processing is triggered by a trans-activating CRISPR RNA (tracrRNA), which is complementary to the repeat sequence and forms a duplex with each crRNA. The crRNA: tracrRNA duplex directs the Cas9 endonuclease to its complementary sequence in the foreign DNA. After Cas9 finds its target, based on Watson-Crick complementarity, it makes cuts in both strands of the DNA, resulting in a blunt double strand break (DSB) [93]. Targeting multiple sites in the invading DNA by the CRSIPR-Cas system leads to degradation of the foreign DNA.

In 2012, Jinek et al., demonstrated that Cas9 can be guided by the crRNA: tracrRNA duplex to make DSB in user-defined sequences in both circular plasmids and linear DNA fragments in a test tube. This study also showed that Cas9 can be programmed by a single chimeric RNA, in which the crRNA and the tracrRNA are attached by a linker[94]. In 2013, two independent studies provided the first proof of concept evidence for CRSIPR-mediated genome editing in mammalian cells by introducing plasmids encoding Cas9 and the chimeric crRNA:tracrRNA, named guide RNA (gRNA), into human cell lines [95,96]. Since 2013, the CRISPR-Cas9 gene editing technology has been broadly utilized for gene disruption, gene replacement and gene modification in cell lines [97,98], zebrafish [99] and mouse [100,101] one-cell embryos, as well as postnatal animal tissues [102-105], and it holds great promise for *in vivo* targeting of the genes mutated in genetic muscle diseases.

Still, in all of the cell and gene therapy approaches discussed above, a persistent concern, even when using autologous cells, is that the ectopic or induced expression of a gene not normally present in patient cells might provoke an undesired immune response, which would lead to clearance of the gene-corrected cells. Indeed, some studies have supported the notion that induced expression of dystrophin can stimulate both humoral and cellular immune responses [106]. Overcoming such immunological barriers remains a significant challenge for the future clinical application of gene therapy approaches in dystrophic disease.

Oligonucleotide-Mediated Approaches

Oligonucleotide-mediated approaches for the treatment of muscular dystrophies offer the advantage of specificity for targets and for mechanism of action (Figure 4). Oligonucleotides have been used in the context of DMD to alter splice site usage in order to modulate the dystrophin open reading frame [107], and have recently showed positive results in the clinic. These antisense oligonucleotides (AONs) are basically designed to mask the splice site for the mutated or additional exons, thereby removing these exons from the mRNA and creating an internally deleted protein that maintains its crucial N- and C-terminal associated functions. As discussed above, such shortened forms of dystrophin are found in BMD patients, whose disease is usually much milder than DMD. Phosphorodiamidate morpholino oligomer (PMO) and 2′-O-methyl-phosphorothioate (2′OMP) are two types of AONs that have been used in DMD exon skipping studies and clinical trials. Both PMO and 2′OMP contain modifications that make them more biologically stable and resistant to nucleases. 2′OMPs designed to target exon 23 of the DMD gene in *mdx* mice restored dystrophin expression in skeletal muscles when injected intramuscularly [108] or intravascularly [109]. This promising result led to testing of a 2′OMP targeting exon 51 of DMD gene (PRO051) in clinical trials. Intramuscular injection of PRO051 resulted in dystrophin expression in 64-97% of muscle fibers at levels between 17 and 35% of normal fibers [110]. A phase I/II clinical trial for PRO051 was also performed by subcutaneous injection of the compound in patients, leading to the

expression of dystrophin in a dose-dependent manner without apparent adverse effects [111]. However, recent results from a phase III clinical trial for PR0051 (Drisapersen) by BioMarin (ClinicalTrials.gov identifier NCT01803412) didn't provide evidence for an increase in DYSTROPHIN expression in patient's muscles. Furthermore, clinical endpoint studies in the same phase III trial and two phase II trials (ClinicalTrials.gov identifier NCT01480245 and NCT01462292) for Drisapersen didn't show consistent improvement in the 6 minute walk test.

PMOs have also been shown to be effective in skipping exon 23 of the *DMD* gene in *mdx* mice [112,113]. The MDEX consortium and AVI Biopharma tested the efficacy of a 30-mer morpholino (AVI-4658 or eteplirsen) to skip exon 51 of human *DMD* in patients. Intramuscular injection of AVI-4658 [114], and also systemic delivery of the morpholino in clinical trials, led to exon 51 skipping and expression of dystrophin when higher morpholino doses were used. Sarepta therapeutics is currently testing the efficacy, tolerability, safety and pharmacokinetics of eteplirsen in phase II clinical trials for patients with early stage DMD (ClinicalTrials.gov identifier NCT02420379) and patients in advanced stage of the disease (ClinicalTrials.gov identifier NCT02286947). A phase III clinical trial by Sarepta for is also ongoing to test the long-term effects of eteplirsen systemic administration in DMD patients amenable to exon 51 skipping (ClinicalTrials.gov identifier NCT02255552).

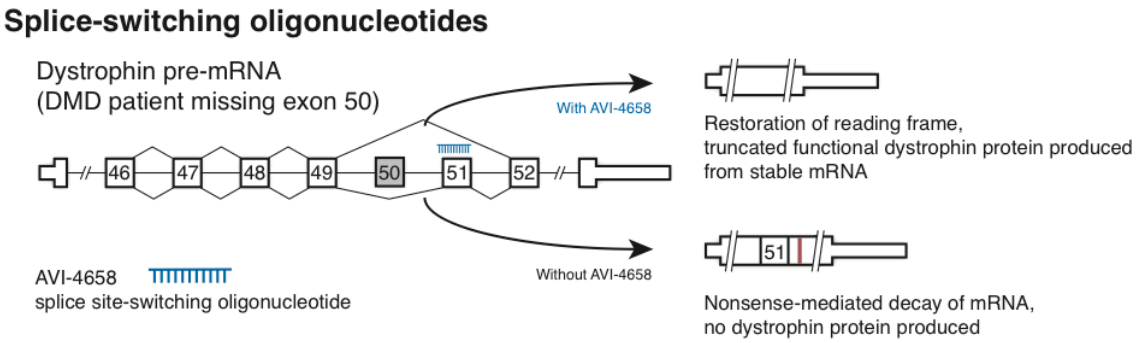

Figure 4. Exon skipping induced by splice-switching oligonucleotides. Schematic for mechanism of action of AVI-4658 antisense oligonucleotide for inducing exon skipping and restoring the mRNA reading frame in a DMD patient missing dystrophin exon 50.

Small Molecule Therapy

The first small molecules used to treat DMD patients were anti-inflammatory compounds from the family of glucocorticoid corticosteroids. Deflazacort, prednisone and prednisolone have been most commonly used in the clinic. In some cases, treated patients showed improved muscle strength, prolonged ambulation and slowed disease progression; however, these interventions do not represent a cure for the disease, and major side effects, including hypertension, diabetes, weight gain and cataract, present obstacles to their prescription [115,116].

About 10-15% of DMD cases are caused by mutations that introduce premature stop codons [117]. Some chemicals are able to interact with ribosomal subunits to cause the translational machinery to “skip” such nonsense mutations by introducing an amino acid in that position instead. Differences in the context of nucleotide sequence surrounding premature and normal stop codons allow for

specificity of action of these compounds [118]. Gentamicin, an aminoglycoside antibiotic that promotes such ribosomal "read-through," can induce dystrophin expression in *mdx* muscle to up to 20% of normal levels [119]; however, this compound has not been effective in human trials [120].

A high throughput screen of ~800,000 chemicals, performed by PTC therapeutics, identified Ataluren (PTC-124) as a compound that efficiently induced nonsense mutation readthrough. Ataluren, which has no structural similarity with aminoglycosides, restores dystrophin expression in cultured myotubes from *mdx* mice and DMD patients. When administrated to *mdx* mice in vivo, Ataluren improved muscle specific force and resistance to contraction-induced injury, and also restored dystrophin expression in up to 25% of fibers [121]. Phase I trials of PTC-124 revealed that the compound is well tolerated; however, three phase II clinical trials were terminated in March 2010 when the predetermined primary outcome (the 6-minute walk test) was not achieved. Results of a phase IIa clinical trial for Ataluren, published in 2013, showed increased dystrophin expression in 61% of the enrolled patients and a decrease in serum CK levels in patients receiving more than 8 mg/kg of Ataluren [122]. A phase III clinical trial for analyzing the efficacy and safety of this compound is currently ongoing (ClinicalTrials.gov identifier NCT01826487).

Another small molecule, BMN 195 (SMT-C1100), emerged from a screen for chemicals that upregulate expression of utrophin. Daily administration of BMN 195 to *mdx* mice ameliorates dystrophic pathology [123], but when tested in phase I clinical trial, plasma concentrations of this compound failed to reach the required

level (http://phx.corporate-ir.net/phoenix.zhtml?c=106657&p=irol-newsArticle&ID=1455247&highlight). However, no adverse effects were reported for BMN 195.

Kawahara et al. used a zebrafish model of DMD to screen a small molecule library to identify compounds that ameliorate dystrophic pathology in newborn fish [124]. The most potent chemical identified in this study was aminophylline, reported to be a non-selective phosphodiesterase (PDE) inhibitor [125]. Interestingly, skeletal muscle structure of affected dystrophin-null fish was restored after treatment with aminophylline for 26 days, although no dystrophin expression was detected in the muscle. The mechanism underlying this compound's activity is not understood, but may relate to elevation of intracellular cAMP levels and activation of cAMP-dependent protein kinase [124]. These authors also reported that Sildenafil citrate, a PDE5 inhibitor, influences muscle pathology in dystrophin-null zebrafish. Sildenafil citrate previously was shown to reverse cardiomyopathy in *mdx* mice, possibly via activation of cGMP-dependent pathways [126]. Tadalafil, another PDE5 inhibitor, reportedly improves the histopathology of dystrophic muscle in *mdx* mice when administrated prenatally [127]; however, existing studies on the effects of PDE5 inhibitors on dystrophic muscle have evaluated compound administration only in the early stages of life, and it remains unclear if these molecules can reverse disease phenotype if animals are treated after disease onset.

Biomarkers for assessing efficacy of therapeutic interventions in DMD patients

Analyzing dystrophin expression in patients' muscle by Western blot and immunofluorescence, measurement of serum creatine kinase (CK) levels, and muscle structure assessment by magnetic resonance imaging (MRI) are among the primary biomarkers used in clinical trials for analyzing the efficacy of the therapeutics used for restoring dystrophin expression [110,122]. A recent study by Somalogic identified 44 proteins with significantly different levels in serums of DMD patients compared to age-matched healthy controls [128] and these proteins can potentially serve as additional biomarkers for future clinical trials. Improvement in the 6 minute walking distance test (6MWT) is the most commonly used primary endpoint in DMD clinical trials [129] and pulmonary function assessment and echocardiogram and muscle strength measurement are also used to assess the efficacy of different compounds in these trials (ClinicalTrials.gov identifier NCT01480245 and NCT01803412).

Chapter 2.

In vitro expansion and gene correction of engraftable dystrophic mouse satellite cells

Addendum:

The data presented in this chapter was originally published as:

Cong Xu*, Mohammadsharif Tabebordbar*, Salvatore Iovino*, Jingxia Liu, Alessandra Castiglioni, Emily Price, Min Liu, Elisabeth R Barton, C. Ronald Kahn, Amy J. Wagers, Leonard I. Zon, A Zebrafish Embryo Culture System Defines Factors that Promote Vertebrate Myogenesis across Species, *Cell,* 2013 Nov 7; 155 (4): 909-21

And

Mohammadsharif Tabebordbar*, Kexian Zhu*, Jason K.W. Cheng, Wei Leong Chew, Jeffrey J. Widrick, Winston X. Yan, Claire Maesner, Elizabeth Wu, Ru Xiao, Ann F. Ran, Le Cong, Feng Zhang, Luk Vandenberghe, George M. Church, Amy J. Wagers, *In vivo* gene editing in dystrophic mouse muscle and muscle stem cells, *Science,* 2015 Dec 31, DOI: 10.1126.

Mohammadsharif Tabebordbar designed and performed all the experiments and analyzed the data presented in figures 7-11 and supplementary figures 1 and 2, except for the Western blot and taqman-quantitative reverse transcription PCR (qRT-PCR) experiments in Figure 11, which were performed by Kexian Zhu, a graduate student in the Wagers lab. Cong Xu, a former graduate student in the Zon lab performed the zebrafish screen and generated the data presented in figures 5 and 6 in this chapter.

Introduction

In vitro expansion, gene correction and autologous transplant of adult muscle stem cells is a promising approach for resorting dystrophin expression in dystrophic muscle. Multiple laboratories have isolated mouse muscle satellite cells from myofiber-associated cells using different combinations of cell surface markers. These cell populations include α7-integrin+, CD34+ cells [130], CXCR4+, β1-Integrin+, CD45-, Mac1-, Sca1- cells [51,131], Syndecan-3/4+ cells[132], CD45-, CD31-, α7-integrin+, V-CAM+ cells [133] and SM/C-2.6+ [134] cells. Cells in all of these populations are localized under the basal lamina on myofibers, express Pax7 as the canonical satellite cell marker and posses myogenic differentiation potential. In addition, transplantation-based studies in animal models have demonstrated the ability of freshly isolated wild type satellite cells to engraft and restore dystrophin in diseased *mdx* muscle [51,135]. Thus, muscle satellite cells are promising targets for cell therapies involving either cell replacement or activation of endogenous repair mechanisms. However, realization of this promise has been hindered by the paucity of satellite cells that can be isolated from adult skeletal muscle and a lack of methods to support their in vitro expansion. Reversible immortalization of myogenic cells with oncogenes has been suggested as a possible approach for expansion of primary myogenic progenitors in culture [136], but introduction of oncogenes into cells that need to be transplanted to patients doesn't have the potential for clinical application. Derivation of myogenic progenitors from embryonic stem cells and iPSCs is an alternative approach to provide sufficient

number of gene-corrected cells for transplantation. Although recent advances in myogenic differentiation of pluripotent cells has led to development of transgene free protocols [85-87], one major challenge that still remains to be addressed is identification of cell surface markers for isolation of myogenic progenitors with engraftment potential from the heterogeneous population of differentiated cells.

Two main obstacles for expansion of primary satellite cells are activation of satellite cells in culture [20] and decline in their engraftment potential after in vitro expansion [135]. Therefore, there is need for culture conditions that expand satellite cells and maintain at least a subset of the cells in an engraftable state. Moreover, transplantation of healthy myogenic progenitors, even with compatible human leukocyte antigen (HLA), into dystrophic patient muscles has been reported to induce immune response in the recipients [137,138]. Thus, a clinically relevant approach for adult muscle stem cell transplantation that avoids immune rejection requires gene correction of *in vitro* expanded dystrophic satellite cells, using a culture condition that keeps the cells in an engraftable state, and allows for transplantation of the corrected autologous cells.

In order to address these issues, we collaborated with the laboratory of Dr. Len Zon, who performed a high-throughput image-based screen using zebrafish blastomere cells. This screen identified 6 chemicals that promote myogenesis. We tested the effect of these muscle-promoting compounds on in vitro expansion of mouse satellite cells. Forskolin, an adenylyl cyclase activator, significantly increased satellite cell proliferation in culture. Forskolin-treated cultured cells retained the immunophenotypic characteristics of engraftable satellite cells, and

transplantation of compound-treated wild type satellite cells into dystrophic muscle yielded a significantly higher level of engraftment compared to control cells. This study also demonstrates that forskolin treatment dramatically expands dystrophic satellite cells from *mdx* mice in culture and provides the opportunity for gene correction. As a proof of concept for a combined gene and cell therapy approach for treating DMD, the mutated *Dystrophin* locus was targeted in expanded forskolin-treated dystrophic satellite cells using CRISPR/Cas9 gene editing technology and the targeted cells were enriched using an endogenous fluorescent reporter system. Gene-corrected dystrophic satellite cells restored dystrophin expression after in vitro differentiation and also after in vivo transplantation into dystrophic mouse muscle. Expansion and gene correction of muscle satellite cells in culture as described here provides the possibility of acheiving combined gene and cell-based therapies for neuromuscular disorders.

Results

Myogenic commitment is signified by expression of *myoD* and *myf5* [139], which are functionally redundant and exhibit overlapping expression in the earliest myogenic precursors [140]. Terminal differentiation of these progenitors produces cells expressing genes encoding muscle-specific structural proteins like *myosin light polypeptide 2* (*mylz2*), found in fast skeletal muscle [141]. To label different developmental states of skeletal muscle cells in zebrafish embryos, the Zon lab generated a *myf5-GFP*;*mylz2-mCherry* double transgenic zebrafish line. At the 11-

somite stage, *myf5-GFP* expression was restricted to the newly formed somite, while no *mylz2-mCherry* expression was detected (Figure 5A). Expression of *mylz2-mCherry* was first detected at 30 hours post fertilization (hpf) in the anterior somites and later spread to the posterior somites (Figure 5A). These data indicate that expression of *myf5-GFP* and *mylz2-mCherry* recapitulate the expression patterns of their corresponding endogenous genes [142], and thus provide a useful surrogate to track myogenic specification from early embryonic progenitors.

Cong Xu, a graduate student in the Zon lab, tested whether zebrafish blastomere cells could form muscle *in vitro* by disassociating myf5-GFP;mylz2-mCherry embryos at the oblong stage and plating them on gelatin-coated dishes. 1-10% became GFP-positive in zebrafish ESC (zESC) medium [143], indicating upregulation of *myf5* expression. Among the GFP-positive cells, 1-5% were also mCherry (*mylz2*) positive, suggesting that myogenic specification and differentiation had occurred in the *in vitro* system (Figure 5B).

Loss of FGF signaling in fgf24 and fgf8 double-deficient zebrafish essentially blocks embryonic muscle development [144], and FGF signals directly activate myoD expression in *Xenopus* [145]. Based on these data, Cong added basic fibroblast growth factor (bFGF) to the embryo cultures. The majority of bFGF-treated cells became GFP and mCherry double positive, indicating a potent muscle-promoting effect (Figure 5B).

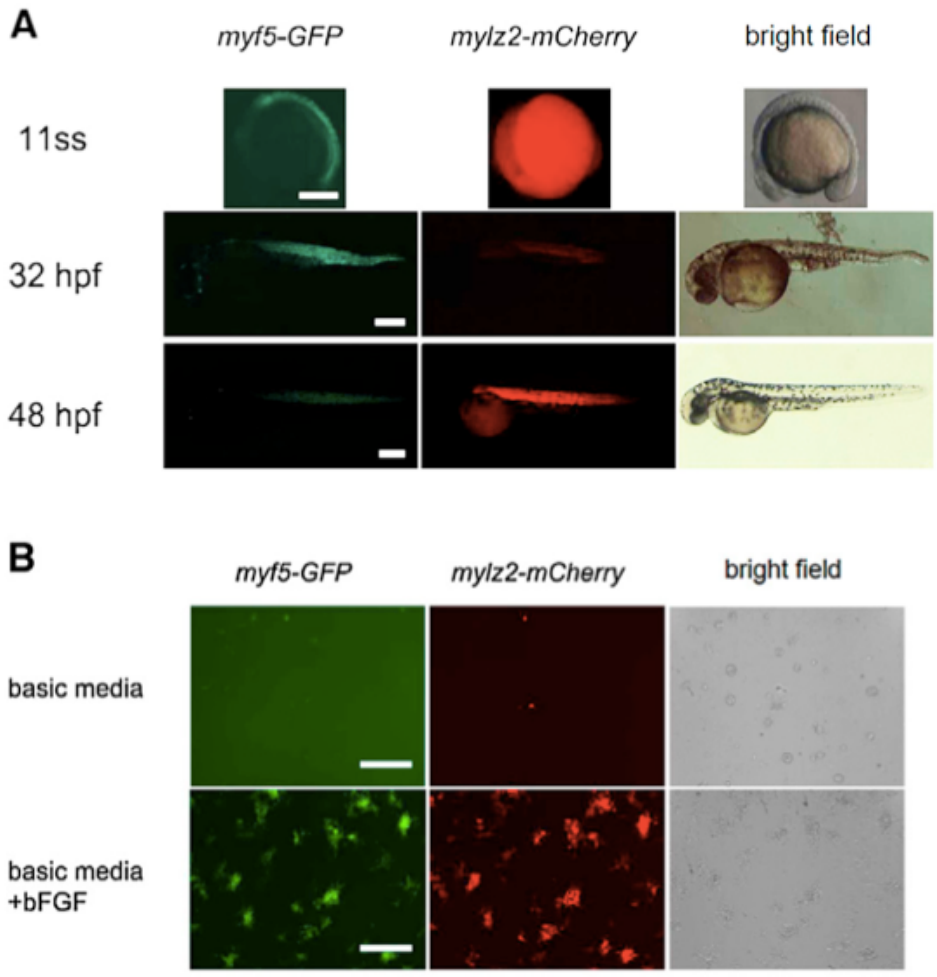

Figure 5. A Double Transgenic Zebrafish as a Reporter of Myogenesis During Development (A) *myf5-GFP*;*mylz2-mCherry* double-transgenic expression recapitulates expression of the endogenous genes. *myf5-GFP* is first detected at the 11-somite stage. *mylz2-mCherry* expression is not observed until 32 hpf. Scale bars represent 200 mm. (B) *myf5-GFP;mylz2-mCherry* embryos were dissociated at the oblong stage and cultured in zESC medium. Images were taken 48 hr after plating. Scale bars represent 250 mm.

To enable higher throughput analysis of myogenesis modifiers, the embryo culture system was adapted to a semi-automated screening platform. myf5-GFP;mylz2-mCherry embryos were disassociated at the oblong stage, and the resulting individual blastomere cells were aliquoted into four 384-well plates with preadded chemicals. The strong muscle-promoting effect of bFGF made it difficult

to identify enhancers of myogenesis in the screen, therefore in order to sensitize the system for enhancers of muscle development, bFGF was not added to the culture medium. After 1 day, the cells were automatically imaged (Figure 6A) and GFP and mCherry signals were quantified. In this sensitized screen, 6 chemicals out of 2,400 were identified to increase the GFP and mCherry signals (Figure 6B). These hits included three GSK3b inhibitors, two calpain inhibitors, and one cAMP activator forskolin.

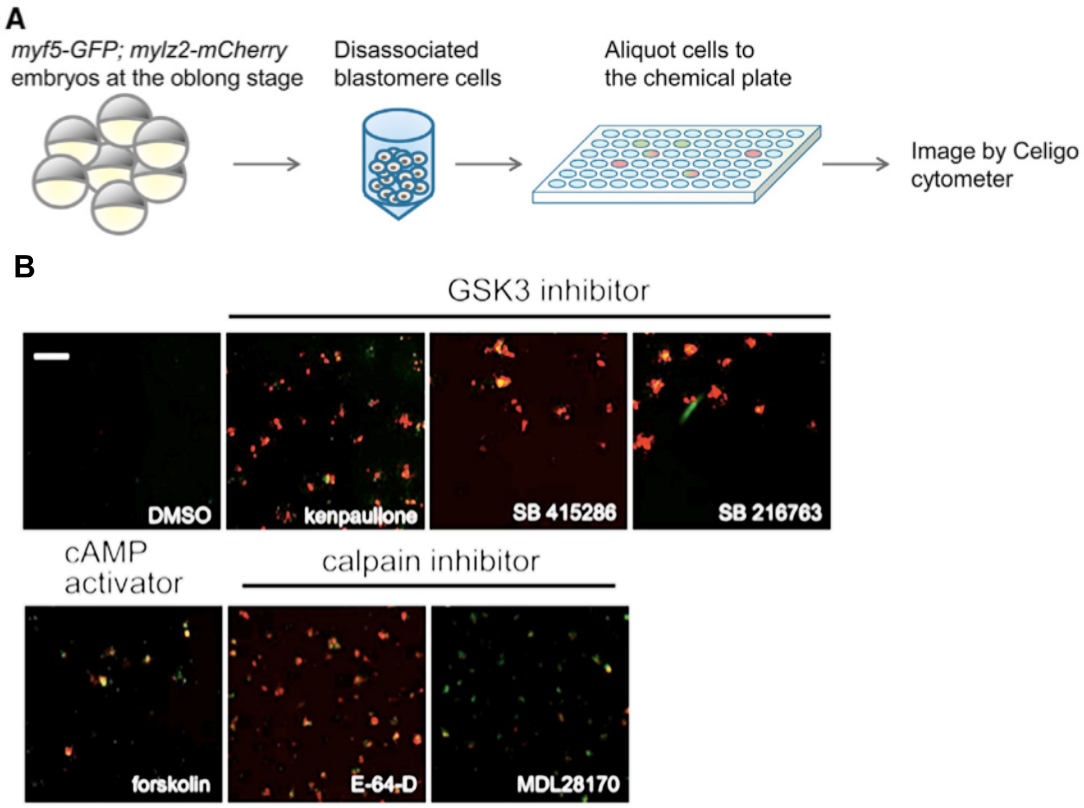

Figure 6. A Chemical Genetic Screens to Identify enhancers of Skeletal Muscle Development (A) Schematic of a high-throughput image-based chemical screening assay. Approximately 800 *myf5-GFP;mylz2-mCherry* double-transgenic embryos were collected and dissociated at the oblong stage. Resulting blastomere cells were aliquotted into 384-well plates with preadded chemicals. The 384-well plates were imaged and analyzed using a Celigo cytometer. (B) Hits from the enhancer screen. Six chemicals that increase the GFP and mCherry signals were identified. Scale bars represent 250 mM.

We hypothesized that chemical hits enhancing skeletal muscle

development in zebrafish blastomeres might likewise promote muscle precursor cell formation and/or expansion in other species. I exposed satellite cells isolated by fluorescence-activated cell sorting (FACS) [51] from adult mouse skeletal muscle to these compounds. Satellite cells were cultured in the presence of different concen- trations of each myogenesis-promoting chemical. Of the six chemicals tested, only forskolin triggered dose-dependent expansion of satellite cell cultures (data not shown). The number of cells in these cultures was increased by forskolin both in the presence and absence of bFGF (Figure 7A). The expanded forskolin-treated cells maintained expression of Pax7 and showed upregulation of MyoD, a marker profile consistent with activated satellite cells (Supplemental figure 1B).

Forskolin treatment also increased cell number in satellite cell cultures seeded from *mdx* mice, a mouse model of DMD [146]. Satellite cells from *mdx* mice typically exhibit defective in vitro expansion under control conditions, and forskolin treatment restored their proliferation to levels seen normally in cultures of untreated wild-type satellite cells (Figures 7B and supplementary figure 1A). To evaluate the mechanism by which forskolin drives increased cell number in satellite cell cultures, I assayed cyclic AMP (cAMP) production [147,148] and found that forskolin treatment increased cAMP levels in mouse satellite cell cultures (Figure 7C). I also performed cell survival and proliferation assays in forskolin-treated cultures. Satellite cells were plated at one cell per well in 96-well plates and treated with forskolin or DMSO. After 6 days, I quantified the number of wells containing any number of myogenic cells (a measure of cell survival; [149]) and the number of cells in those wells (a measure of cell proliferation) (Figure 7D). The

frequency of myogenic colony formation did not differ between forskolin- and DMSO-treated cells (Figure 7E), suggesting that forskolin treatment does not affect cell survival. Consistent with my earlier observations (Figure 7A), myogenic colonies formed in the presence of forskolin contained more cells than DMSO-treated colonies (Figure 7F). Forskolin-treated satellite cells were not immortalized, however, and maintained proliferative capacity in culture for approximately the same length of time as DMSO-treated cells (data not shown).

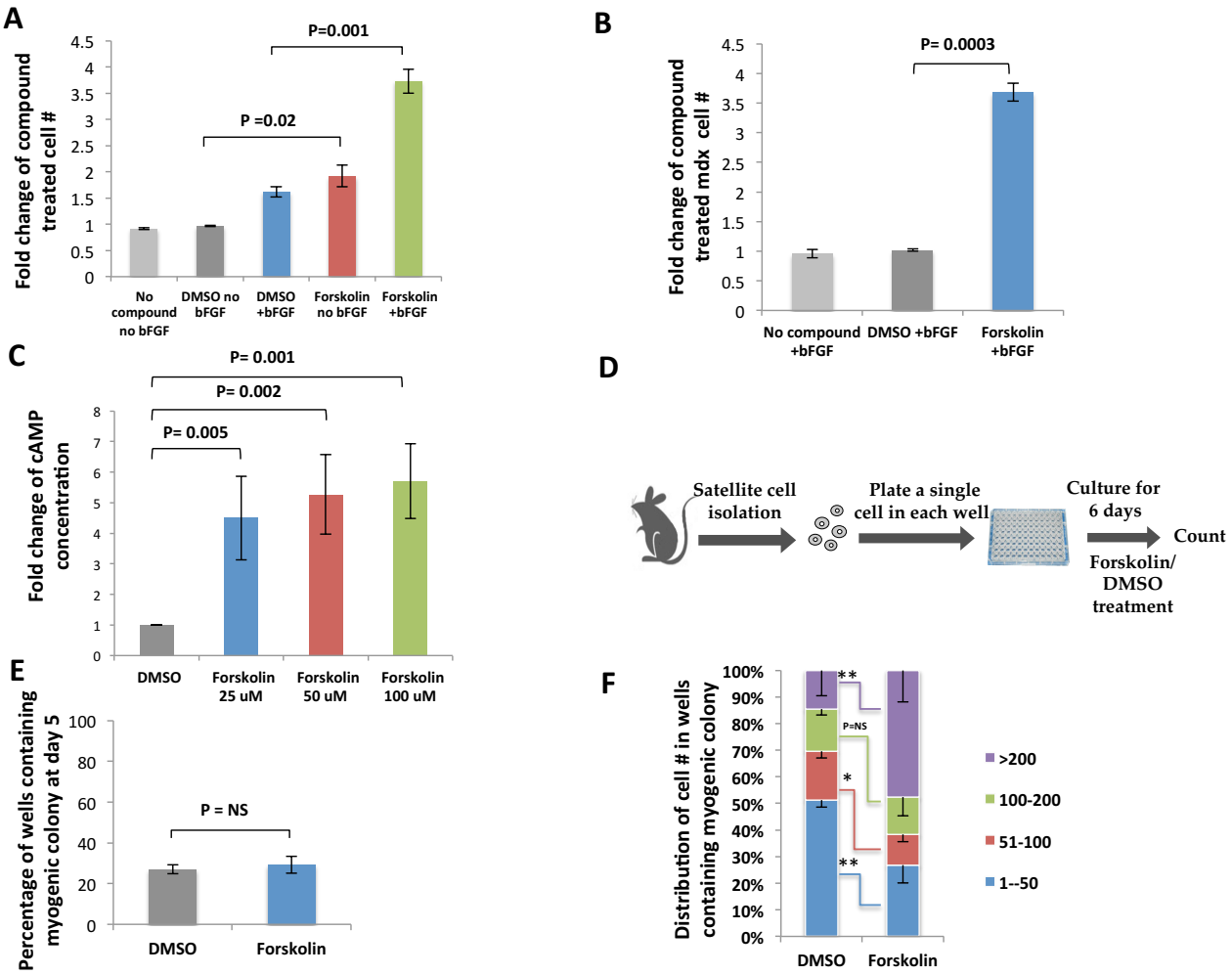

Figure 7. Forskolin Treatment Elevates cAMP Level and Increases Proliferation of Satellite Cells from Both Healthy and Dystrophic Mice (A) Satellite cells from C57BL/6J mice were cultured and treated with DMSO or forskolin in the absence or presence of bFGF, as indicated. Total cell number was determined after 5 days (mean ± SEM, n = 4). Data are presented as fold change, normalized to ‘‘DMSO no bFGF’’ controls. (B) Fold change in cell number from cultures of *mdx* satellite cells after 5 days *in vitro* with bFGF alone, DMSO + bFGF, or forskolin + bFGF (mean ± SEM, n = 4). Data are normalized to ‘‘DMSO +bFGF’’ controls. (C) Concentration of cAMP in cultured satellite cells is increased after treatment with 25 mM, 50 mM, or 100 mM of forskolin, as compared to the DMSO-treated cells (mean ± SD, n = 5). Data are normalized ‘‘DMSO’’ controls. (D) Experimental scheme for myogenic colony- forming assay. Satellite cells were isolated from C57BL/6J mice, and a single cell was plated into each well of 96-well plates. Cells were cultured for 6 days and treated with DMSO or forskolin. The number of wells containing a myogenic colony and the number of cells in each colony were counted after 6 days. (E) Clonal plating efficiency of satellite cells is not altered by forskolin treatment, as compared to DMSO-treated cells (mean ± SD, n = 4). (F) Forskolin treatment increases the number of myogenic cells arising from a single satellite cell in each well, showing an increase in cell proliferation. Data are plotted as the % of colonies containing the indicated number of cells (mean ± SD, n = 4). *, $p < 0.05$; **, $p < 0.01$.

To test whether the increase in cell proliferation was caused by an inhibitory

effect of forskolin on satellite cell differentiation, I expanded cultured satellite cells and induced them to differentiate in the presence or absence of forskolin. The percentage of nuclei in myotubes in each culture was quantified as a measure of myogenic differentiation (Figure 8A) and was not different between the forskolin and DMSO-treated groups (Figures 8B and 8C). Satellite cells that were exposed to forskolin during growth and then induced to differentiate after removal of the compound (Figure 8D) also formed myotubes with the same efficiency as control-treated cells (Figures 8E and 8F). Treatment with forskolin during both the proliferative and differentiation phases of culture also did not affect differentiation (Supplemental figures 2D–2F). Thus, forskolin-treated satellite cells exhibit unperturbed differentiation in vitro regardless of the timing of compound exposure. Unlike the synergistic effect of bFGF and forskolin for satellite cell expansion (Figure 7A), however, addition of bFGF during differentiation slightly reduced the number of nuclei incorporated into myotubes (Supplemental figures 2A–2C), suggesting an inhibitory effect of bFGF on myogenic differentiation in the presence of forskolin (Supplemental figures 2A–2C).

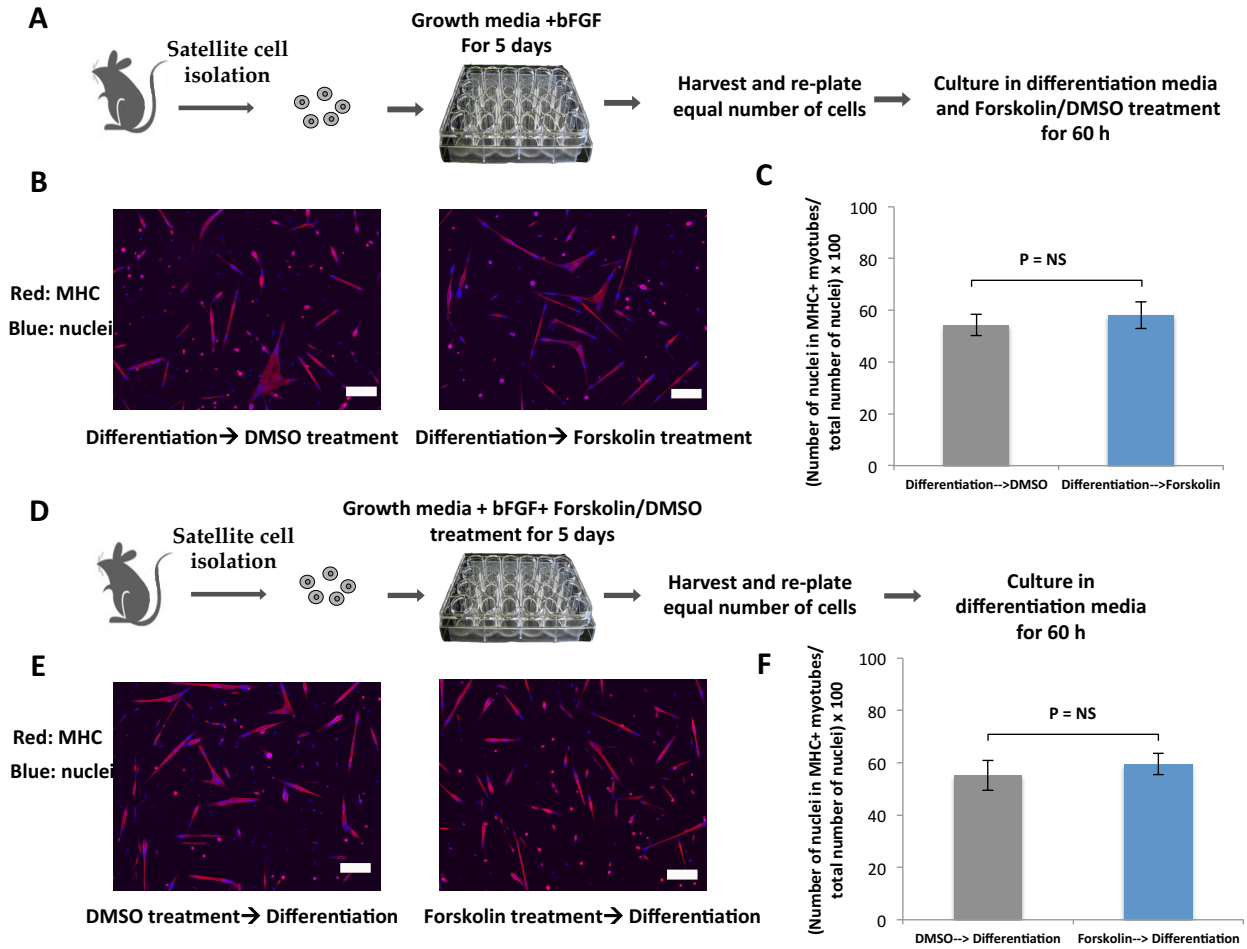

Figure 8. Forskolin-Treated Satellite Cells Exhibit Effective Differentiation *In Vitro* (A) Experimental scheme. Satellite cells from C57BL/6J mice were cultured in the presence of bFGF for 5 days. Cells were harvested on day 5, and equal numbers of cells were induced to differentiate in the presence of forskolin or DMSO. (B) Images of satellite cells differentiated in the presence of DMSO (left) or forskolin (right) and stained for myosin heavy chain (MHC, red) and nuclei (blue). Scale bars represent 200 mm. (C) Quantification of percentage of nuclei in myotubes after satellite cell differentiation in the presence of forskolin or DMSO (mean ± SEM, n = 4). Differentiation potential of satellite cells is unaffected by forskolin (p = nonsignificant [NS]). (D) Satellite cells from C57BL/6J mice were cultured with bFGF and forskolin/DMSO for 5 days. Cells were harvested on day 5, and equal numbers of cells were induced to differentiate after removal of the compound. (E) Images of DMSO- (left) or forskolin (right)-treated satellite cells differentiated after removal of compound and were stained for MHC (red) and nuclei (blue). Scale bars represent 200 mm. (F) Quantification of percentage of nuclei in myotubes after differentiation of forskolin- or DMSO-treated cells (mean ± SEM, n = 5). Forskolin-treated satellite cells show no defect in myotube formation.

Muscle satellite cells are highly enriched within the subset of myofiber-associated cells that co-expresses *Cxcr4* and *1- Integrin* , and myogenic cells lacking CXCR4 and 1-integrin fail to engraft into *mdx* muscle [51]. High levels of *Cxcr4* expression also predict high levels of *Pax7* expression, which identifies a subset of serially transplantable satellite cells with muscle-stem-cell-like properties [25]. Freshly isolated satellite cells are 100% positive for CXCR4 and 1-integrin expression, and flow cytometric analysis revealed that 78.9% ± 1.52% of forskolin-expanded cells maintained co-expression of both these markers after 5 days in culture (Figures 9A and 9B). Thus, most satellite cells cultured in forskolin retain phenotypic characteristics of freshly isolated, engraftable muscle stem cells.

To assess directly the engraftment potential of cultured forskolin-treated satellite cells, I isolated cells from -actin-GFP transgenic mice [150], using GFP as a marker for cell tracking in transplantation experiments. 6,000 GFP-expressing satellite cells were cultured for 5 days with forskolin, and the resulting cells were transplanted into the preinjured muscles of *mdx* mice (Figure 9C). Recipient muscles were harvested 3–4 weeks after transplant and analyzed for the presence of donor-engrafted, GFP-expressing myofibers. Consistent with the ability of forskolin to expand a primitive and engraftable myogenic cell population, the number of GFP+ fibers was higher in animals receiving forskolin-expanded cells as compared to those receiving the original number of freshly isolated satellite cells or those receiving expanded DMSO-treated cells (Figures 9E and 9F). In contrast, the number of engrafted fibers did not differ significantly when recipients were transplanted with equal numbers of cultured DMSO or forskolin-treated cells

(Figures 9G and 9H). Thus, exposure to forskolin expands mouse satellite cells in culture while maintaining their engraftment potential. This effect provides more cells for transplantation (Figure 9D) and a greater yield of engrafted fibers *in vivo* if the same number of satellite cells is first expanded with forskolin *in vitro*, compared to control. Myofibers engrafted by forskolin-treated cells stained for dystrophin, which normally is absent in *mdx* muscle (Supplemental figure 1C), indicating that forskolin-expanded donor cells maintain *in vivo* myogenic activity and can produce functional myoblasts that incorporate into myofibers and produce muscle-specific proteins.

Figure 9. Forskolin-Treated Cultured Satellite Cells Retain Immunophenotypic Characteristics of Freshly Isolated Satellite Cells and Engraft Skeletal Muscle In Vivo (A) Representative FACS plots depict $CD45^{-}SCA\text{-}1^{-}MAC1^{-}$ cells gated for the $CXCR4^{+}$ and b1 $Integrin^{+}$ subset of freshly isolated (left) and cultured satellite cells (initially sorted as 100% $CXCR4^{+}$ and b-1 $Integrin^{+}$) treated with DMSO (middle) or forskolin (right). (B) Average frequency (mean ± SEM, n = 6) of $CXCR4^{+}$b1-$Integrin^{+}$ cells among cultured satellite cells treated with DMSO or forskolin, quantified by FACS. Most cultured satellite cells were treated with either DMSO or forskolin retain expression of CXCR4 and b1 Integrin. (C) Experimental scheme. GFP^{+} satellite cells were harvested from b-*actin-GFP* mice and were transplanted into the TA muscle of recipient *mdx* mice, injured 1 day previously by injection of cardiotoxin. Cells were transplanted either immediately after isolation or following 5 days in culture with DMSO or forskolin treatment. (D) Total number of cultured GFP+ satellite cells that were obtained from 6,000 freshly isolated cells and used for transplantation into *mdx* muscle. Cell number was, on average, 2.5 times greater in forskolin-treated as compared to DMSO-treated cultures (mean ± SD, n = 6) . (E) Transverse frozen section of TA muscle from *mdx* mice transplanted with 6,000 freshly isolated satellite cells (left), cultured DMSO-treated satellite cells expanded from 6,000 freshly isolated cells (middle), or cultured forskolin-treated satellite cells expanded from 6,000 freshly isolated cells (right). Laminin staining is shown in red. Scale bars represent 200 mm. (F) Transverse frozen sections of TA muscle from *mdx* mice transplanted with 200,000 cultured DMSO-treated (left) or 200,000 cultured forskolin-treated (right) GFP+ satellite cells. Laminin staining is shown in red. Scale bars represent 200 mm. (G) Quantification of donor-derived (GFP+) myofibers in *mdx* muscles transplanted with freshly isolated, DMSO-cultured, or forskolin-cultured satellite cells (mean ± SD, n = 6). (H) Quantification of donor-derived myofibers in *mdx* muscle transplanted with 200,000 cultured DMSO-treated or 200,000 cultured forskolin-treated satellite cells (mean ± SD, n = 4).

Figure 9 (continued)

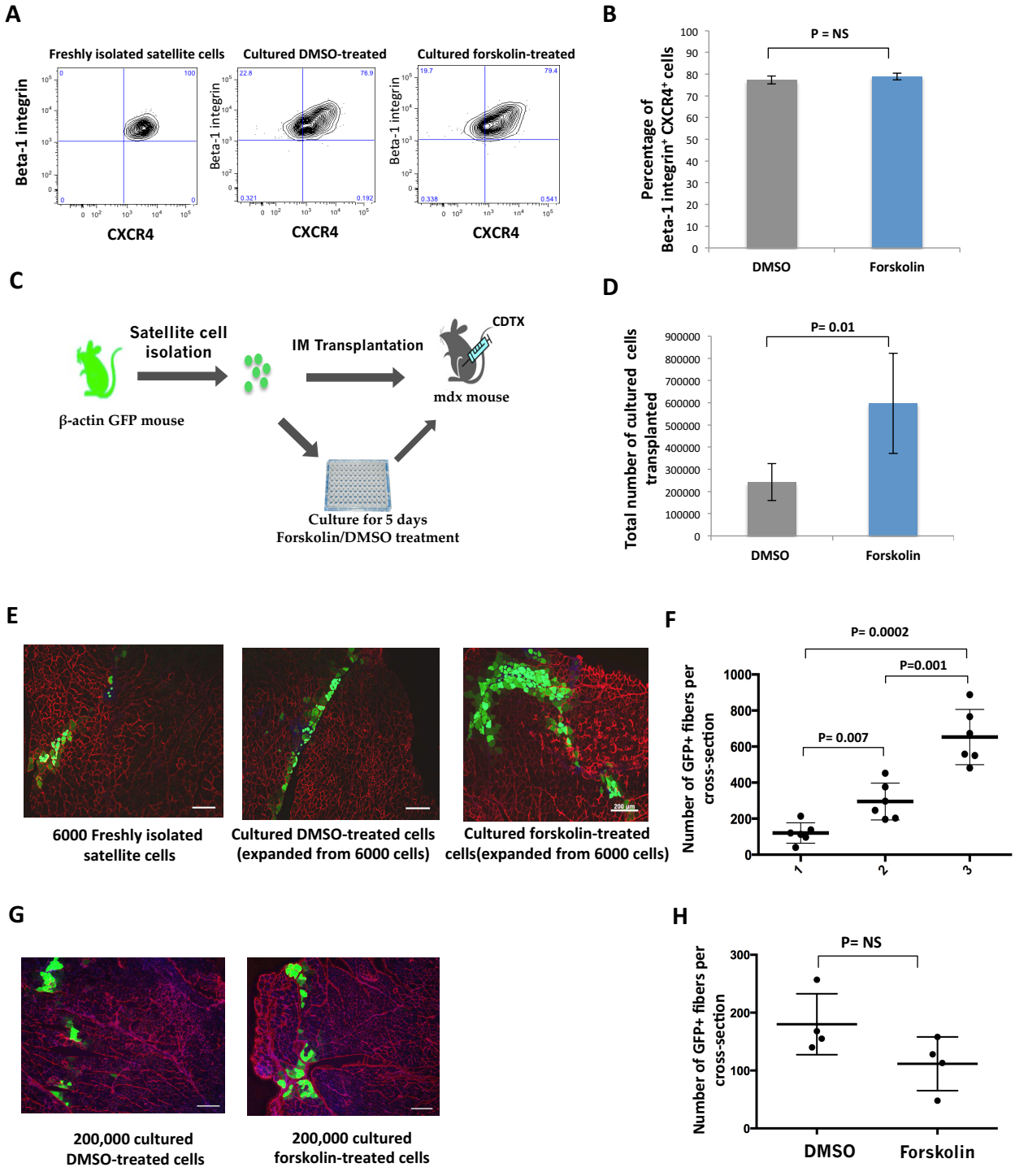

Next, we used forskolin treatment to expand dystrophic satellite cells isolated from *mdx* mice in culture in order to provide sufficient number of cells that can be used for gene correction and transplantation. To apply CRISPR/Cas9 gene editing for targeting the mutated locus in *Dmd*, we first sought to develop a robust reporter system for CRISPR activity. For this, we "repurposed" an existing mouse reporter allele, Ai9, which encodes the fluorescent tdTomato protein downstream of a ubiquitous CAGGS promoter and "floxed" STOP cassette [151] (Figure 10A). Exposure to SpCas9, together with paired gRNAs targeting near the 5' and 3' loxP sites of the Ai9 allele (hereafter Ai9 gRNAs), results in precise excision of the intervening DNA and expression of the downstream tdTomato gene (Figures 10A and 10B). This system thereby provides sensitive, fluorescence-based detection of CRISPR activity with single cell resolution and the capacity to prospectively detect and isolate gene-edited cells and their progeny by FACS (Figure 10B). We also designed and tested a pair of gRNAs directed at 5' and 3' sequences flanking exon 23 of the mouse *Dmd* gene (hereafter *Dmd23* gRNAs) that enabled efficient excision of the intervening DNA (Figure 10C). *Mdx* mice, a genetic model of human DMD, carry a nonsense mutation in *Dmd* exon 23, resulting in loss of dystrophin and destabilization of DMD mRNA [146]. Prior studies with AONs indicate that skipping of exon 23 restores dystrophin reading frame and produces an internally truncated, but still highly functional protein that can complement dystrophin-deficiency in dystrophic muscle [108]. To facilitate detection of *Dmd* gene-edited cells in our studies, we coupled the *Dmd23* gRNAs to Ai9 gRNAs using a two plasmid system in which the 3' gRNAs for Ai9 and *Dmd* were encoded in one

vector and the 5' gRNAs in another (Figure 10D, top pannel). This hybrid vector system effectively links expression of the CRISPR activity reporter (tdTomato) to genome editing events at the *Dmd* locus, because in order to express tdTomato after co-transfection with these vectors and SpCas9, the target cell must have received both the 5' and 3' Ai9 gRNAs, and therefore must also have received both of the linked *Dmd23* gRNAs.

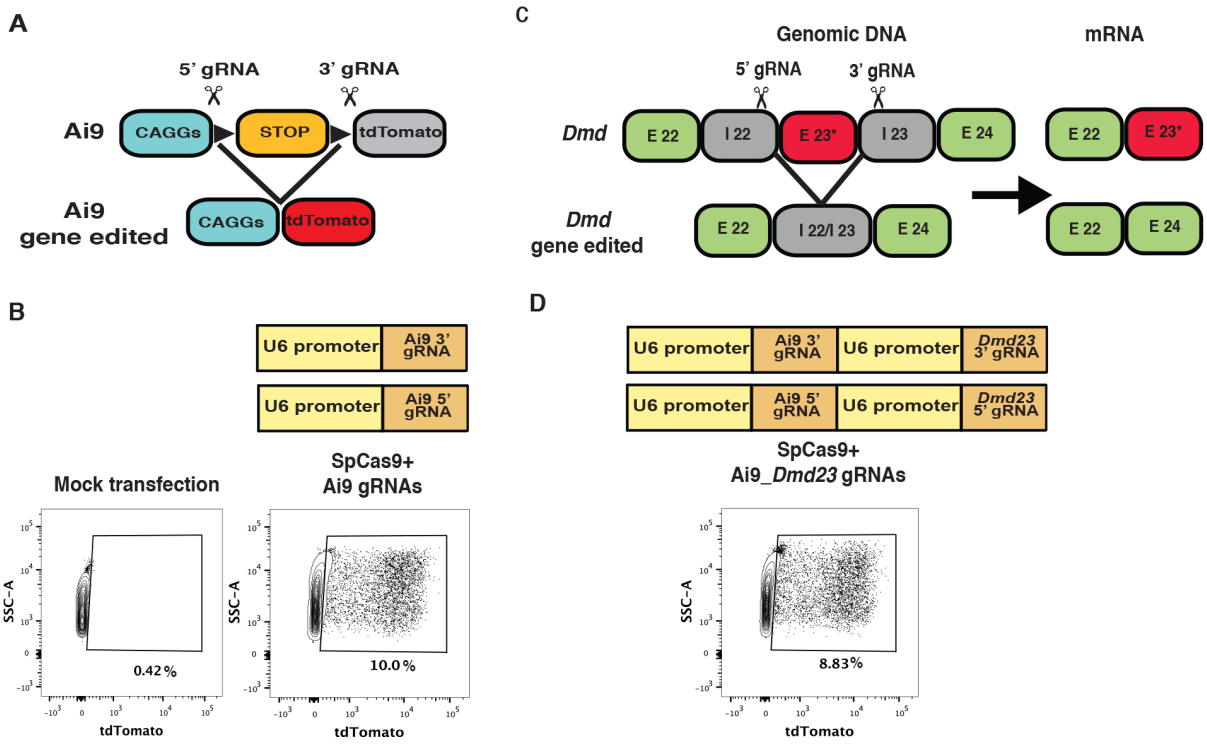

Figure 10. A Sensitive Fluorescent CRISPR Activity Reporter System Facilitates Detection And Isolation of Gene-targeted Cells. (A) Schematic of the Ai9 allele and its use as a fluorescent CRISPR activity reporter. (B) Schematics of Ai9 targeting gRNA constructs (top) and representative FACS plots from *mdx;Ai9* satellite cells transfected with plasmids encoding SpCas9 and gRNAs targeting Ai9 locus (bottom right) or with no DNA (bottom left). (C) Schematic of CRISPR-mediated excision of *Dmd* exon 23. (D) Schematics of coupled Ai9-*Dmd23* targeting gRNA constructs (top) and a representative FACS plot from *mdx;Ai9* satellite cells transfected with plasmids encoding SpCas9 and coupled gRNAs targeting Ai9 and *Dmd23* loci (bottom).

Indeed, *in vitro* transfection of primary satellite cells from *mdx* mice carrying the Ai9 allele (hereafter *mdx;Ai9* mice) with SpCas9 + Ai9-*Dmd*23 coupled gRNAs induced gene editing at both the Ai9 locus (demonstrated by tdTomato expression, Figure 10D, bottom panel) and the *Dmd* locus (detected by genomic PCR using primers flanking exon 23 together with amplicon sequencing indicating precise excision and generation of a fused intron 22/23, Figure 11A). DMD gene editing was not detected in *mdx;Ai9* cells receiving Ai9 gRNAs alone (Figure 11A), although tdTomato expression was equivalently induced (Figure 10B, bottom panel), confirming that locus specificity in this system is determined by the genomic complementarity of the gRNAs used for programming Cas9.

To confirm that CRISPR-mediated editing of the *Dmd* locus results in irreversible genomic modification and production of exon-deleted mRNA and protein, co-transfected primary satellite cells were isolated by FACS based on tdTomato expression, expanded *in vitro* by forskolin treatment [85], and differentiated to myotubes. RNA and protein were then harvested for RT-PCR and Sanger sequencing analysis, which demonstrated the presence of the exon 23-deleted DMD mRNA in cells receiving SpCas9 and coupled Ai9-*Dmd*23 gRNAs, but not in cells receiving SpCas9 and Ai9 gRNAs only (Figure 11B). Levels of exon 23-deleted transcripts were quantified using Taqman analysis [152], and represented 24-47% of total DMD mRNA in cells receiving Ai9-*Dmd*23 coupled gRNAs (Figure 11C). In contrast, exon 23 deletion was undetectable in cells receiving SpCas9 with only Ai9 gRNAs (Figure 11C). Dystrophin protein expression was also restored in CRISPR-modified *mdx;Ai9* cells, and was detectable by Western blot

(Figure 11D) in *in vitro* differentiated myotubes and immunofluorescence (Figure 11E) in *in vivo* engrafted muscle fibers derived from gene-edited satellite cells.

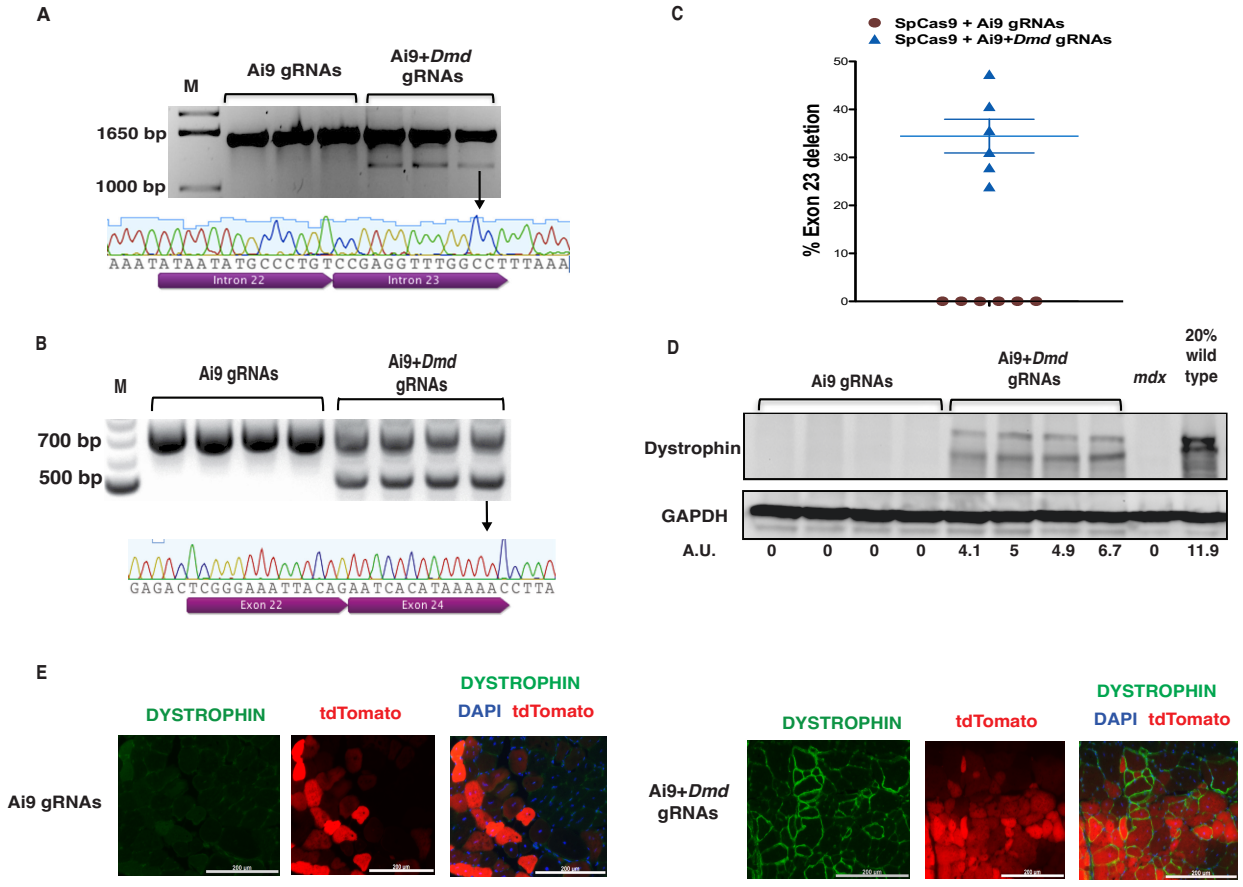

Figure 11. Gene-corrected Dystrophic Satellite Cells Restore dystrophin Expression After Differentiation *In Vitro* and *In Vivo*. (A) Detection of exon 23 excision by genomic PCR in myotubes derived from satellite cells transfected with SpCas9 and Ai9 gRNAs (left lanes) or coupled Ai9-*Dmd*23 gRNAs (right lanes). Unedited genomic product, 1572bp; gene-edited product, 1189bp. Sanger sequencing confirms precise excision of exon 23 from the genome. (B) Detection of exon 23-deleted mRNA using RT-PCR. M, molecular weight marker. Unedited RT-PCR product: 738bp; exon 23-deleted product: 525bp. Sanger sequencing confirms absence of exon 23 in the mRNA. (C) Quantification of percent exon 23-deleted transcripts in targeted satellite cell-derived myotubes by Taqman-based real-time PCR. Plotted as individual data points for *Dmd*23 gRNAs (blue) and Ai9 gRNAs (red), overlaid with mean +/- SEM (n=6 transfections analyzed per group) (D) Western blot for dystrophin and GAPDH (loading control) in lysates of myotubes derived from gene-edited satellite cells. A.U.: Arbitrary Unit normalized to GAPDH. (E) Dystrophin immunofluorescence in *mdx* muscles transplanted with satellite cells transfected in vitro with SpCas9 + Ai9 gRNAs (left) or SpCas9 + Ai9-*Dmd*23 coupled gRNAs (right). Green: dystrophin; Red: tdTomato; Blue: DAPI (nuclei). Scale bar: 200 um.

Discussion

Autologous adult stem cell transplant is considered as a promising therapeutic approach for treating genetic muscle diseases. However, *in vitro* expansion of engraftable muscle stem cells and efficient gene correction of the cultured satellite cells are two major hurdles for clinical application of this approach. To develop a culture condition that allows for expansion of engraftable satellite cells, we took advantage of chemical genetic approaches available in zebrafish to reveal conserved mechanisms controlling the specification and expansion of myogenic progenitor cells. The culture-based screening system reported here takes one-sixth the time and uses one-tenth the embryos compared to conventional screening strategies using whole zebrafish embryos. Such throughput enables screening of larger chemical libraries with greater speed than chemical screening on mammalian cell lines. Transgenic zebrafish with fluorescent reporters known to label a particular cell type *in vivo* can be used, and images can be automatically captured and stored such that the cells need not be fixed or scored immediately.

A noteworthy attribute of the zebrafish embryo culture system is its ability to identify pathways that influence tissue specification and progenitor cell expansion across species. Chemicals found in our zebrafish system expand postnatal muscle satellite cells from mice, thus helping to address another vexing challenge in the production of mammalian muscle precursors for experimental applications and, ultimately, cell therapy. One major obstacle in using purified skeletal muscle satellite cells for therapy is their very low frequency in adult tissue. High numbers

of engraftable cells are required for functional recovery of skeletal muscles throughout the body in genetic muscle disorders, and efforts to expand purified satellite cells in culture while maintaining their engraftment potential have been largely unsuccessful [135]. We show that mouse muscle progenitors treated with the adenylyl cyclase activator forskolin exhibit enhanced proliferation in culture. These data are consistent with a previous report showing that activation of cAMP signaling in transgenic mice expressing an activated form of cAMP response element binding protein (CREB) increases the *in vitro* proliferation of primary myoblasts [153] and contrast with the cell-cycle inhibitory effects of this chemical in some other systems (e.g., human T cells [154] and thyroid cancer cell lines [155]). Forskolin does not inhibit satellite cell differentiation *in vitro*, and forskolin- treated muscle progenitors differentiate normally after removal of the compound or in its continued presence. Satellite cells cultured with forskolin retain most phenotypic characteristics of freshly isolated satellite cells. Forskolin may mimic activation of a natural G-protein-coupled receptor involved in the genesis or maintenance of muscle progenitors. When transplanted into preinjured *mdx* muscle, forskolin-expanded satellite cells engrafted to generate dystrophin-expressing myofibers.

Forskolin treatment also enhanced proliferation of satellite cells from dystrophic *mdx* mice, which exhibited defective *in vitro* expansion under control conditions. We used forskolin to expand primary dystrophic satellite cells in culture and used a sensitive fluorescent reporter system to enrich for the gene-targeted cells after *in vitro* transfection of the cells with CRISPR/Cas9 gene editing components. Gene-corrected satellite cells restored DYSTOPHIN expression after myogenic

differentiation *in vitro* and *in vivo*, providing proof of concept evidence for the feasibility of an autologous adult stem cell transplantation approach for treating DMD. Together, these data are consistent with recent reports of *DMD* gene editing in immortalized human myoblast cell lines [156] and human induced pluripotent stem cells [157] and demonstrate the utility of CRISPR/Cas9 gene editing for modification of disease-specific alleles in primary muscle stem cells that retain muscle engraftment capacity. These results also establish a robust, programmable system for fluorescent detection and enrichment of gene-edited cells *in vitro* and *in vivo*.

Chapter 3.

In vivo gene editing in dystrophic mouse muscle and muscle stem cells

Addendum:

The data presented in this chapter was originally published as:

Mohammadsharif Tabebordbar*, Kexian Zhu*, Jason K.W. Cheng, Wei Leong Chew, Jeffrey J. Widrick, Winston X. Yan, Claire Maesner, Elizabeth Wu, Ru Xiao, Ann F. Ran, Le Cong, Feng Zhang, Luk Vandenberghe, George M. Church, Amy J. Wagers, *In vivo* gene editing in dystrophic mouse muscle and muscle stem cells, *Science,* 2015 Dec 31, DOI: 10.1126.

Mohammadsharif Tabebordbar and Kexian Zhu designed the experiments. Mohammadsharif Tabebordbar generated the SaCas9 gRNAs, the two-vector AAV constructs and the modified gRNA scaffold, performed the *in vitro* plasmid transfection and AAV DJ transduction, Flow cytometry, mouse handling, satellite cell isolation, culture and transplantation, histology and immunofluorescence. Kexian Zhu from the Wagers lab generated the single vector AAV constructs, performed genomic DNA PCR, end point RT-PCR and Taqman-qRT-PCR, Western blot, capillary immunoassay and prepared the Next generation sequencing (NGS) library. Jason Cheng from the Wagers lab helped with AAV production, cryosectioning, plasmid preparation and immunofluorescence. Jeffrey J. Widrick from the Children's hospital performed the physiology experiments. Winston Yan from the Feng lab performed the NGS and analyzed the data.

Introduction

The potential efficacy of exon-skipping strategies has been supported by the relatively mild disease course of Becker Muscular Dystrophy (BMD) patients with in-frame deletions in *DMD* that lead to "natural" exon skipping [158,159]. Morpholino AON mediated strategies designed to mask the splice donor or acceptor sequences of mutated exons in the dystrophin mRNA have been shown to restore expression of a truncated but biologically active dystrophin protein in mice [108,160] and human patients [161], and show some promise [161,162], although they have failed to meet predetermined clinical endpoints, likely reflecting insufficient rescue of dystrophin protein expression in key target tissues [129]. Indeed, while progress has been made recently through the use of tricyclo-DNA (tcDNA) and Pip5 transduction peptide-based approaches [152,163], early AON chemistries induced relatively low levels of exon skipping in skeletal muscles and were particularly inefficient at delivery to cardiac muscle. Furthermore, even with relatively stable chemistries [152], AONs have a defined half-life [152,164], requiring patients to undergo repeated rounds of treatment. This need for multiple injections increases both the cost and potential side effects of AON therapy. Finally, delivery of AONs of any chemistry to resident muscle satellite cells, if it occurs, is likely to be ineffective because the AONs are diluted during proliferation. Strategies in which AONs are delivered virally, by embedding within small nuclear RNAs, suffer similarly from progressive loss of the viral genome, and its encoded AONs, from dystrophic muscles [165]. Thus, ironically, in the context of gene therapy for DMD,

the regenerative activities of muscle satellite cells pose a potential threat to therapeutic dystrophin restoration, as the addition of new, non-targeted nuclei would reduce the fraction of myonuclei in muscle fibers producing therapeutic exon skipped mRNA or shortened forms of dystrophin. Of course, on the other hand, successful targeting of satellite cells *in vivo* would provide a mechanism for continual replenishment of gene-edited myonuclei through normal muscle repair mechanisms, and may be important to correct satellite cell-intrinsic polarity defects arising from dystrophin loss-of-function [52].

It was with these considerations in mind that we sought to adapt the gene-editing potential of the CRISPR/Cas9 system, which enables irreversible modification of targeted gene loci, for enduring production of functional dystrophin protein in dystrophic heart, skeletal muscle and satellite cells. Our data provide exciting support in DMD model mice for recovery of dystrophin expression and function in dystrophic skeletal muscle, cardiac muscle, and satellite cells, through local or systemic dissemination of gene editing complexes targeting the *Dmd* locus. Our system employs a clinically relevant delivery strategy, already in use in human trials [166,167], and our data provide strong proof-of-concept evidence for the feasibility and efficacy of this approach. As it has been estimated that more than 60% of DMD patients could benefit from skipping one or more exons in the exon 45-55 region [168,169], clinical translation of this novel strategy has the potential to transform the clinical course of disease for a significant number of DMD patients.

Results

To assess the utility of the CRISPR system for genomic modification of muscle cells *in vivo*, we adapted the CRISPR machinery for delivery via adeno-associated virus (AAV). AAVs are currently in use in human clinical trials [166,167] and provide the opportunity for both local and systemic delivery of virally encoded gene editing complexes. However, the limited packaging capacity of AAVs (4.8 kb) presents an obstacle for their use in delivering large genes such as SpCas9 (4.2kb) [170,171]. To overcome this problem, we used the orthologous Cas9 protein from *Streptococcus aureus* (Sa), which is ~1 kb smaller and can be programmed to target any locus in the genome containing a "NNGRR" PAM sequence [105]. To employ tdTomato expression as a reporter of *in vivo* CRISPR activity, we generated paired Sa gRNAs targeting sequences flanking the STOP cassette of the Ai9 allele. Using the Ai9 reporter, we next attempted to optimize the SaCas9 gRNA scaffold by incorporating base modifications previously reported to remove a putative RNA polymerase III transcription terminator [172,173] and enhance the assembly of gRNA and catalytically inactive orthologous SpCas9 [173]. We found that the same base modifications in the gRNA scaffold that increase the efficiency of Sp CRISPR complex formation also enhance gene targeting by SaCas9 (Figure 12A-C). We therefore used the modified Sa gRNA scaffold to generate *Dmd*23 Sa gRNAs. We screened 16 pairs of *Dmd*23 Sa gRNAs and identified the pair with highest efficiency for precise DNA excision at exon 23 (Figure 12D).

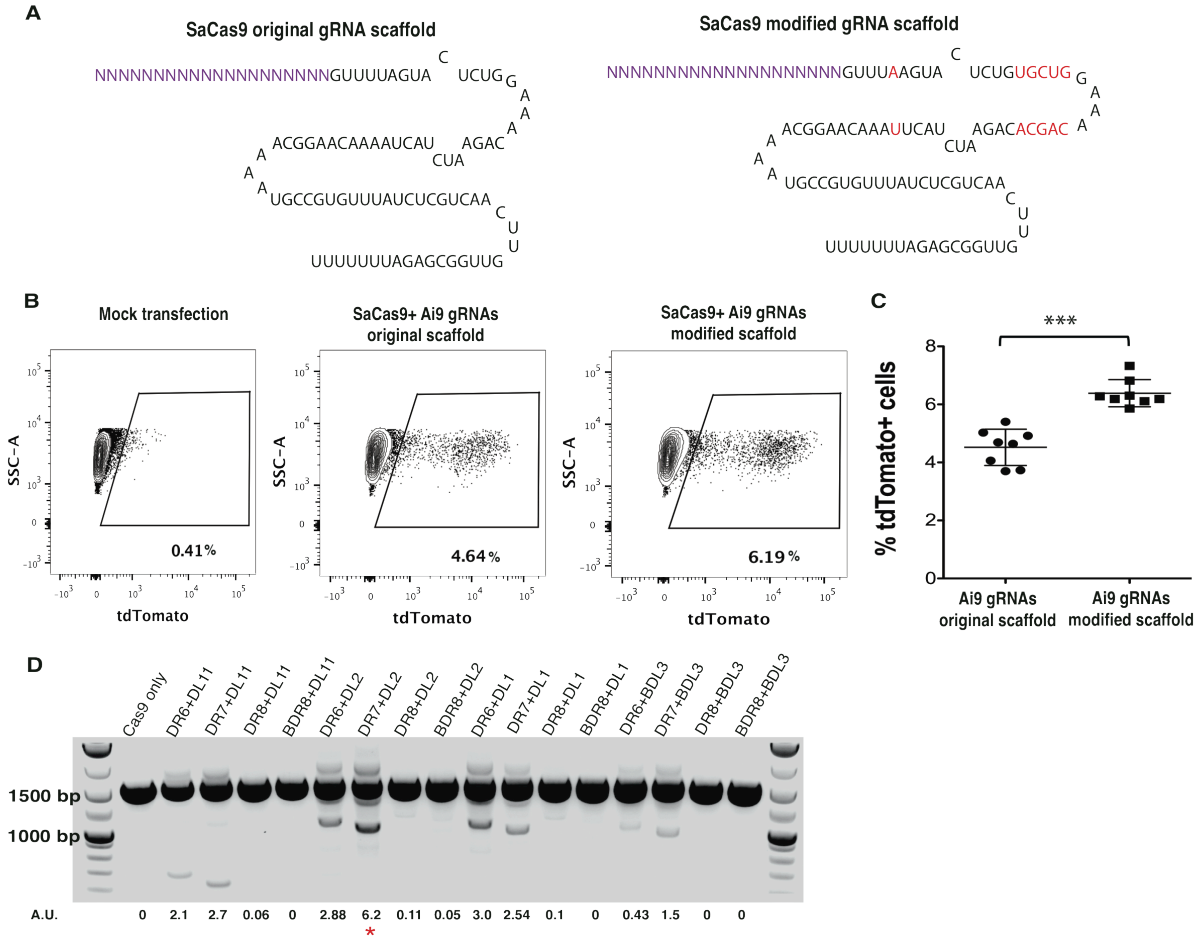

Figure 12. A modified Sa gRNA Scaffold Results in Higher Gene Targeting at the Ai9 Locus. (A) Sequence of the original (left) and modified (right) Sa gRNA scaffold. Base substitutions are noted in red font. (B) Representative FACS plots from Ai9 mouse tail tip fibroblasts transfected with no plasmids (left panel), or with plasmids encoding SaCas9 and Ai9 gRNAs with the original scaffold (middle panel) or the modified scaffold (right panel). Numbers indicate percent tdTomato+ cells. (C) Quantification of percent tdTomato+ targeted cells in transfected Ai9 tail tip fibroblasts transfected with Ai9 gRNAs with the original scaffold or the modified scaffold. Data are plotted as individual data points overlaid with mean ± SD (n=8 per condition). P-value calculated by Mann-Whitney test; ***: P<0.001. (D) Result of screening in C2C12 cells of 16 pairs of Sa *Dmd*23 gRNAs, using the modified Sa gRNA scaffold (panel A, right), by genomic PCR using primers spanning exon23. Intensity of the gene-edited band was quantified by densitometry. A.U.: Arbitrary Unit normalized to the unedited band. The combination of DR7+DL2 gRNAs (red asterisk) yielded the highest efficiency of precise DNA excision at exon23, and was therefore chosen for use in further studies.

We then produced AAV constructs encoding SaCas9 and Ai9 Sa gRNAs or *Dmd*23 Sa gRNAs in two different vectors (Figure 13A) or in a single vector (Figure 13B). Two different small promoters (173CMV [174] or elongation factor 1 short (EFS) [175]) were used to drive expression of SaCas9 in the single vector CRISPR constructs, while SaCas9 was expressed from the SV40 enhancer and CMV promoter in the dual vector system. Dual or single CRISPR AAV constructs targeting *Dmd*23 (AAV-*Dmd* CRISPR) were used to generate AAV serotype DJ and transduce myotubes derived from *mdx* primary satellite cells in order to compare the efficiency of different constructs for inducing exon 23 deletion. Quantification of exon 23-deleted transcripts in transduced *mdx* myotubes showed that dual AAV constructs induce deletion more efficiently than the single vector constructs and that EFS-driven SaCas9 is more efficient than 173CMV-driven SaCas9 (Figure 13C). Based on these data, we proceeded with the dual vector system for *in vivo Dmd* targeting.

For *in vivo* injections, dual AAVs were pseudotyped to serotype 9, which exhibits robust transduction of mouse skeletal and cardiac muscle [176]. We first injected the tibialis anterior (TA) muscles of *mdx;Ai9* mice with AAV9-SaCas9 + AAV9-Ai9 gRNAs (hereafter AAV9-Ai9 CRISPR), with the dose of 7.5E+11 vg each, or vehicle, to test the potential for *in vivo* targeting of an endogenous gene in multinucleated muscle fibers. Four weeks later, muscles were harvested for immunofluorescence to assess genome-editing events. TdTomato fluorescence was detected in muscles injected with AAV-Ai9 CRISPR, but not in muscles injected with vehicle alone (Figure 14A), providing strong evidence for effective

genome editing in multinucleated skeletal muscle fibers after *in vivo* delivery of CRISPR AAV. Similar to targeting at the Ai9 locus, co-delivery of AAV9-SaCas9 + AAV9-*Dmd*23 gRNAs (hereafter AAV9-*Dmd* CRISPR) resulted in robust and specific modification of the *Dmd* locus in skeletal muscles *in vivo*.

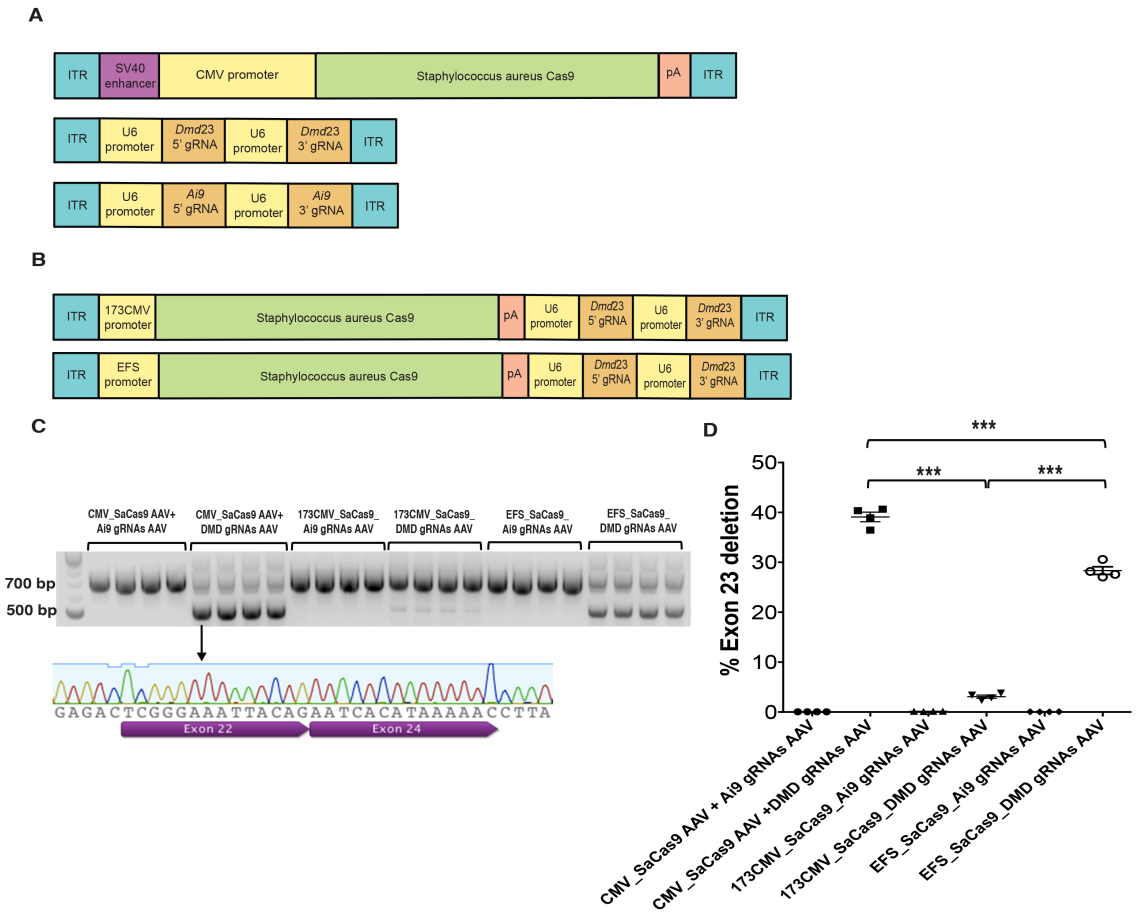

Figure 13. Dual AAV-*Dmd* CRSIPR Constructs Target the *Dmd*23 Locus More Efficiently than Single AAV-*Dmd* CRISPR Constructs *In Vitro*. (A) Schematics of AAV-SaCas9 (4728bp including ITRs) (top) AAV-*Dmd*23 gRNAs (middle) and AAV-Ai9 gRNAs (bottom) constructs (1393bp including ITRs) used for dual CRISPR AAV experiments. (B) Schematics of 173CMV_SaCas9_*Dmd*23 gRNAs (4691bp including ITRs) and EFS_SaCas9_Dmd23 gRNAs (4760bp including ITRs) single AAV constructs. (C) Detection of exon 23 deletion by RT-PCR using primers flanking DMD exon 23. RNA was isolated from *mdx;Ai9 in vitro* differentiated myotubes, transduced with AAV DJ encoding the indicated constructs. Exon 23-deleted mRNA is detected only in myotubes receiving AAV-*Dmd* CRISPR. Sequencing result from unedited and truncated mRNA, confirms absence of exon 23 in the mRNA. (D) Taqman-based quantification of exon 23-deleted transcripts in myotubes transduced with AAV DJ encoding dual or single *Dmd*23 CRISPR constructs. Plotted as individual data points overlaid with mean ± SEM, n=4. The EFS-driven SaCas9 was more efficient than the 173CMV-driven SaCas9; however, the dual AAV system induced deletion more efficiently than either of the single vector constructs.

Genomic PCR and Sanger sequencing demonstrated precise excision of exon 23 in muscles of mice injected with AAV9-*Dmd* CRISPR, but not AAV9-Ai9 CRISPR (Figure 14B). Consistent with genomic data, RT-PCR and Sanger sequencing demonstrated the presence of exon 23-deleted DMD mRNA specifically in muscles receiving AAV9-*Dmd* CRISPR (Figure 14C). Quantification of exon 23-deleted transcripts by Taqman assay indicated an average exon-deletion rate of 39% ±1.8% (Figure 14D).

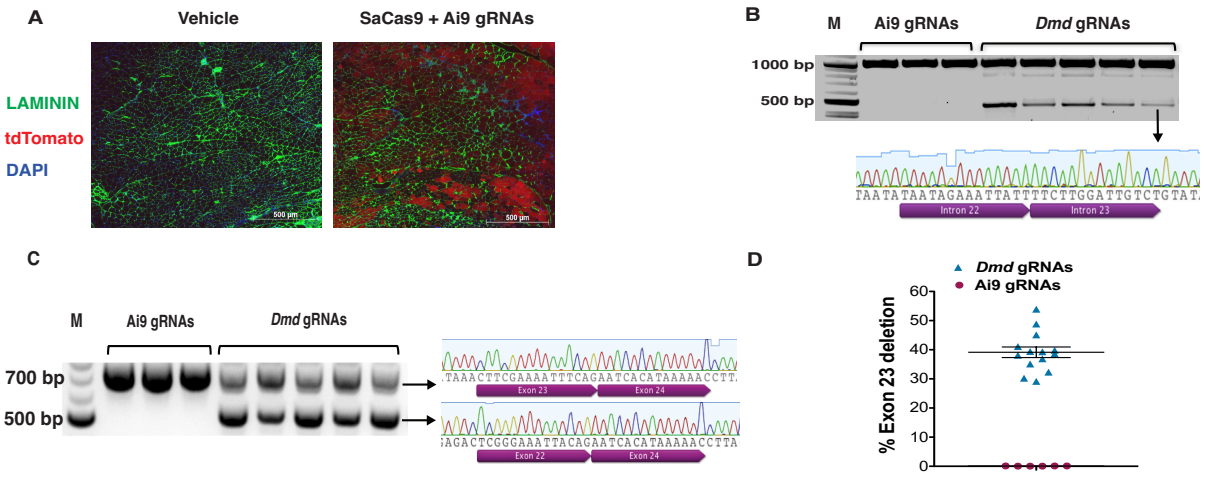

Figure 14. Local delivery of AAV-CRISPR enables *in vivo* excision of *Dmd* exon23 from the genomic DNA and results in DMD mRNA exon 23 skipping in adult dystrophic muscle. (A) Representative immunofluorescence analysis of muscles from adult *mdx;Ai9* mice injected intramuscularly with vehicle (left) or dual AAVs encoding SaCas9 and Ai9 gRNAs (right). Green: LAMININ; Red: tdTomato; Blue: DAPI (nuclei). Scale bar: 500um. (B) Detection of exon 23 excision in TA muscles from *mdx;Ai9* mice injected intramuscularly with AAV-CRISPR targeting Ai9 (left lanes) or *Dmd*23 (right lanes) by genomic PCR. M, molecular weight marker. Unedited PCR product 1012bp; exon-excised product 470bp. Sanger sequencing confirms precise excision of exon 23 from the genome. (C) Detection of exon 23 deletion in the mRNA from the AAV-CRISPR injected TA muscles by RT-PCR (left). Sequencing result from unedited and exon-deleted amplicons, confirms absence of exon 23 in the mRNA (right). (D) Quantification of exon 23-deleted transcripts in injected muscles by Taqman-based real-time PCR. Data plotted for individual mice (n=14 receiving *Dmd*23 gRNAs (blue) and n=6 receiving Ai9 gRNAs (red)) and overlaid with mean +/- SEM.

As seen for targeting of primary satellite cells in culture (Figure 11), local, *in vivo* CRISPR-mediated targeting of *Dmd* exon23 in skeletal muscle restored expression of dystrophin, which was robustly detected by Western blot (Figure 15A), capillary immunoassay (Supplementary figure 3A) and immunofluorescence (Figure 15B) at the surface of muscle fibers of *mdx;Ai9* mouse muscle for at least four weeks after AAV transduction. Other pathological hallmarks of dystrophy were also restored in AAV-*Dmd* CRISPR injected muscles, including sarcolemmal localization of the multimeric dystrophin-glycoprotein complex and neuronal nitric-oxide synthase (Supplementary figures 4 and 5). Next- generation sequencing indicated minimal activity at the predicted highest-ranking genomic off-target sites (Supplementary figure 6). Dystrophin expression was undetectable by Western blot (Figure 15A) and present only on rare revertant fibers in *mdx;Ai9* mice receiving AAV9-Ai9 CRISPR (Figure 15B; [177]).

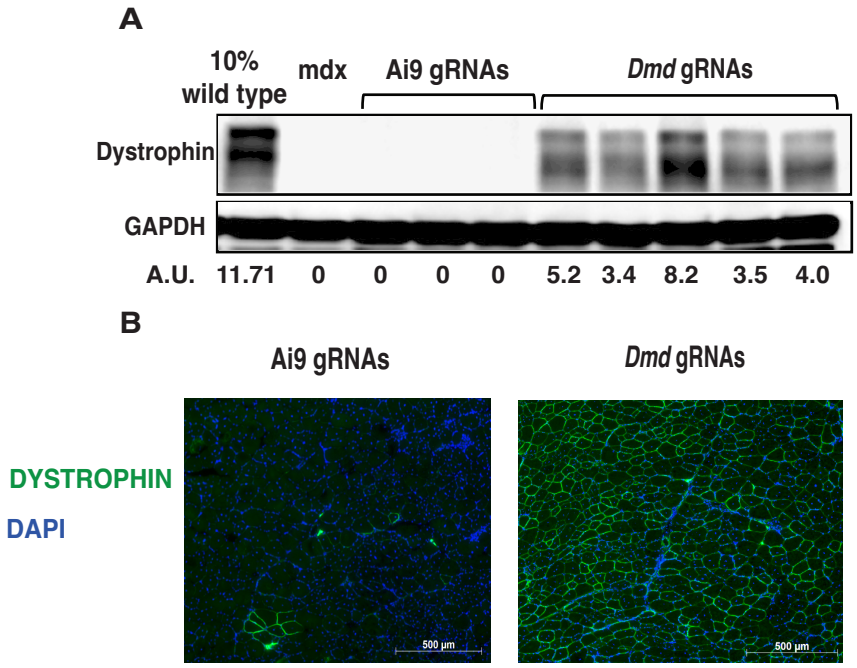

Figure 15. Local Delivery of AAV-CRISPR Restores dystrophin Expression in Adult Dystrophic Mouse Muscle. (A) Western blot for dystrophin and GAPDH (loading control) in muscles injected with AAV-CRISPR using Ai9 (left) or *Dmd*23 (right) gRNAs, quantified by densitometry at the bottom. A.U.: Arbitrary Unit normalized to GAPDH. (B) Representative images of immunofluorescence staining for dystrophin (green) in *mdx;Ai9* muscles injected with CRISPR AAVs targeting Ai9 (Left) or DMD23 (Right).

Finally, to evaluate the functional consequences of CRISPR-mediated induction of exon-deleted DMD mRNA in *mdx* muscle, we subjected a subset of mice injected intramuscularly with AAV-*Dmd*23 CRISPR to *in situ* muscle force assessment. Muscles receiving AAV9-*Dmd* CRISPR showed significantly increased specific force (Figure 16A), and attenuated force drop after eccentric damage (Figure 16B) compared to the contralateral vehicle injected muscle. In contrast, differences in specific force (Figure 16A) and force drop (Figure 16B) for AAV9-Ai9 CRISPR injected mice were not statistically significant between the

virus-injected and vehicle-injected muscles. Taken together, these data demonstrate that the CRISPR/Cas9 gene editing system is effective for *in vivo* genomic modification, including the introduction of therapeutic gene deletions, even in highly multinucleated, post-mitotic cell types such as muscle fibers. The CRISPR-Cas9 system enables irreversible modification of the targeted loci, providing enduring production of the modified gene product for as long as the targeted cell/nucleus survives.

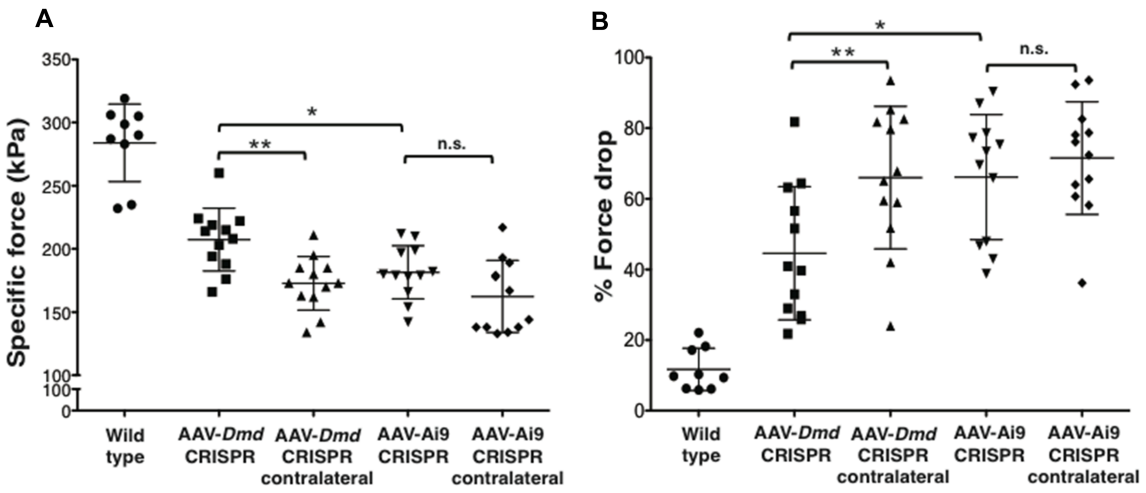

Figure 16. Local Delivery of AAV9-*Dmd* CRISPR Increases Adult Dystrophic Mouse Muscle Specific Force and Protects the Muscle Against Eccentric Damage. (A) Muscle specific force and (B) decrease in force after eccentric damage for wild type mice injected with vehicle (n=9), *mdx;Ai9* mice injected with AAV-*Dmd* CRISPR in the right TA and vehicle in the left TA (n=12), *mdx;Ai9* mice injected with AAV-Ai9 CRISPR in the right TA and vehicle in the left TA (n=12). *P<0.05, **P<0.01, n.s., not significant, One-Way ANOVA with Newman-Keuls multiple comparisons test.

Given the robust restoration of dystrophin expression obtained after intramuscular delivery of AAV-*Dmd* CRISPR in *mdx* mice, we next wished to evaluate the potential of this system for multisystemic delivery of gene editing complexes. Dual AAV-Ai9 CRISPR vectors (1.5E+12 vg each) were co-injected

intraperitoneally into *mdx;Ai9* mice at postnatal day 3 (P3), and 3 weeks later, muscles were harvested and analyzed for expression of tdTomato. Widespread tdTomato expression was detected in all the cardiac and skeletal muscles analyzed (Figure 17A).

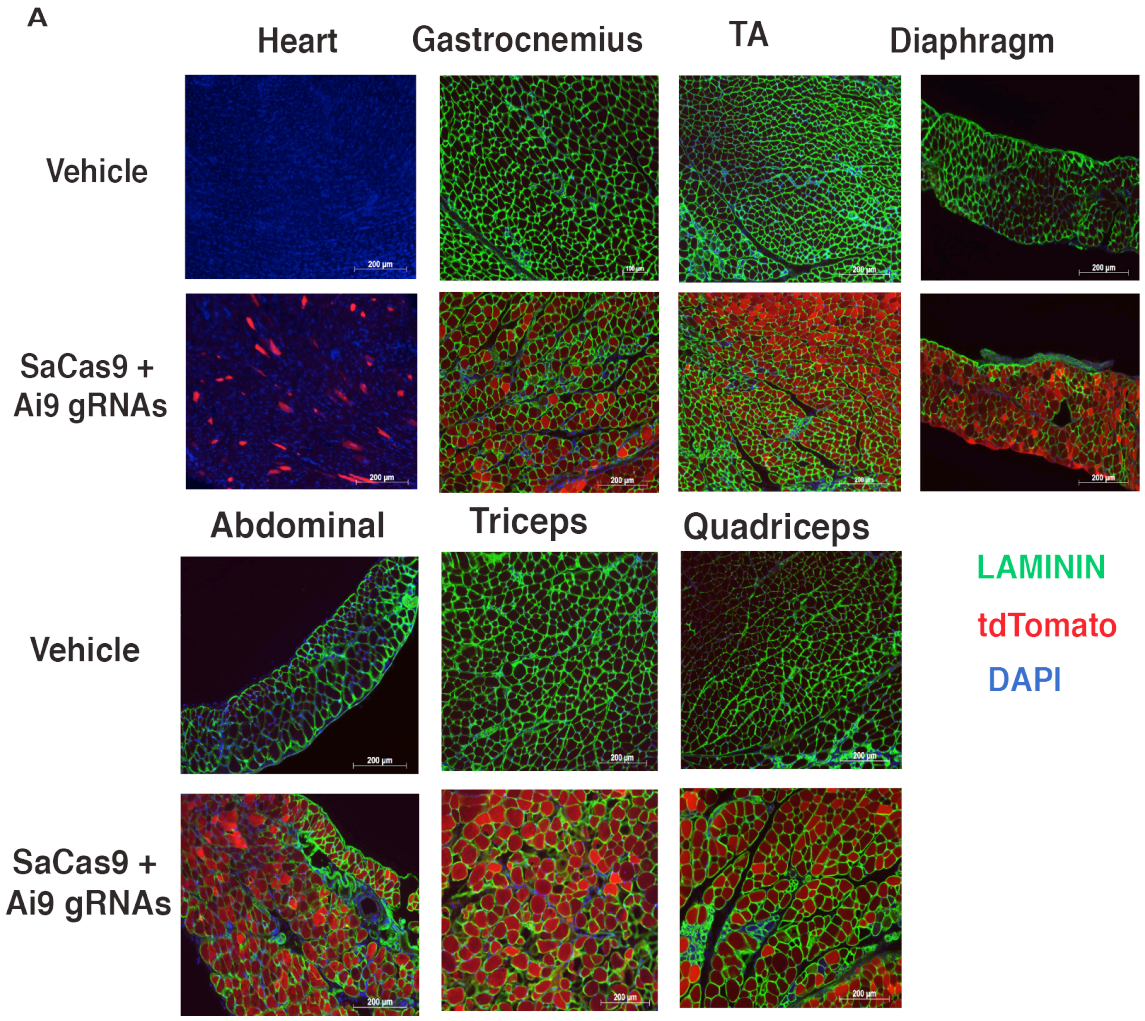

Figure 17. Systemic Delivery of AAV-Ai9 CRISPR in Dystrophic Mice Targets the STOP Cassette in the Ai9 Locus and Results in tdTomato Expression in Cardiac and Skeletal Muscles. (A) Representative immunofluorescence images of muscles from 3 wk. old *mdx;Ai9* mice systemically injected on P3 with vehicle or dual AAVs encoding SaCas9 and Ai9 gRNAs. Green: LAMININ; Red: tdTomato; Blue: DAPI (nuclei). Scale bar: 200um.

We also injected 7 *mdx;Ai9* mice with AAV9-*Dmd* CRISPR systemically. RT-PCR and Sanger sequencing demonstrated detectable exon 23-deleted transcripts in multiple skeletal muscles and cardiac muscle of these mice. In contrast, no loss of exon 23 was apparent in dystrophin mRNA in animals receiving Ai9 gRNAs instead (Figure 18A). Quantification of exon 23-deleted transcripts as a percentage of total DMD mRNA confirmed widespread targeting in animals receiving systemic AAV9-*Dmd* CRISPR, with levels varying from 3-18% in different muscle groups (Figure 18B).

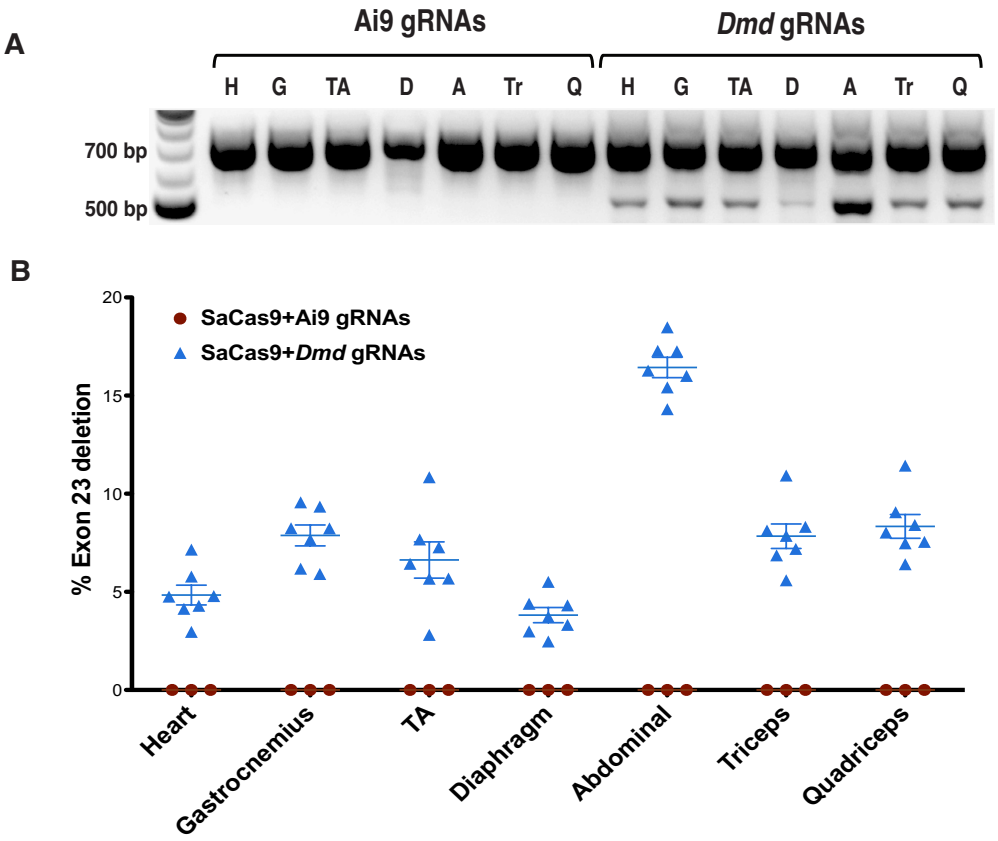

Figure 18. Systemic Delivery of AAV9-*Dmd* CRISPR in *mdx* Mice Results in DMD mRNA Exon 23 Skipping in Cardiac and Skeletal Muscles. (A) Exon 23-deleted transcripts are detected in muscles of *mdx;Ai9* mice injected with CRISPR AAVs targeting *Dmd*23 (Right), but not Ai9 (Left) by RT-PCR. (B) Quantification of exon 23-deleted transcripts in muscles by Taqman-based real time PCR. Data plotted for individual mice (n=7 receiving *Dmd*23 gRNAs (blue) and n=3 receiving Ai9 gRNAs (red)) and overlaid with mean +/- SEM.

Finally, Western blot (Figure 19A), immunofluorescence (Figure 19B) and and capillary immunoassay analysis (Supplementary figure 3B) of dystrophin expression, which is normally lacking in mdx mice and absent from cardiac and skeletal muscles of mdx;Ai9 mice receiving AAV9-Ai9 CRISPR, showed restoration of dystrophin in mice receiving AAV9-*Dmd* CRISPR in all muscle groups examined. Levels of dystrophin in AAV-*Dmd* CRISPR treated mice varied among individual mice and muscle groups, with amounts as high as 5% and as low as <0.1% of wild-type.

Figure 19. Systemic Delivery of AAV9-*Dmd* CRISPR in *mdx* Mice Results in DYSTROPHIN Expression in Cardiac and Skeletal Muscles. (A) Detection of DYSTROPHIN and GAPDH (loading control) by Western blot in the indicated muscles of *mdx;Ai9* mice receiving systemic AAV-CRISPR. Right lanes correspond to muscles from 7 different mice injected systemically with AAV-*Dmd* CRISPR. Signal intensity is quantified by densitometry at the bottom. A.U.: Arbitrary Unit normalized to GAPDH. (B) Representative images of immunofluorescence staining for DYSTROPHIN (green) in *mdx;Ai9* muscles injected with CRISPR AAVs targeting Ai9 or *Dmd*23. Scale bar: 200 um.

Figure 19 continued

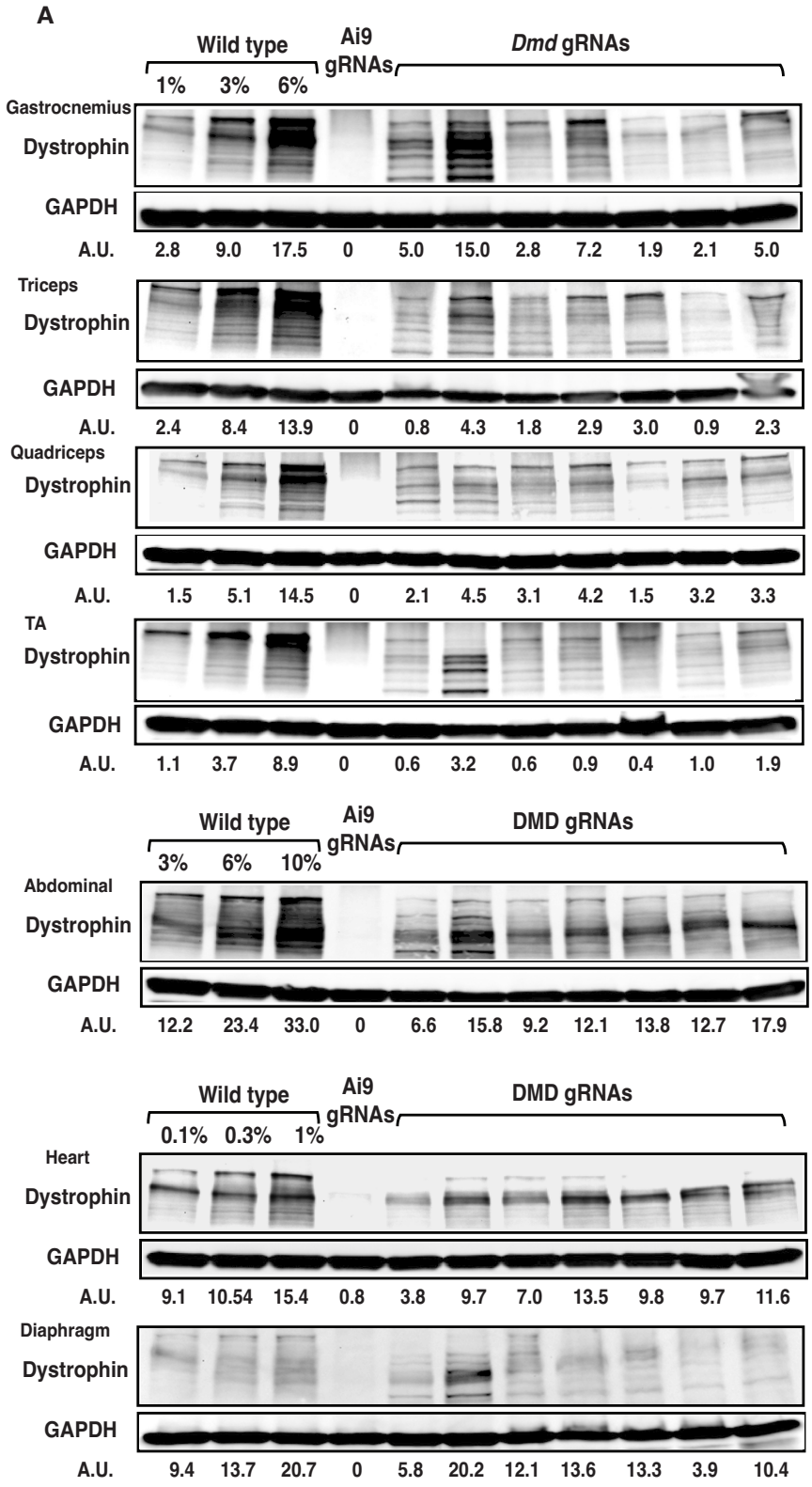

Figure 19 continued

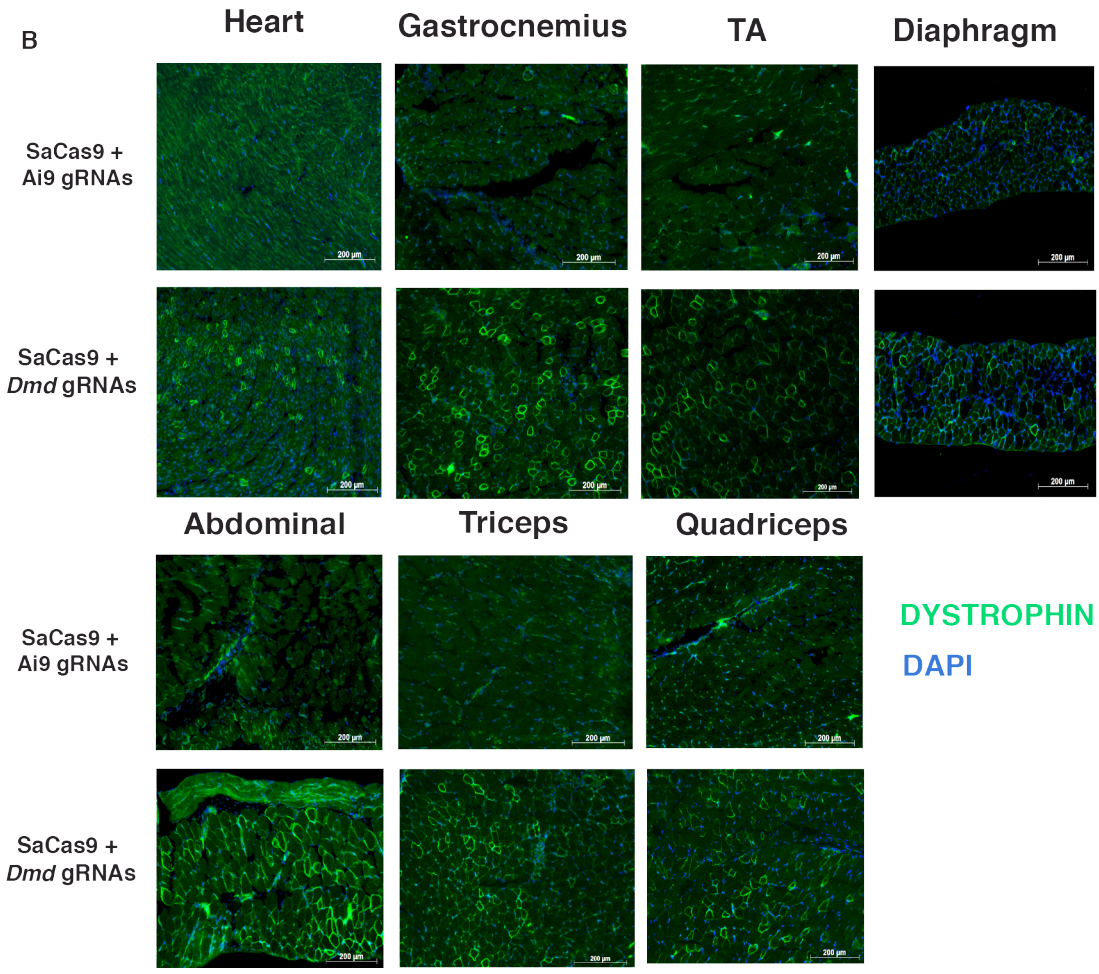

Similar systemic dissemination of AAV and excision of exon23 in multiple organs were seen in two adult mice injected intravenously with AAV-*Dmd* CRISPR at 6 weeks of age (Supplementary figure 7).

Local and systemic injection of the single vector AAV-*Dmd* CRISPR, in which SaCas9 is expressed under the control of the EFS promoter, yielded significantly lower exon deletion efficiencies compared to the dual AAV-*Dmd* CRISPR system (Figures 20A,B). Together, these data provide exciting support in DMD model mice for recovery of dystrophin expression in dystrophic muscle through systemic gene editing of the *Dmd* locus.

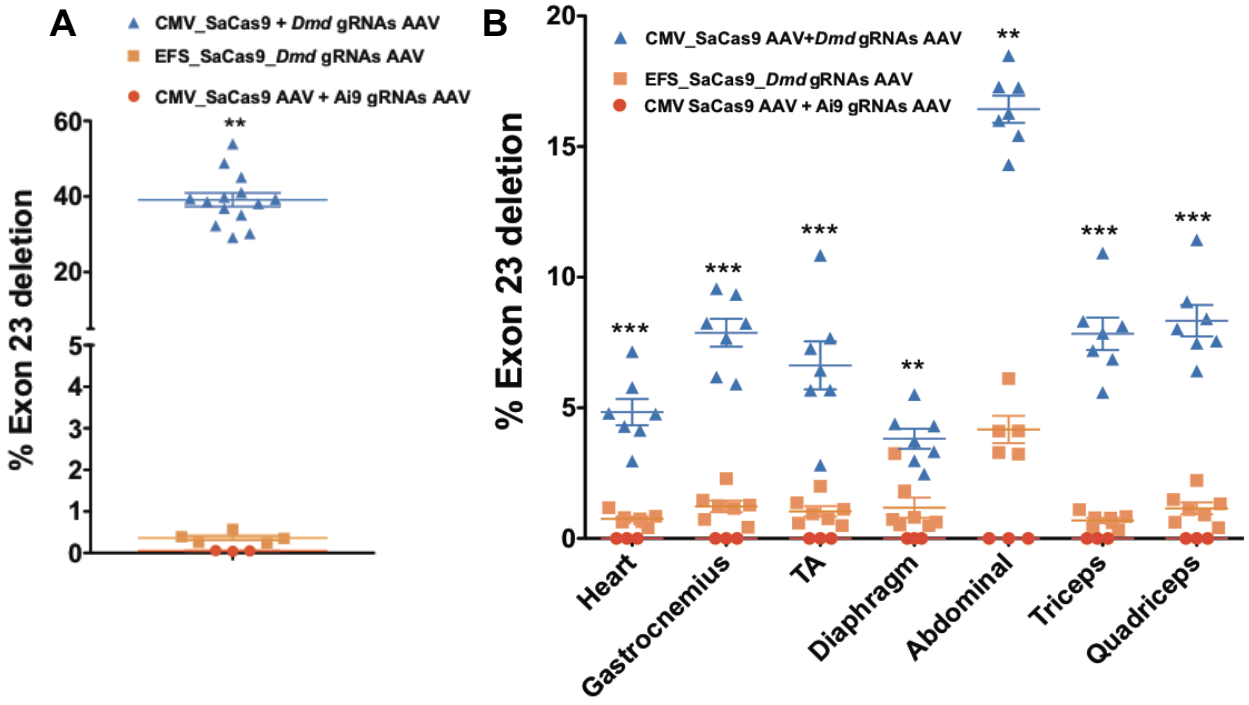

Figure 20. Dual AAV-*Dmd* CRSIPR Constructs Target the *Dmd*23 Locus More Efficiently than Single AAV-*Dmd* CRISPR Constructs *In Vivo*. (A) Taqman-based quantification of exon 23-deleted transcripts in muscles injected locally with dual AAVs encoding SaCas9 + *Dmd*23 gRNAs (7.5E+11 vg each) or a single AAV encoding EFS_SaCas9_*Dmd*23 gRNAs (1.5E+12 vg). Data points for dual AAV injected muscles are reproduced from Fig. 2D for comparison. *: P<0.05. Overlay indicates mean +/- SEM. (B) Taqman-based quantification of exon 23-deleted transcripts in different muscles of mice systemically injected with dual AAVs encoding SaCas9 + *Dmd*23 gRNAs (1.5E+12 vg each) or a single AAV encoding EFS_SaCas9_*Dmd*23 gRNAs (3E+12 vg). Data points for dual AAV injected muscles are reproduced from Fig. 3C for comparison. **: P<0.01 and ***: P<0.001 by Mann-Whitney test for comparison of CMV_SaCas9 AAV + *Dmd* gRNAs (blue triangles) to EFS_SaCas9_Dmd gRNAs AAV (orange squares). N=7 for SaCas9 + *Dmd*23 gRNAs injected muscles, n=5 (abdominal muscle) or 7 (all other muscles) for EFS_SaCas9_*Dmd*23 gRNAs injected muscles and n=3 for SaCas9 + Ai9 gRNAs. Data shown for individual muscles and overlaid with mean ± SEM.

To evaluate the potential for AAV9-CRISPR gene editing in satellite cells *in vivo,* we used our sensitive Ai9 fluorescent reporter system. To facilitate the discrimination of satellite cells in these studies, we crossed the *mdx;Ai9* mice with previously described Pax7-ZsGreen animals, in which satellite cells are specifically marked by green fluorescence [178]. *Pax7-ZsGreen$^{+/-}$;Mdx;Ai9* mice were injected intramuscularly or systemically with AAV9 encoding Cre recombinase or Ai9 CRISPR components, and skeletal muscles were harvested 2 weeks later for isolation of ZsGreen+ muscle satellite cells by FACS (Figure 21A). Flow cytometric analysis demonstrated that about 36% (+/- 1.9%) of Pax7-ZsGreen+ cells expressed tdTomato when isolated from muscles injected locally with AAV9-Cre (6E+11 vg), suggesting significant transduction by AAV of endogenous satellite cells in these mice (Figures 21B,C).

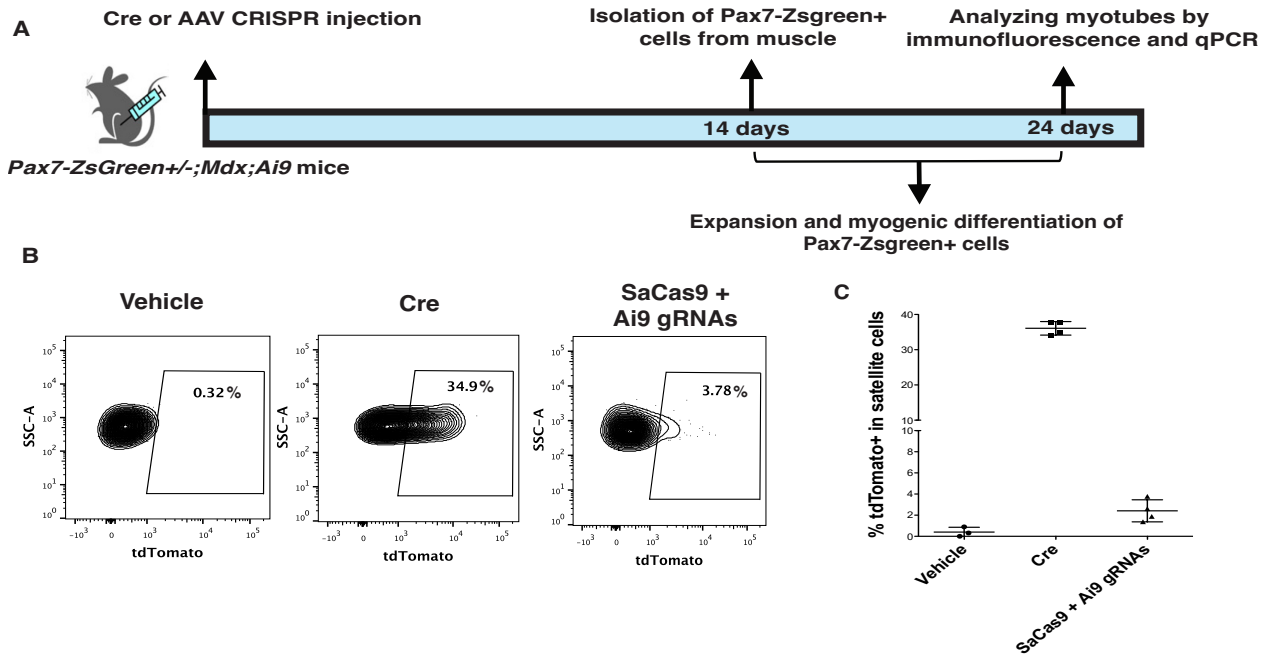

Figure 21. Satellite Cells in Dystrophic Muscles are Transduced and Targeted with AAV CRISPR After Intramuscular Injection. (A) Experimental design. *Pax7-ZsGreen*$^{+/-}$*;Mdx;Ai9* mice were injected intramuscularly or systemically with Cre or CRISPR AAVs targeting Ai9 or *Dmd*23. Two weeks later, Pax7-ZsGreen+ satellite cells were isolated by FACS, expanded in culture, differentiated to myotubes and analyzed for gene editing. (B) Representative FACS plots of tdTomato expression among ZsGreen+ satellite cells isolated from mice injected intramuscularly with vehicle (left), AAV9-Cre (middle) or AAV9-Ai9 CRISPR (right). Numbers indicate percent tdTomato+ cells for each plot. (C) Quantification of tdTomato+ cells among Pax7-ZsGreen+ satellite cells isolated from mice injected intramuscularly with vehicle, AAV9-Cre or AAV9-Ai9 CRISPR. Individual data points overlaid with mean +/- SD; n=3 mice for vehicle and n=4 mice for Cre and Ai9 CRISPR.

Myogenic differentiation of ZsGreen+ satellite cells isolated from mice receiving intramuscular AAV9-Cre produced tdTomato+ myotubes, demonstrating that permanent recombination at the Ai9 locus was induced in these muscle progenitors by AAV9-Cre (Figure 22A). TdTomato expression was also detected in Pax7-ZsGreen+ satellite cells harvested from mice receiving AAV9-Ai9 CRISPR intramuscularly (Figures 21B,C). These CRISPR-targeted satellite cells also differentiated to produce tdTomato+ myotubes (Figure 22A), again consistent with

stable modification of the Ai9 allele following *in vivo* exposure to Ai9-CRISPR. The lower efficiency of recombination in satellite cells seen with the CRISPR, as opposed to Cre system, likely reflects the need for co-transduction by two AAVs in the CRISPR system, a compromise necessitated by current payload limits of AAV (see Figure 13 and Figure 20).

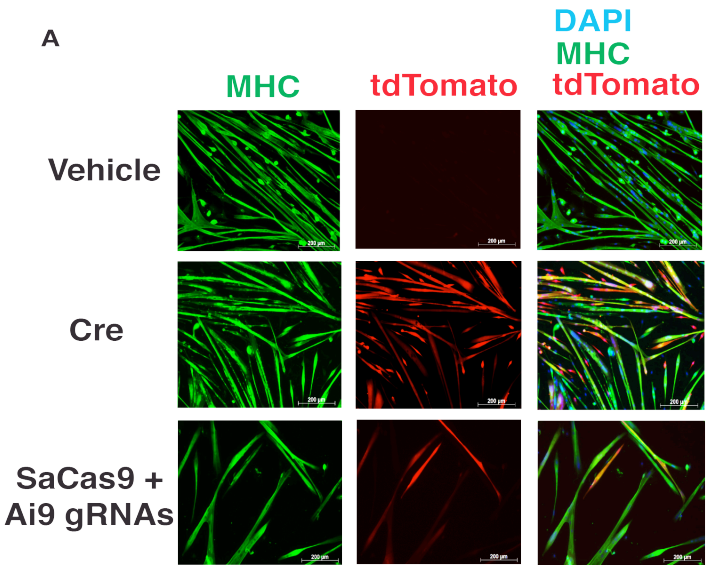

Figure 22. Transduced Satellite Cells Isolated from Muscles Locally Injected with AAV Differentiate to Myotubes in Culture. (A) Representative immunofluorescence images of myotubes differentiated from FACSorted Pax7-ZsGreen+ cells from vehicle (top), AAV9-Cre (middle) and AAV9-Ai9 CRISPR (bottom) injected muscles. Green: Myosin heavy chain (MHC); Red: tdTomato. Blue: DAPI (nuclei) Scale bar: 200 um.

TdTomato expression was also detected in Pax7-ZsGreen+ satellite cells after systemic injection of AAV9-Cre and AAV9-Ai9 CRISPR in dystrophic mice (Figures 23A and 23B). Myogenic differentiation of these satellite cells resulted in formation of tdTomato+ myotubes as well (Figure 23C).

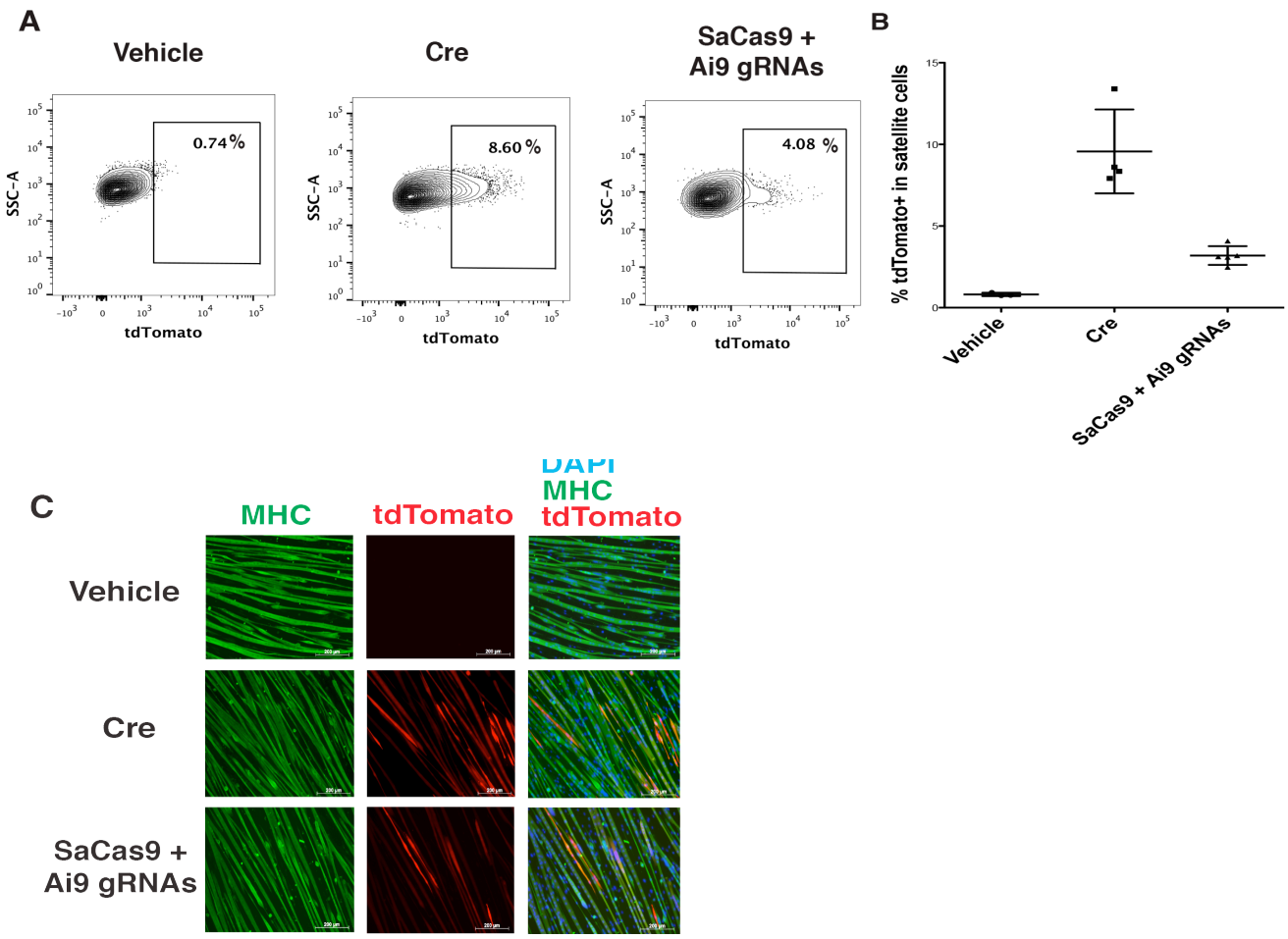

Figure 23. Satellite Cells in Dystrophic Muscles are Transduced and Targeted with AAV CRISPR After Systemic Injection. (A) Representative FACS plots of tdTomato expression among ZsGreen+ satellite cells isolated from mice injected systemically with vehicle (left), AAV9-Cre (middle) or AAV9-Ai9 CRISPR (right). Numbers indicate percent tdTomato+ cells for each plot. (B) Quantification of tdTomato+ cells among Pax7-ZsGreen+ satellite cells isolated from mice injected systemically with vehicle, AAV9-Cre or AAV9-Ai9 CRISPR. Individual data points overlaid with mean +/- SD; n=3 mice for vehicle and n=4 mice for Cre and Ai9 CRISPR.

TdTomato^{+} gene–edited satellite cells also engrafted recipient *mdx* muscle and contributed to in vivo muscle regeneration after transplantation (Figure 24).

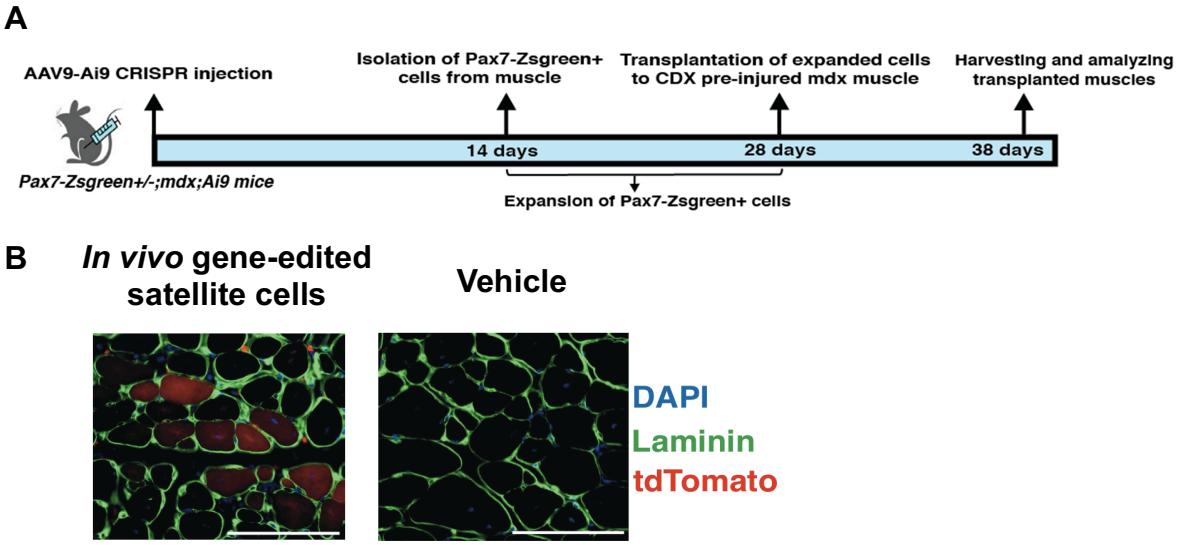

Figure 24. In vivo gene edited satellite cells engraft dystrophic muscle. (A) Experimental design. (B) Detection of tdTomato+ donor-derived myofibers (left image) demonstrates the capacity of gene-edited satellite cells to contribute to muscle regenerative responses *in vivo.* TdTomato+ myofibers were not detected in muscles injected with vehicle only (right image). Green: LAMININ; Red: tdTomato; Blue: DAPI (nuclei). Scale bar: 100 μm.

In any event, these data clearly demonstrate the ability of AAV9 to transduce and genomically modify endogenous satellite cells, raising the possibility that programming of CRISPR with gRNAs targeting *Dmd* could result in directed gene editing in this critical precursor cell population in dystrophic muscles. To test this, we isolated Pax7-ZsGreen+ satellite cells from *Pax7-ZsGreen*$^{+/-}$*;Mdx;Ai9* mice injected intramuscularly or systemically with AAV9-*Dmd* CRISPR or AAV9-Ai9 CRISPR gRNAs and expanded and differentiated these cells *in vitro*. RT-PCR analysis of mRNA isolated from satellite cell-derived myotubes demonstrated the presence of a truncated transcript of the expected size for gene-edited *Dmd* in many of the AAV-*Dmd* CRISPR injected muscles, but not AAV-Ai9 CRISPR injected muscles. In addition, sequencing of this shorter transcript confirmed site directed excision of exon 23 and production of an exon-deleted

mRNA in which exon 22 is fused to exon 24 (Figures 25A and 25C). Quantification of exon 23-deleted transcripts in the differentiated myotubes by Taqman-based real time PCR revealed variable efficiencies (Figures 25B and 25D), likely reflecting the inability to isolate the total pool of satellite cells from any single muscle and the survival and expansion of only a subset of these cells in culture. Regardless, these data provide clear evidence for *in situ* gene editing in muscle stem cells as well as terminally differentiated multinucleated fibers.

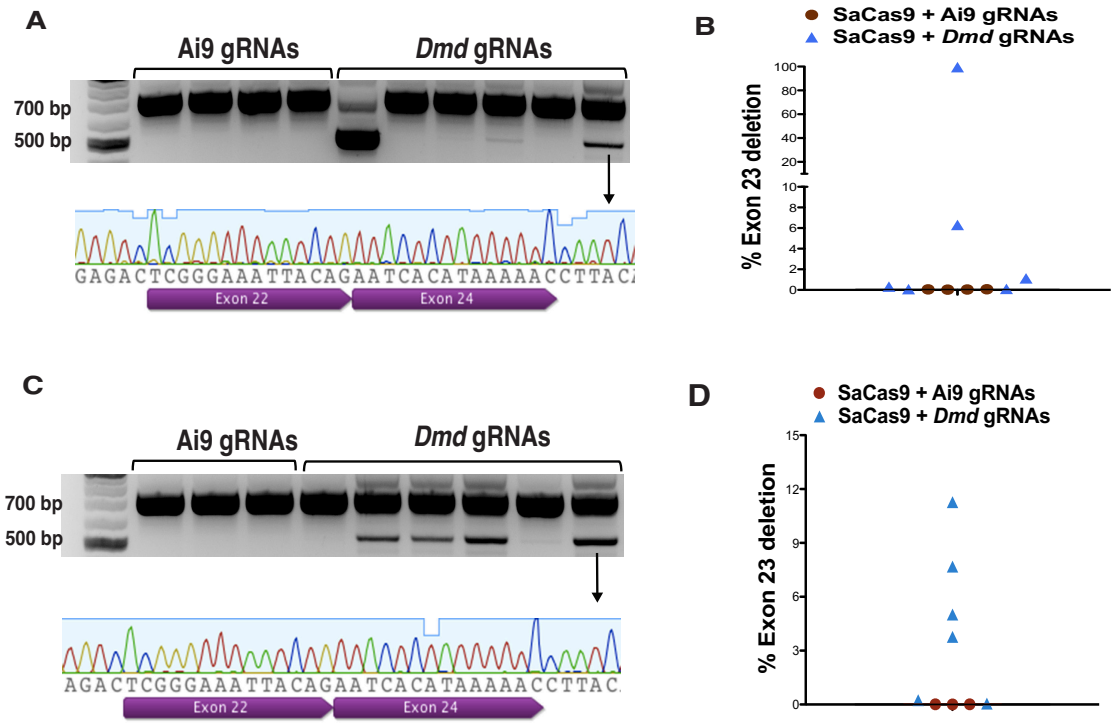

Figure 25. AAV-*Dmd* CRISPR Transduces Dystrophic Satellite Cells and Targets *Dmd* Exon 23 After Local and Systemic Injections. (A) RT-PCR with primers flanking exon 23 indicates expression of exon 23-deleted DMD mRNA in myotubes differentiated *in vitro* from satellite cells isolated from adult TA muscles receiving AAV-*Dmd* CRISPR (right lanes), but not those from muscles injected with AAV-Ai9 CRISPR (left lanes). Sanger sequencing result confirms absence of exon 23 in the mRNA. (B) Quantification of exon 23-deleted transcripts in myotubes derived from satellite cells isolated from intramuscularly injected muscles by Taqman assay. (C) RT-PCR and Sanger sequencing confirm expression of exon 23-deleted mRNA in myotubes derived from satellite cells isolated from mice injected systemically with AAV-*Dmd* CRISPR. (D) Quantification of exon 23-deleted transcrips in myotubes derived from satellite cells isolated from systemically injected mice by Taqman assay.

Genomic PCR and amplicon sequencing confirmed targeted excision at the *Dmd* locus in satellite cell-derived myotubes (Figure 26A), and capillary immunoassay analysis revealed restored dystrophin expression (Figure 26B).

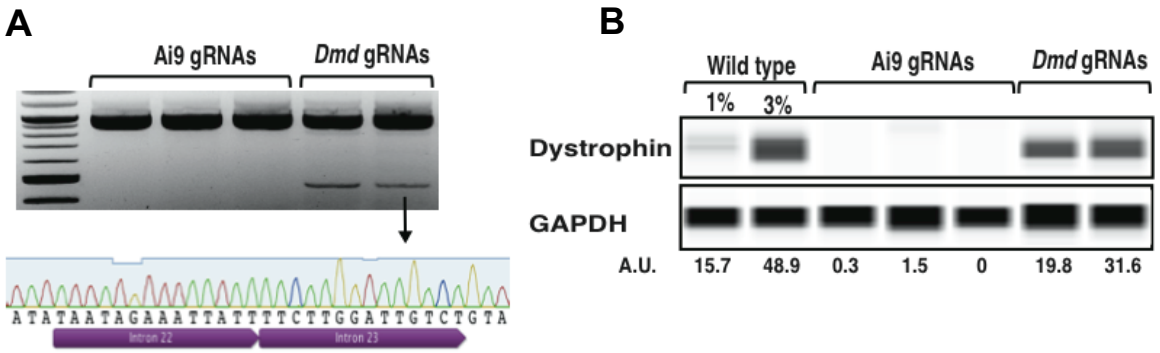

Figure 26. Excision of *Dmd* exon 23 and DYSTROPHIN restoration in satellite cell-derived myotubes isolated from mice systemically injected with AAV-*Dmd* CRSIPR. A) Genomic PCR and sequencing confirming targeted excision of exon23 and generation of a hybrid intron 22/23 in genomic DNA of myotubes derived from satellite cells isolated from *Pax7-ZsGreen*$^{+/-}$*;mdx;Ai9* mice injected intraperitoneally with AAV-CRISPR targeting *Dmd*23. A representative trace is shown from the band indicated by the arrow. (B) Capillary immunoassay analysis (Simple Western, WES instrument, ProteinSimple) indicating restored DYSTROPHIN expression in myotubes derived from satellite cells harvested from mice receiving AAV-*Dmd* CRISPR, but not mice receiving AAV-Ai9 CRISPR. For this experiment, AAV-CRISPR was provided systemically, by intraperitoneal injection into P3 neonatal mice, and satellite cells were isolated from TA, gastrocnemius, triceps, quadriceps and abdominal muscles. Data obtained from ProteinSimple analysis (Wes) are presented as virtual Western blots for DYSTROPHIN and GAPDH, which serves as a loading control. A.U.: Arbitrary Unit normalized to GAPDH, determined by analysis of chromatograms from each sample.

Discussion

These results provide proof-of-concept evidence supporting the efficacy of *in vivo* genome editing to correct frame-disrupting mutations in DMD in a relevant dystrophic mouse model. We show that programmable CRISPR complexes can be delivered directly to terminally differentiated skeletal muscle fibers and

cardiomyocytes, as well as muscle satellite cells, where they mediate targeted gene deletion, restore dystrophin expression and partially recover functional deficiencies of dystrophic muscle. As prior studies in mice and humans indicate that dystrophin levels as low as 3-15% of wild-type are sufficient to ameliorate pathologic symptoms in the heart and skeletal muscle [179-182], and levels as low as 30% can suppress the dystrophic phenotype altogether [183], the levels of dystrophin restoration achieved here by the dual AAV-*Dmd* CRISPR system clearly encourage further evaluation of this system as a new candidate modality for the treatment of DMD.

The capacity to target DMD mutations in endogenous satellite cells, in addition to dystrophic myofibers, ensures the capacity of the muscle to repair injured fibers with gene-corrected muscle precursors. Although a prior study suggested that AAVs do not transduce endogenous satellite cells [184], this result likely stems from use of a relatively less sensitive, transient GFP or mCherry expression system for marking transduced cells, in which dilution of the AAV genome during cell division would result in extinction of fluorescence. In contrast, because the AAV-CRISPR system irreversibly marks transduced cells and their progeny, these cells remain distinguishable even after loss of the viral genome, allowing sensitive detection of even very rare gene-modified cells *in vivo*.

In comparison to AONs, our AAV-CRISPR system has several attractive features. While both systems are amenable for systemic delivery, AAV-CRISPR provides irreversible genome modification with one-time administration of the therapeutic vectors and supports restoration of dystrophin in both the skeletal

muscle and heart, which has been notoriously challenging to target with AONs [185]. Low immunogenicity of AAV makes it a preferable vector for systemic delivery of CRSIPR compared to other cytotoxic and immunogenic vectors such as adenovirus [186,187]. Still, the AAV-CRISPR system will require further optimization. In particular, levels of gene correction in muscle satellite cells are currently rather low, suggesting a need to investigate additional AAV serotypes to identify those with optimal tropism for muscle satellite cells. In this regard, it may be of particular interest to engineer novel AAV serotypes by directed evolution and select for the serotypes with high tropism for satellite cells *in vivo* [166]. Further studies are also needed to evaluate the long-term safety of the *in vivo* AAV-CRISPR approach, although the relative improvements seen in muscle function argues against any severe, acute toxicity in our experiments. The off-target activity of CRISPR/Cas9 is highly dependent on the gRNA spacer sequence. On-targets, as well as potential off-targets, from this study are not conserved between mouse and human genomes, and so assessment of off-target activity with gRNAs targeting human *DMD* is required for pre-clinical studies. In this regard, the muscle could be considered a somewhat privileged target for *in vivo* genome modification, as its multi-nucleation provides a "buffer" against potential toxic events; however, the long-term safety of gene editing in muscle satellite cells will require further investigation. Furthermore, development of new Cas9 variants with lower off-target activity [188,189] is a promising advancement towards increasing the specificity of gene editing.

With regard to the human disease, more than 60% of DMD patients could benefit from skipping one or more exons in the exon 45-55 region [168], and skipping exon 51 alone can be therapeutic for DMD deletions of exon(s) 50, 45-50, 48-50, 49-50, 52 and 52-63, which together constitute 15% of DMD mutations. Skipping of exon 45 can potentially cover another 13% of patients [190]. Future identification of Sa gRNAs optimized for maximal on-target and minimal off-target activity at broadly relevant DMD mutations (including mutational 'hotspots' in the exon 45-55 region) could enable rapid translation of the results from our studies for the many DMD patients who could potentially benefit from this approach. *In vivo* gene editing holds promise to overcome limitations of conventional gene therapy approaches not only for DMD, but also for a wide range of other genetic muscle diseases.

Chapter 4.

Future directions and considerations for clinical translation

Future directions

In this thesis, I identified a small molecule (forskolin) that supports *in vitro* expansion of both healthy and dystrophic mouse muscle stem cells and provided proof of concept evidence for *in vitro* expansion, gene correction and transplantation of dystrophic satellite cells. However, one of the major limitations of current approaches to satellite cell expansion is that they activate satellite cells, downregulate Pax7 expression in these cells [20], and impair their subsequent potential to replenish the satellite cell pool after transplantation [130]. Prior studies indicate that higher expression of Pax7, a satellite cell specific transcription factor [191], marks more quiescent daughter cells during asymmetric division of satellite cells. Pax7-high satellite cells also exhibit slower cycling kinetics and can generate Pax7-high and -low populations after transplant, indicating their self-renewal potential [25] Yet, despite its critical influence on satellite cell function, precisely how Pax7 expression is regulated in satellite cells is not well understood. Identification of genes and pathways that can upregulate Pax7 expression in activated satellite cells in future studies, will pave the way to establishing culture conditions that support expansion of these cells while maintaining their ability to replenish the satellite cell pool after transplantation. Genome-scale gene activation with CRISPR has recently been reported as a powerful tool for identifying genes regulating particular cellular processes, such as BRAF inhibitor resistance in melanoma cells [192] or cell growth in K562 cells [193]. Using a Pax7-reporter cell line, genome-wide CRISPR-mediated gene activation can be used to identify targets that can be manipulated to upregulate Pax7 expression and revert ex vivo

expanded, activated satellite cells into highly functional muscle stem cells with self-renewal capacity.

These studies also provide evidence for AAV-mediated transduction and correction of *Dmd* in dystrophic muscle stem cells. Correction of *Dmd* in dystrophic satellite cells provides a reservoir of myogenic progenitors capable of producing dystrophin-expressing muscle fibers, and represents a potential advantage compared to conventional transgene-mediated gene therapy, Transgenes delivered by AAV will be diluted during expansion of satellite cells as myoblasts, but CRISPR- mediated gene editing results in irreversible correction of *Dmd* in satellite cells and their progeny. This will be even more advantageous if the gene-corrected cells are selected for, or enriched, in dystrophic tissue. Expansion of clusters of naturally occurring dystrophin-expressing revertant fibers in *mdx* muscle, which depends on muscle regeneration, suggests a selective advantage for dystrophin-expressing satellite cells in dystrophic muscle [194]. It would be interesting to test if gene-corrected satellite cells in dystrophic muscles are selectively enriched after induced muscle degeneration and regeneration. It will also be informative to examine the hypothesis that permanent gene correction of dystrophic satellite cells (and their progeny) prevents the loss of dystrophin-expressing nuclei in muscle fibers seen with traditional gene therapy approaches [165].

Furthermore, levels of gene targeting in muscle satellite cells are currently rather low, suggesting a need to investigate additional AAV serotypes to identify those with optimal tropism for muscle satellite cells. Directed evolution and *in vivo*

selection has been recently used to engineer novel AAV capsids with high tropism for tissues that are difficult to transduce with naturally occurring AAVs, such as human hepatocytes in a xenograft liver model [195] and the outer retina after injection into the eye's vitreous humor [196]. Therefore, an exciting next step would be to use a directed evolution and *in vivo* selection strategy for generating novel AAV serotypes with high tropism for satellite cells.

Consideration for clinical translation

Engineering efficient single vector CRISPR AAV constructs

Our results demonstrate that with the current state of the art gene editing technology, there is need for the use of dual AAV vectors to deliver the CRISPR components *in vivo*. The need for dual AAV administration is an obstacle for clinical translation of the technology that can be overcome by identification and engineering smaller versions of the Cas9 protein, which provide the ability to fit all the CRISPR components in one AAV vector without compromising Cas9 expression levels or gene editing efficiency. This is also specifically important for improving gene targeting in multinucleated muscle fibers, since gRNAs used for CRISPR gene editing experiments in eukaryotic systems are expressed under the control of the U6 promoter and are transcribed by RNA polymerase III. RNA polymerase III transcripts don't leave the nucleus after the transcription [197], therefore functional CRISPR complex is only formed in muscle fiber nuclei that received the gRNA coding sequence, and therefore, incorporating the Cas9 coding sequence in the same vector as the gRNA can potentially increase the probability

of gene editing in nuclei, receiving that vector.

Minimizing off target activity of Cas9 nuclease

CRISPR/Cas9 can generate unwanted mutations at off-target genomic sites that are similar to the on-target sequence [198,199]. These off-target effects can be the source of potential complications for therapeutic uses of the technology. Recent advances in the field of genome engineering have led to development of different strategies to reduce genome-wide off-target mutations of the SpCas9. These strategies include using paired SpCas9 nickases [200], reducing the length of the guide sequence in gRNAs [201] and engineering SpCas9 variants with amino acid substitutions in the DNA binding domains that show lower off-target rates [188,189]. However, there is still need for improving the specificity of SpCas9 and its smaller orthologs (e.g. SaCas9) before making further steps towards clinical application of CRISPR/Cas9. This issue is particularly important in terms of targeting muscle stem cells, which have substantial proliferative capacity. The risk of generating undesired mutations at proto-oncogene loci by CRISPR in these cells needs be to rigorously analyzed.

Analyzing potential immune responses against CRISPR components

Exogenous expression of the bacterial SpCas9 protein in mouse liver has been reported to induce humoral immune response in the animals [186], which highlights the need for more carful analysis of the potential immune response complications as a result of Cas9 expression in mammalian tissues. Identifying immunodominant epitopes of the protein might help to engineer Cas9 variants with

lower immunogenicity or to identify strategies for inducing immunological tolerance to Cas9. Furthermore, the use of delivery methods that provide the possibility for transient expression of Cas9 such as modified RNA [202] or ribonucleoprotein (RNP)-mediated [203] delivery can avoid long-term expression of the protein and induction of a chronic immune response.

Assessing the efficacy of *in vivo* gene editing in dystrophic dog and human muscle xenograft models

This study and two studies from other groups [204,205] have provided the proof of concept evidence for restoring dystrophin expression in the *mdx* mouse model by AAV-mediated *in vivo* gene editing. However the efficacy and safety of this approach in other animal models is yet to be studied. Canine models of DMD, including the golden retriever muscular dystrophy (GRMD), have more severe dystrophic phenotypes than the mouse models, which is more similar to the DMD phenotypes in patients [206]. Therefore, preclinical studies in the dog models might be a better indicative of the *in vivo* gene editing efficacy. Recently developed human muscle xenograft model also provides a unique opportunity for studying the efficacy of AAV CRISPR in correcting mutations in human dystrophic muscle fibers and satellite cells *in vivo* [207].

Ethical considerations regarding systemic *in vivo* gene editing

To assess the likelihood of vertical transfer of the gene editing events to the next generation after systemic gene editing, germline and also transplacental transmission of AAV CRISPR needs to be rigorously analyzed. AAV9 has been

shown to penetrate the placenta [208] in mice and this needs to be taken into consideration for clinical application of the technology. On the other hand, if the issues with specificity of CRISPR-mediated gene editing are resolved in the future, germline transmission of gene-editing events might provide the opportunity of having healthy children for patients with genetic diseases.

Chapter 5.

Materials and methods

Satellite Cell Isolation, Culture and Transfection

Satellite cell isolation was performed as previously described [51], For *in vitro* expansion experiments, $CD45^-$ $Sca\text{-}1^-$ $Mac\text{-}1^-$ $CXCR4^+$ $b1\text{-}integrin^+$ cells were seeded on collagen/laminin- coated plates in F10 (GIBCO) containing 20% horse serum (Atlanta Biologics), 1% penicillin-streptomycin (Invitrogen), and 1% glutamax (Invitrogen). Where indicated, 5 ng/ml bFGF (Sigma) was added to the medium daily. 50 mM forskolin (Santa Cruz) or 0.1% DMSO was added to the wells 24 hr after plating, and the medium was changed with fresh medium containing DMSO or forskolin 48 hr after plating with treatment continued for 36 more hours, after which the medium was changed for fresh medium without compound. Cells were counted or used for transplant after 5 days in culture. For myogenic colony- forming assays, cells were fixed and counted after 6 days in culture. For differentiation, cells were cultured 5 days with or without compound, and on day 5, equal numbers (8,000) of cells were replated in each well of a 96-well plate in growth medium. Medium was changed after 4 hr to DMEM (GIBCO) containing 2% horse serum (Atlanta Biologics), 1% penicillin-streptomycin (Invitrogen), with or without 50 mM Forskolin or 0.1% DMSO. Cells were fixed after 60 or 72 hr in differentiation medium.

For satellite isolation from locally AAV-injected muscles, TA muscles were harvested and cut into small pieces using a curved scissor. Mononuclear cells were obtained by enzymatic digestion with 0.2% collagenase type II and 0.05% dispase in DMEM (LifeTech) at 37°C for 15 min followed by another 10 min

digestion. The cells were centrifuged, filtered through a 70 um strainer and stained with the antibody mix (APCCy7-CD45 (BD, clone 30-F11, 1:200), APCCy7-CD11b (BD, clone M1/70, 1:200), APCCy7-TER119 (Biolegend, clone TER-119, 1:200). APC conjugated Sca-1 (eBioscience, clone D7, 1:200)) for 30 min on ice in HBSS (LifeTech) containing 2% Donor Bovine Serum (DBS). For isolating satellite cells from *Pax7-ZsGreen* $^{+/-}$*;Mdx;Ai9* mice, Zsgreen + cells were isolated after gating for live mononuclear cells lacking expression of Sca1, CD45, Ter119 and Mac1. For *in vitro* expansion of satellite cells isolated from AAV CRISPR injected muscles, satellite cells were seeded on collagen/laminin-coated plates in F10 (GIBCO) containing 20% horse serum (Atlanta Biologics), 1% penicillin-streptomycin (LifeTech), and 1% glutamax (Lifetech). 5 ng/ml bFGF (Sigma) was added to the medium daily. Medium was changed for fresh medium every other day. After 7 days, satellite cells were harvested, cell numbers were counted and cells were re-plated in multiple wells of a 96 well plate for differentiation. The next day, medium was changed to DMEM (GIBCO) containing 2% horse serum (Atlanta Biologics), 1% penicillin-streptomycin (LifeTech). Myotubes were fixed with 4% PFA or harvested in TriZol reagent for RNA analysis after 60 or 72 hr in differentiation medium. Satellite cells from *mdx;Ai9* mice, used for *in vitro* transfection, were cultured on 6-well plates in the presence of forskolin (50 uM) for 5 days [85]. On day 6, cells were harvested and re-plated in 10 cm dishes and transfected with plasmids encoding SpCas9 and gRNA plasmids using lipofectamine 3000 reagent per manufacturer's instructions. TdTomato+ gene-targeted cells were double-

sorted 2 days after transfection and expanded in culture for 5 days before *in vitro* myogenic differentiation/*in vivo* transplantation.

Tissue Injury and Mouse Satellite Cell Transplantation

25 ml (0.03 mg/ml) of Naja mossambica mossambica cardiotoxin (Sigma) was injected in the tibialis anterior (TA) muscle of anesthetized *mdx* mice 1 day before cell transplantation. The next day, 6,000 freshly isolated double-sorted GFP^+ satellite cells or the total number of cells expanded from 6,000 SMPs after 5 days in culture were injected directly into these pre-injured muscles in 20 ml PBS. For transplantation with equal numbers of cultured compound treated cells, 200,000 forskolin or 200,000 DMSO-treated cells were injected. The contralateral TA was injected with PBS only as a negative control. Muscles transplanted with *in vitro* transfected satellite cells were harvested 3 weeks after injection, and muscles transplanted with satellite cells from intramuscular AAV-Ai9 CRISPR injected muscles were harvested 10 days after transplantation for cryosectioning and immunofluorescence/ epifluorescence analysis.

Immunofluorescence and Imaging of Satellite Cells

Cultured satellite cells were fixed in 4% paraformaldehyde (PFA) and stained with 10 mg/ml Hoechst (Invitrogen). Pictures from the whole well were taken using a Celigo cytometer (Cyntellect) under the UV channel. The images were analyzed and numbers of cells were counted by the built-in software. Differentiated cells were stained for myosin heavy chain (Primary antibody: anti-skeletal myosin type

II (fast-twitch) 1:200 and anti-skeletal myosin type I (slow-twitch) 1:100, Sigma. Secondary: goat anti-mouse IgG Alexa-555 conjugate (Molecular Probes) 1:250) and 10 mg/ml Hoechst (Invitrogen) and pictures from the whole well were taken using Celigo cytometer (Cyntellect) under UV and red channels. The images were analyzed and percentage of nuclei in myotubes was calculated using a modified ImageJ macro developed in-house. Sections of the transplanted muscles were stained for GFP (rabbit anti-GFP Alexa 488 conjugate (Invitrogen) 1:250) and for dystrophin (Primary: rabbit anti-dystrophin (Abcam) 1:50. Secondary: goat anti-rabbit IgG Alexa-555 conjugate (Molecular probes) 1:250) and imaged using an upright Zesis fluorescent microscope.

Flow Cytometry of Satellite Cells

Flow cytometry analysis was performed using a BD LSR II, provided through the Harvard Stem Cell Institute Flow Cytometry Core Facility. Flow cytometry data were collected using DIVA (Becton Dickinson (BD), Franklin Lakes, NJ) software and analyzed offline using Flowjo software (Tree Star, Inc., Macintosh version 8.1.1, Ashland, OR). Antibodies used for flow cytometry included: APC/ Cy7 anti-mouse Ter119, clone Ter119 (1:200, Biolegend 116223), APC/Cy7 anti-mouse CD45, clone 30-F11 (1:200, Biolegend 103116), APC/Cy7 anti-mouse CD11b, clone M1/70 (1:200, Biolegend 101226), APC Anti-mouse Ly-6A/E (Sca-1), clone D7 (1:200, Biolegend 108112), Biotin anti-mouse CD184 (CXCR4, Fusin) (1:100, BD Biosciences 551968), Streptavidin PE-Cy7 (1:100, eBioscience 25-4317-82), PE anti-mouse / rat CD29 Antibody (1:100, Biolegend 102208). Live cells were identified by positive staining with calcein blue (1:1000) (Invitrogen, Carlsbad, CA)

and negative staining for propidium iodide (PI, 1 mg/ml). Antibody incubations were performed in staining medium (SM = Hank's Buffered Saline Solution (HBSS, (GIBCO)) + 2% donor horse serum), on ice for 15 min.

Constructs

Plasmid encoding SpCas9 and the Sp gRNA cloning plasmid were gifts from George Church. Sp gRNA plasmids targeting Ai9 and *Dmd*23 loci were derived from the parental construct by amplifying the plasmid using a forward primer that includes the gRNA target sequence in the 5' end and anneals to the gRNA scaffold in the 3' end along with a reverse primer that anneals to the 3′ end of the U6 promoter. Target sequences of the gRNAs are provided in Supplementary table 1. PCR products were treated with DpnI (NEB), purified using QIAquick PCR Purification Kit (Qiagen), phosphorylated with T4 Polynucleotide Kinase (NEB), self-ligated using the Quick Ligation Kit (NEB) and transformed into Top10 competent cells (LifeTech). Individual colonies were analyzed by Sanger sequencing. Coupled Ai9-*Dmd*23 Sp gRNAs were generated from the single Sp gRNA plasmids using standard restriction enzyme and ligation-based cloning methods. Plasmid encoding SaCas9 and the Sa gRNA cloning plasmids were gifts from Feng Zhang. Sa gRNA plasmids targeting Ai9 and *Dmd*23 loci were derived from the parental constructs using the same strategy as the Sp gRNA plasmids.

The 173CMV_SaCas9_Ai9/*Dmd*23 gRNAs constructs were generated by isothermal assembly of 4 fragments using Gibson Assembly Master Mix (NEB). 173CMV promoter followed by SaCas9 was amplified from Zhang lab plasmid using primers 173cmv_f and saCas9_r (Supplementary table 3). Two gBlocks

each were synthesized (IDT) to together cover SV40-polyA, U6 promoter, left gRNA, U6 promoter, right gRNA for Ai9 and *Dmd23* guides, respectively (Supplementary table 4). gBlocks were PCR amplified using gBlock_f and gBlock_r primers and digested with BbsI (NEB). The final piece, pUC19 backbone, was PCR amplified with pUC19_f and pUC19_r from pUC19 control plasmid (LifeTech). All PCR products were gel extracted prior to Gibson Assembly. EFS_SaCas9_Ai9/*Dmd*23 gRNAs constructs were similarly constructed with EFS promoter amplified from a plasmid containing full length EF1 promoter (a gift from John Rinn) with EFS_f and EFS_r primers, followed by SaCas9 amplified with primers SaCas9_f and SaCas9_r (Supplementary table 3) and the two gBlocks as well as the pUC19 backbone as previously mentioned. Correctly assembled plasmids were confirmed by Sanger sequencing and subsequently used to construct AAV plasmid with pZac2.1 backbone. The pZac2.1 AAV backbone plasmid was purchased from University of Pennsylvania Vector Core. AAV constructs were inserted into the pZac2.1 backbone using a restriction enzyme digestion and blunt end ligation approach and transformed into Stbl3 competent cells (LifeTech).

Genomic DNA extraction and genomic PCR

Genomic DNA was extracted from tissues and *in vitro* cultured cells using Quick Extract solution (Epicenter) according to manufacturer's instruction. DNA samples in Quick Extract of volumes equal to 10% of the final PCR reaction were used. Phusion Human Specimen Direct PCR Kit (ThermoFisher) was used to amplify

*Dmd*23 locus from the *in vitro* transfected satellite cell-derived myotubes using Genomic_Dmd23_f and Genomic_Dmd23_r primers (Supplementary table 2) with the following PCR condition: 98˚C for 3 min, 6x [98˚C for 5s, 68˚C (-1˚C/cycle) for 10s, 68˚C for 1 min], 29x (98˚C for 5s, 62˚C for 10s, 68˚C for 1 min), 68˚C for 3 min. Nested PCR was performed for locally injected TA muscles using Phusion Green Hot Start II High-Fidelity PCR Master Mix (ThermoFisher) with 20 cycles of first round amplification using with above mentioned primers and thermocycling conditions followed by 25 cycles of second round amplification using Genomic_Dmd23_nested_f and Genomic_Dmd23_nested_r (Supplementary table 2) with a 1:10 dilution between the two rounds and the following conditions: 98˚C for 3 min, 25x (98˚C for 5s, 66˚C for 10s, 72˚C for 15s), 72˚C for 5 min. Unedited and exon-excised bands were gel extracted and cloned into TOPO plasmids using Zero Blunt TOPO PCR cloning kit (LifeTech) and subsequently transformed into TOP10 competent cells. Individual colonies were analyzed by Sanger sequencing to confirm the correct excision of sequence flanked by two guide RNAs.

RT-PCR and Taqman-based real time PCR

Total RNA was isolated from tissues using TRIzol reagent (LifeTech) per manufacturer's instructions. For tissues harvested from animals, 1ug of RNA was used for cDNA synthesis with SuperScript III First Strand Synthesis SuperMix (LifeTech) in 20uL reactions. For *in vitro* cultured samples, 400ng of RNA was used for cDNA synthesis with SuperScript VILO MasterMix (LifeTech) in 20uL reactions. RT-PCR was performed using 1uL cDNA with Q5 HotStart MasterMix

(NEB) using RT_Dmd23_f and RT_Dmd23_r (Supplementary table 2) primers with the following condition: 98°C for 3 min, 40x (98°C for 10s, 60°C for 15s, 65°C for 30s), 65°C for 3 min. Both unedited and exon 23-deleted bands were gel extracted and cloned into TOPO vectors using Zero Blunt TOPO PCR cloning kit (LifeTech) and subsequently transformed into TOP10 competent cells. Individual colonies were analyzed by Sanger sequencing. Alignment to genomic sequence was performed using Geneious software. Taqman quantitative Real-Time PCR was performed as previously described [152]. A taqman probe against exon 4-5 junction was used for quantification of total DMD transcripts, and another probe against exon 22-24 junction was used for quantification of exon 23-deleted transcripts (Supplementary table 2). A taqman assay for 18s ribosomal RNA was used as housekeeping control (ThermoFisher, Cat # 4333760). Assays were carried out in triplicates of 10uL reactions for each probe and with 20ng of cDNA input. Taqman Fast Advanced Master Mix (LifeTech) was used with fast cycling conditions recommended by the manual, 50°C for 2 min, 95°C for 20s, 40x (95°C for 1s, 60°C for 20s), with data collection at the end of each PCR cycle. Delta-Ct values between exon 4-5 and exon 22-24 were used to quantify the percentage of exon 23-deleted transcripts in comparison to total DMD transcripts.

AAV Production

CRISPR AAVs were generated through the Gene Transfer Vector Core (GTVC) at the Grousbeck Gene Therapy Center at the Schepens Eye Research

Institute and Massachusetts Eye and Ear Infirmary(SERI/MEEI). AAV9 encoding Cre was purchased from University of Pennsylvania Vector Core.

Western blotting:

Protein was extracted from tissues and cultured cells using RIPA buffer (Cell Signaling). Tissues were homogenized using GentleMACS M-tubes (Miltenyi Biotech) with protein 1.1 program. Protein was concentrated using Amicon Ultra 10k centrifugal filter units. Protein concentration was determined by BCA assay (Pierce). 25ug, 25ug and 50ug of total protein per lane were used for myotubes, IM injected TA muscle and IP injected tissues, respectively. Different percentages of wild-type muscle proteins were diluted in mdx proteins from the same muscle so that the total protein of that lane was kept the same. Samples were denatured at 99°C for 5 minutes before being loaded on to 4-20% Tris-HCl precast Criterion gels (Bio-Rad). Dystrophin and GAPDH (loading control) were detected by primary antibodies NCL_DYS1 (1:100, Novocastra) and sc-32233 (1:25,000, Santa-Cruz Biotechnology) followed by horse anti-mouse IgG HRP-linked (1:1,000, Cell Signaling Technology 7076P2). ChemiDoc imaging system (Bio-Rad) was used to detect chemiluminescence after using Supersignal west Dura ECL kit (ThermoFisher). Intensity of dystrophin and GAPDH bands were quantified using ImageJ gel analysis function. Different exposures were used for some membranes for dystrophin and GAPDH quantification to avoid overexposed bands. Relative abundance of dystrophin in total protein was computed by the ratio of dystrophin signal and GAPDH and presented in Arbitrary Unit (AU). Detection of multiple

bands for dystrophin with NCL-Dys1 antibody is consistent with the previous reports in literature [209].

Detection of dystrophin by capillary immunoassay (Simple Western)

Protein was extracted and processed as described for Western blotting (above). The Wes 66-440 kDa Mouse Master Kit (PS-MK09) was used for all Simple Western experiments on the ProteinSimple Wes system. Specifically, 5uL of protein extract from each sample was loaded to the kit at the final concentration of 2ug/uL. Dystrophin and Vinculin (loading control) were detected by primary antibodies NCL_DYS1 (1:100, Novocastra) and MAB6896 (1:12.5, R&D). Goat Anti-Mouse Secondary HRP Conjugate (ready-to-use reagent) was used according to manufacturer's instructions (ProteinSimple). Default running and detection programs were used across all the assays (Separation time 30 minutes, Separation Voltage 475 Volts, Antibody Diluent time 5 minutes, Primary Antibody time 30 minutes, Secondary Antibody time 30 minutes). Compass software (ProteinSimple) was used to visualize virtual gels. Relative protein quantification was generated from chromatograms of the indicated samples.

Histology and immunofluorescence:

Mouse skeletal and heart muscles were dissected. Samples used for dystrophin immunofluorescence were embedded in O.C.T compound (Tissue-Tek) immediately after dissection and frozen in liquid-nitrogen-cold isopentane. Sample used for tdTomato epifluorescence were fixed in 4% PFA for 1 h at room

temperature and immersed in 30% sucrose until submersion, before embedding in O.C.T. and freezing. For dystrophin immunostaining of *mdx* muscle sections transplanted with tdTomato+ satellite cells, tissues were fixed in 2% PFA for 30 min before embedding in O.C.T. and freezing. Subsequent cryosectioning was performed using a Microm HM550 (Thermo Scientific) at the thickness of 12 µm for skeletal muscles and 30 um for heart. For dystrophin, nNos and Syntrophin immunostaining, cryosections were blocked with 5% Normal Goat Serum (NGS) (Jackson ImmunoResearch), 2% Bovine Serum Albumin (BSA) (Sigma), 2% protein concentrate (M.O.M. Kit, Vector Laboratories, BMK-2202), and 0.1% tween-20 (Sigma) for 1h at room temperature, followed by 2 x 5 min DPBS washes. Sections were subsequently stained with rabbit polyclonal anti-dystrophin (1:50, Abcam, ab15277), rabbit polyclonal anti-nNos (1:100, Immunostar, 24431) or rabbit monoclonal anti-Syntrophin (1:200, Abcam, ab11187) antibody at 4°C overnight, followed by 4 x 5min DPBS washes each. Slides were then incubated with secondary goat-anti-rabbit IgG Alexa Fluor 488 (1:250, LifeTech) at room temperature for 1 h, followed by 4 x 5 min DPBS washes. Slides were then mounted with mounting media containing DAPI (Vector Laboratories). For alpha-Sarcoglycan, beta-Sarcoglycan, beta-Dystroglycan and Dystrobrevin stainings, cryosections were blocked with 5% Normal Goat Serum (NGS) (Jackson ImmunoResearch), 2% Bovine Serum Albumin (BSA) (Sigma), 2% protein concentrate (M.O.M. Kit, Vector Laboratories, BMK-2202), 1 drop/ml of M.O.M. blocking reagent (M.O.M. Kit, Vector Laboratories, BMK-2202) and 0.1% tween-20 (Sigma) for 1h at room temperature, followed by 2 x 5 min DPBS washes.

Sections were subsequently stained with mouse monoclonal anti-alpha Sarcoglycan (1:50, abcam, ab49451), anti-beta Sarcoglycan (1:100, Novacastra, NCL-L-b-SARC), anti-beta Dystroglycan (1:100, Novacastra, NCL-b-DG) or anti-Dystrobrevin (1:100, BD Biosciences, 610766) antibody, at 4°C overnight, followed by 4 x 10 min DPBS washes each. Slides were then incubated with secondary goat-anti-mouse IgG Alexa Fluor 488 (1:250, LifeTech) at room temperature for 1 h, followed by 4 x 10 min DPBS washes. Slides were then mounted with mounting media containing DAPI (Vector Laboratories).

For LAMININ staining, sections were fixed on the slide using 4% PFA for 10 min, washed with DPBS for 3 x 5 min, blocked and stained with a rabbit polyclonal anti-laminin antibody (1:200, Millipore, AB2034) as described above for the dystrophin staining. For MHC staining of *in vitro* differentiated myotubes, myotubes were permeablized using 0.5% TritonX-100 (Sigma) for 15 min at RT, washed 2 x 5 min with DPBS, blocked with 5% NGS, 2% BSA, 2% protein concentrate, and 0.1% tween-20 for 1h at room temperature, washed 2 x 5 min with DPBS, incubated with anti-skeletal myosin type II (fast-twitch) (1:200, Sigma) and anti-skeletal myosin type I (slow-twitch) (1:100, Sigma) at 4°C overnight, washed 4 x 5min with DPBS, incubated with goat anti-mouse IgG Alexa-488 conjugate secondary antibody (1:250, LifeTech), washed 4 x5 min with DPBS and stained with 10 mg/ml Hoechst (Invitrogen). 12 µm sections were fixed in 4% PFA for 10 min and washed with DPBS for 3 x 5 min before H&E staining.

Mice

Animal care and experimental protocols were approved by the Harvard University Institutional Animal Care and Use Committee (IACUC). *Mdx* mice (JAX, #001801) were bred with Ai9 mice (JAX, #007905) in the Harvard Biological Research Infrastructure to generate the *mdx;Ai9* mice. *Pax7-ZsGreen* mice (kindly provided by Dr. Michael Kyba, University of Minnesota) were bred with *mdx; Ai9* mice to generate the *Pax7-ZsGreen* $^{+/-}$*;mdx;Ai9* mice. Wild type C57BL6/J mice (JAX, #000664) were purchased from Jackson laboratories.

AAV injections

For intramuscular injections into adult mice, animals were anesthetized using isoflurane and virus was injected into the TA muscle (6E+11 vg for AAV-Cre or 1.5E+12 vg for AAV CRISPR). For systemic injections into neonatal mice, virus was injected intraperitoneally (3E+11 vg for AAV-Cre or 3E+12 vg for AAV CRISPR) to mice on postnatal day 3 (P3). For adult systemic injections, virus was injected via tail vein (3.6E+13 vg/mouse).

Analyzing muscle contractile properties:

Mice were anesthetized with sodium pentobarbital (80-100 mg/kg body mass). Supplemental doses were provided as necessary during the experiment. Small incisions were made to expose the right tibialis anterior (TA) tendon and right patellar tendon. The mouse was placed on the temperature-controlled platform (38 °C) of an in situ test stand (Aurora Scientific model 809B, Aurora, Ontario, Canada). Silk suture (4-0) was used to attach the severed TA tendon to the lever

arm of a dual mode muscle lever system (Aurora Scientific model 305C-LR). The lower right limb was stabilized by using suture attached to the patellar tendon to secure the knee to a horizontal support. Supramaximal 200 μs square-wave pulses, output by a high current muscle stimulator (Aurora Scientific, model 701A), were delivered to platinum electrodes inserted behind the knee to depolarize the peroneal nerve. The lever system was interfaced to a PC using a multi-function data acquisition board (National Instruments model USB-6229, Austin, TX). Custom software written in LabVIEW (National Instruments) was used to configure and trigger stimulation, control lever arm position, and record data to disk. After the right leg was studied, the animal was removed from the test stand and the left leg prepared and studied in an identical manner. All contractile measurements were initiated at the empirically determined optimal length (L_0) for tetanic tension (200 Hz stimulation). Fiber length (FL) was calculated as 0.60 L_0 [210]. Susceptibility to mechanical strain was evaluated by subjecting the muscle to 5 lengthening (eccentric) trials. During each lengthening trial the muscle was tetanically stimulated at L_0 for 100 ms and then lengthened to 1.20 FL at a velocity of +1.5 FL/s. Stimulation ceased at the conclusion of the lengthening ramp. The muscle was held for 200 ms before being returned to its L_0 at a velocity of -1.5 FL/s. The series of lengthening contractions was bracketed by fixed-end tetanic contractions, which were used to evaluate the overall change in force due to the lengthening contractions. One minute separated all contractions.

Specific force was calculated as active tetanic force divided by physiological cross-sectional area (pCSA). The pCSA of the TA was calculated as muscle mass

divided by the product of FL and muscle density. Muscle density was taken as 1.06 mg/mm^3 [211].

Appendix: Supplementary figures and tables

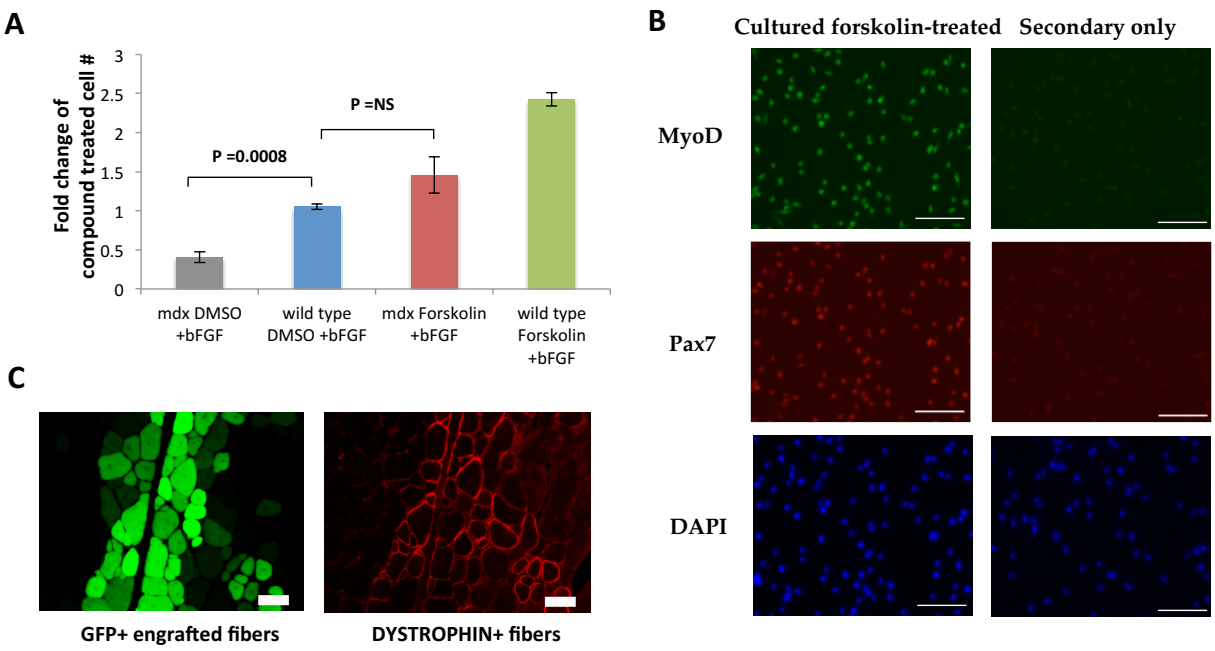

Supplementary figure 1. Forskolin Treatment Restores Proliferation of *mdx* Satellite Cells, and Transplantation of Forskolin-treated Wild-type Satellite Cells Provides *Dystrophin* Expression to Dystrophic Muscle. (A) Satellite cells from C57BL/6J (wild type) or *mdx* mice were cultured with DMSO or forskolin in the presence of bFGF. Cell numbers were determined at day 5. *Mdx* satellite cells show defective *in vitro* expansion under control conditions (compare grey bar and blue bar) and forskolin treatment increases the number of cells recovered after culture of *mdx* satellite cells (compare blue and red bars). Data are presented as fold change (mean +/- SEM, n=4), normalized to "DMSO + bFGF" controls. (B) Immunofluorescence images of forskolin-cultured cells stained for MyoD (top), Pax7 (middle) and nuclei (DAPI, bottom). Scale bars represent 100 μm. (C) Transverse frozen section of *mdx* muscle transplanted with cultured forskolin-treated GFP^+ satellite cells showing GFP (left, green) and Dystrophin (right, red) in the engrafted fibers. Scale bars represent 50 μm.

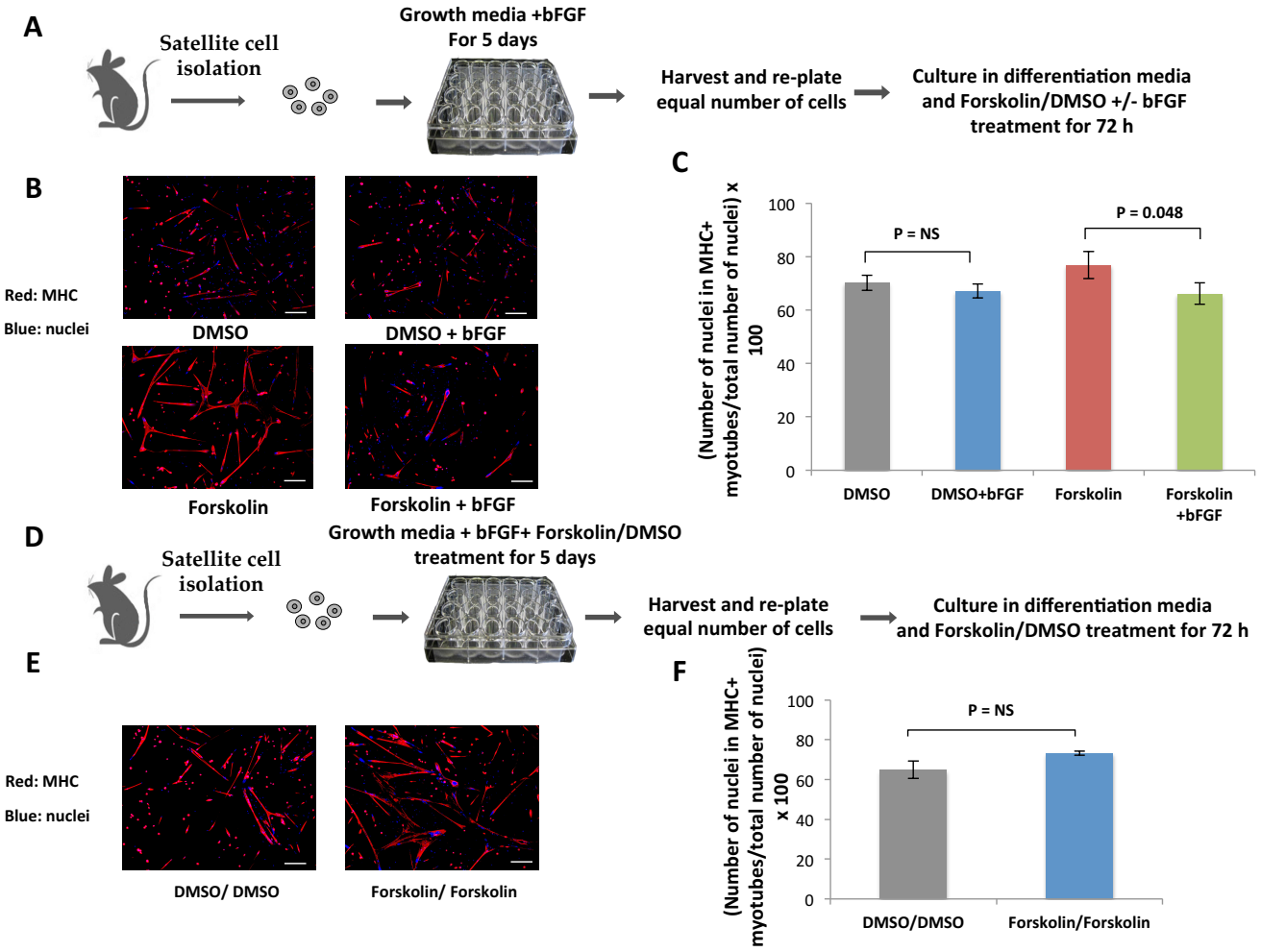

Supplementary figure 2. Forskolin and bFGF Do Not Have a Synergistic Effect on Differentiation of Mouse Satellite cells. (A) Experimental scheme for data shown in (B, C). Satellite cells from C57BL/6J mice were cultured in the presence of bFGF for 5 days. In order to test potential synergistic effects of bFGF and forskolin on satellite cell differentiation in vitro, cells cultured with bFGF were harvested on day 5 and equal numbers of cells were replated under pro-differentiation conditions with forskolin or DMSO in the presence or absence of bFGF. (B) Images of satellite cells differentiated with DMSO (top row) or forskolin (bottom row) in the absence (left column) or presence (right column) of bFGF. Cultures were stained for Myosin Heavy Chain (MHC, red) and nuclei (DAPI, blue). Scale bars represent 200 µm (C) Quantification of percentage of nuclei in myotubes after differentiation of satellite cells in the presence of forskolin or DMSO with or without bFGF (mean +/- SD, n=3). The differentiation potential of satellite cells appears to be reduced slightly in the presence of bFGF when the cells are also treated with forskolin during differentiation. (D) Experimental scheme for data shown in (E, F). Satellite cells from C57BL/6J mice were cultured in the presence of bFGF and forskolin/DMSO treatment for 5 days. In order to test the differentiation potential of satellite cells treated with forskolin during both the proliferation and differentiation phases, cells were harvested on day 5 and equal numbers of cells were induced to differentiate in the continued presence of forskolin or DMSO. (E) Images of differentiated satellite cells treated with DMSO (left) or forskolin (right) during proliferation and differentiation. Myotubes are stained for MHC (red) and nuclei (DAPI, blue). Scale bars represent 200 µm. (F) Quantification of percentage of nuclei in myotubes after differentiation of forskolin or DMSO treated cells in the continued presence of the compound (mean +/- SD, n=3). Forskolin-treated and DMSO-treated satellite cells differentiate normally into myotubes in the continued presence of the compound.

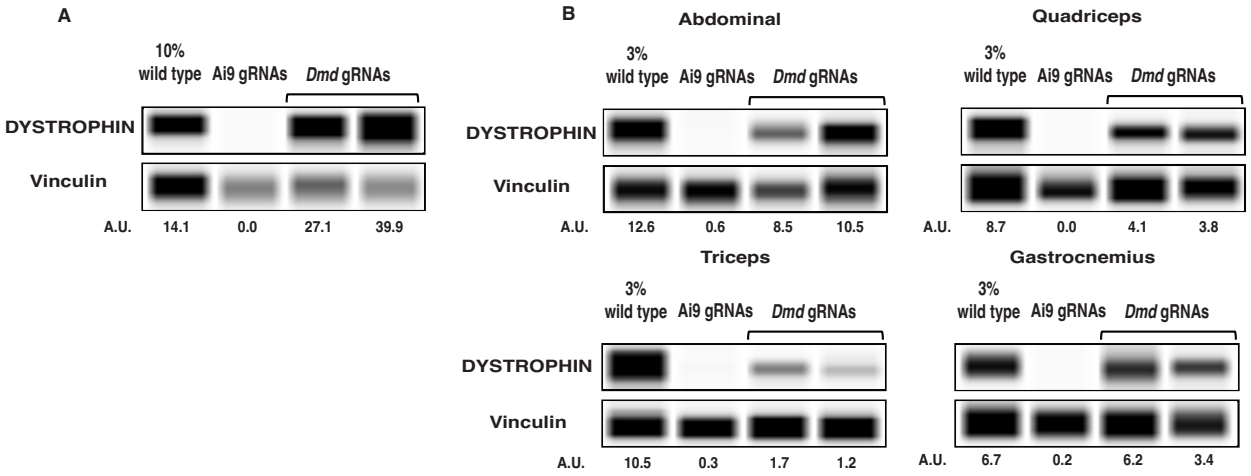

Supplementary figure 3. Detection of DYSTROPHIN Protein in AAV-*Dmd* CRISPR Treated Mice Using Capillary Immunoassay from ProteinSimple**.** To confirm data obtained by classical Western blot analysis (Figs. 2, 3, and S8), a subset of muscle samples was analyzed using ProteinSimple capillary immunoassay technology (ProteinSimple Wes instrument). Data are presented as virtual Western blots for DYSTROPHIN and Vinculin, which serves as a loading control. A.U.: Arbitrary Unit normalized to Vinculin, determined by analysis of chromatograms from each sample. (A) Detection of DYSTROPHIN protein in TA muscles of *mdx;Ai9* mice injected intramuscularly with AAV-CRISPR + *Dmd* gRNA or AAV-CRISPR Ai9 gRNAs as control. Analysis of a sample containing 90% *mdx* + 10% wild-type muscle lysate is provided for comparison. A.U.: Arbitrary Unit normalized to Vinculin. (B) Detection of DYSTROPHIN protein in abdominal, quadriceps, triceps and gastrocnemius muscles of *mdx;Ai9* mice injected intraperitoneally with AAV-CRISPR + *Dmd* gRNA or AAV-CRISPR Ai9 gRNAs as control. Analysis of a sample containing 97% mdx + 3% wild-type muscle lysate is provided for comparison of relative protein levels. A.U.: Arbitrary Unit normalized to Vinculin.

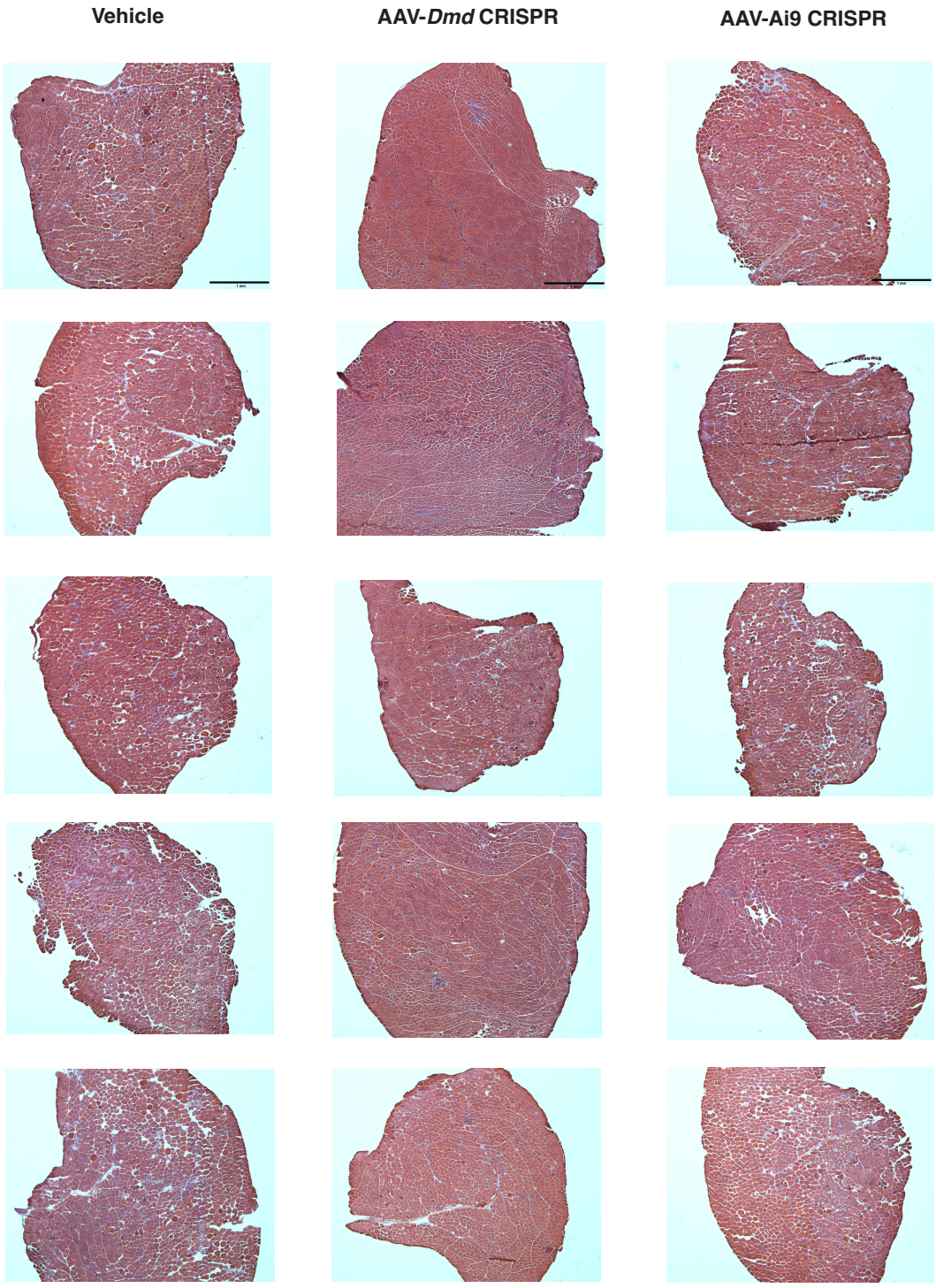

Supplementary figure 4. Histological Analysis of AAV-CRISPR Injected Muscles. Representative hematoxylin & eosin (H&E) staining of TA muscle sections from *mdx;Ai9* mice injected intramuscularly with vehicle (left), AAV-*Dmd* CRISPR (middle) or AAV-Ai9 CRISPR (right). Scale bar: 1mm.

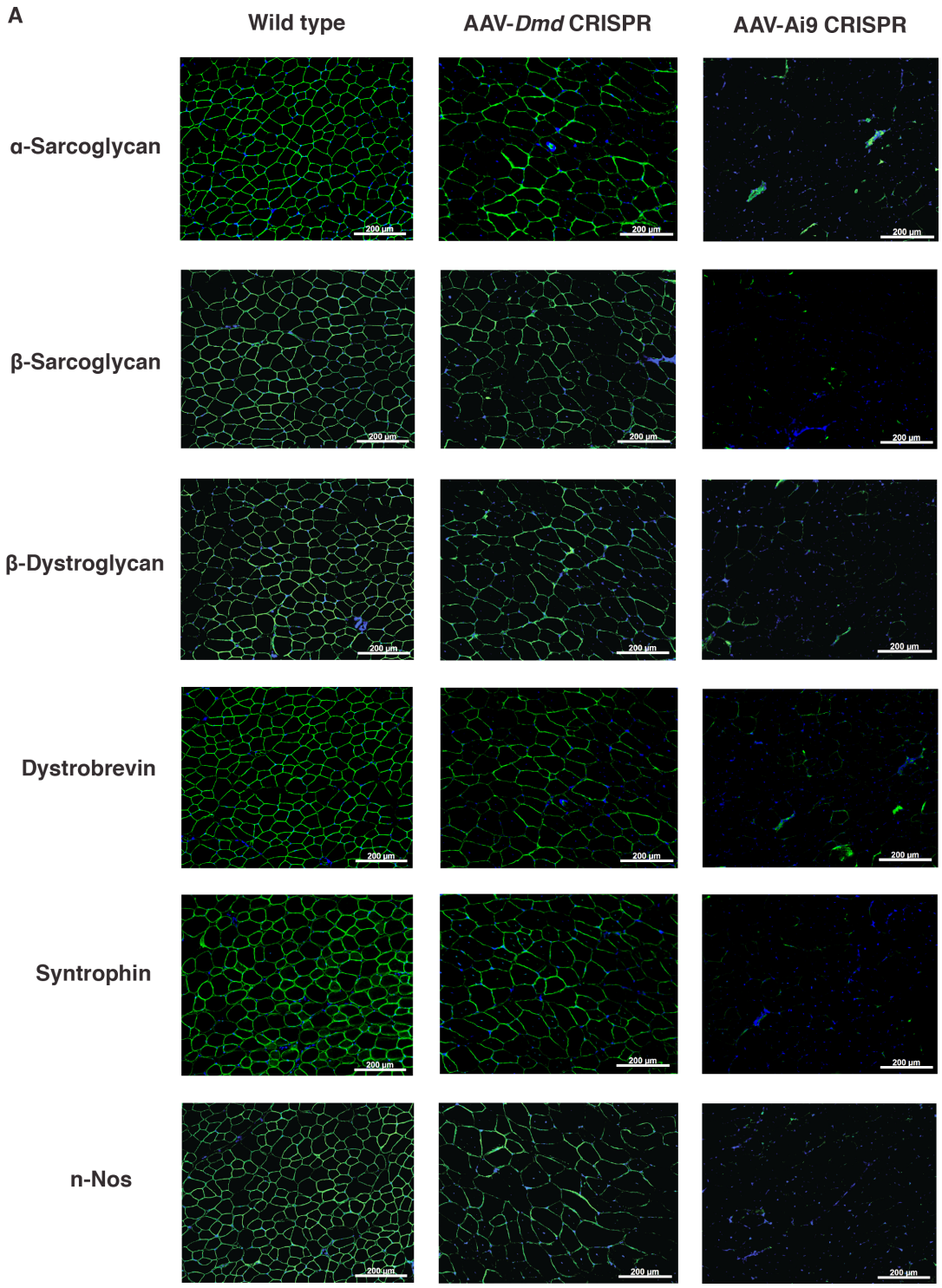

Supplementary figure 5. DGC and nNos are Restored at the Sarcolemma of AAV9-*Dmd* CRISPR Injected Muscles. (A) Transverse frozen section of wild type muscles (left column), *mdx-Ai9* muscles injected with SaCas9 and *Dmd23* gRNAs (middle column) and *mdx-Ai9* muscles injected with SaCas9 and Ai9 gRNAs and stained for different members of DGC and nNos. Scale bars represent 200 µm.

	#	Sequence	PAM	Chromosome	Position	% Indel (MLE)
Left *Dmd23* gRNA	ON	ATATAATAGAAATTATTCAT	AAGAA	chrX	83803158	2.30782198
	OFF1	ATATAATAAAAATTATTCAT	GGGAG	chr15	29264846	0.00098245
	OFF2	GTTTAATATAAATTATTCAT	TTGAA	chr12	96693430	0.01689232
	OFF3	TTCTATTAGAAATTATTCAT	AGGAA	chr9	39999808	0.00085581
	OFF4	ATAGAATAGTAATTATTCTT	CAGAA	chr2	136343268	0.01360306
	OFF5	GTATACAAGAAATTATTCAT	TTGAA	chr13	114710644	0.02998372
	OFF6	AGATAATAAACATTATTCAT	CAGGG	chr9	65881154	0.01739191
	OFF7	ATATAATTGAAATAATTCAT	CAGAG	chr2	57798779	0.00087477
	OFF8	TTAAAACAGTAATTATTCAT	GTGAA	chrX	121305872	0.00084999
Right *Dmd23* gRNA	ON	CAGTAATGTGTCATACCTTC	TTGGA	chrX	83803700	2.0575122
	OFF1	AGGTAATGTGTCATACTTTC	TGGAG	chrX	165166989	0.00821828
	OFF2	TATTCATATGTCATACCTTC	CAGAA	chr13	112470224	0.01384562
	OFF3	GCTTAATGTATCATACCTTC	CAGGA	chr18	88209239	0.01298753
	OFF4	CACTGATGTGTCATACATTC	TGGAA	chr5	91135977	0.00863797
	OFF5	GTGTCAAGTGTCATACCTTC	ATGAA	chr14	31346645	0.01833734
	OFF6	CATAAAGCTGTCATACCTTC	AGGAA	chr5	90764217	0.00085218
	OFF7	TAGTAATTCTTCATACCTTC	CAGGG	chr13	16839031	0.0042576
	OFF8	CTGTGATATGTCATACCTTT	CAGAA	chr11	10335862	0.01346439

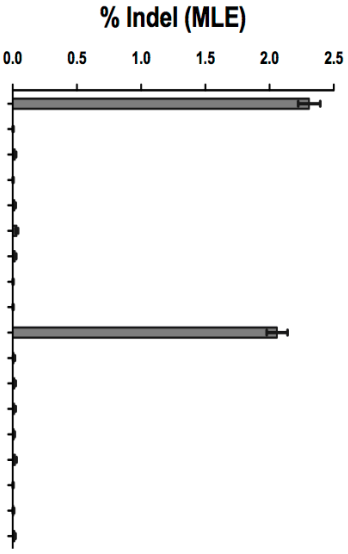

Supplementary figure 6. Next generation sequencing analysis of ON- and OFF-target modifications in AAV-CRISPR targeted muscles. List of predicted off-target sites for the left and right *Dmd*23 gRNAs and the Maximum Likelihood Estimate (MLE) calculated to determine the frequency of on-target and predicted off- target sites with true indels (*28*) in muscles injected with AAV-*Dmd* CRISPR. Targeting efficiency at the on-target sites underestimates CRISPR activity at these sites because deletion of the intervening DNA between the two gRNAs (which leads to recovery of DYSTROPHIN expression) is not detected as an indel by Next generation Sequencing (NGS) due to the large size of the deletion induced. None of the predicted off-target sites are in exonic regions of the genome. n=6 for AAV-*Dmd* CRISPR injected muscles and n=6 for AAV-Ai9 CRISPR injected muscles. AAV-Ai9 CRISPR injected muscles were used as the control for calculating the MLE. Data indicate minimal activity, close to the detection limit of Next Generation Sequencing, at all evaluated off-target sites.

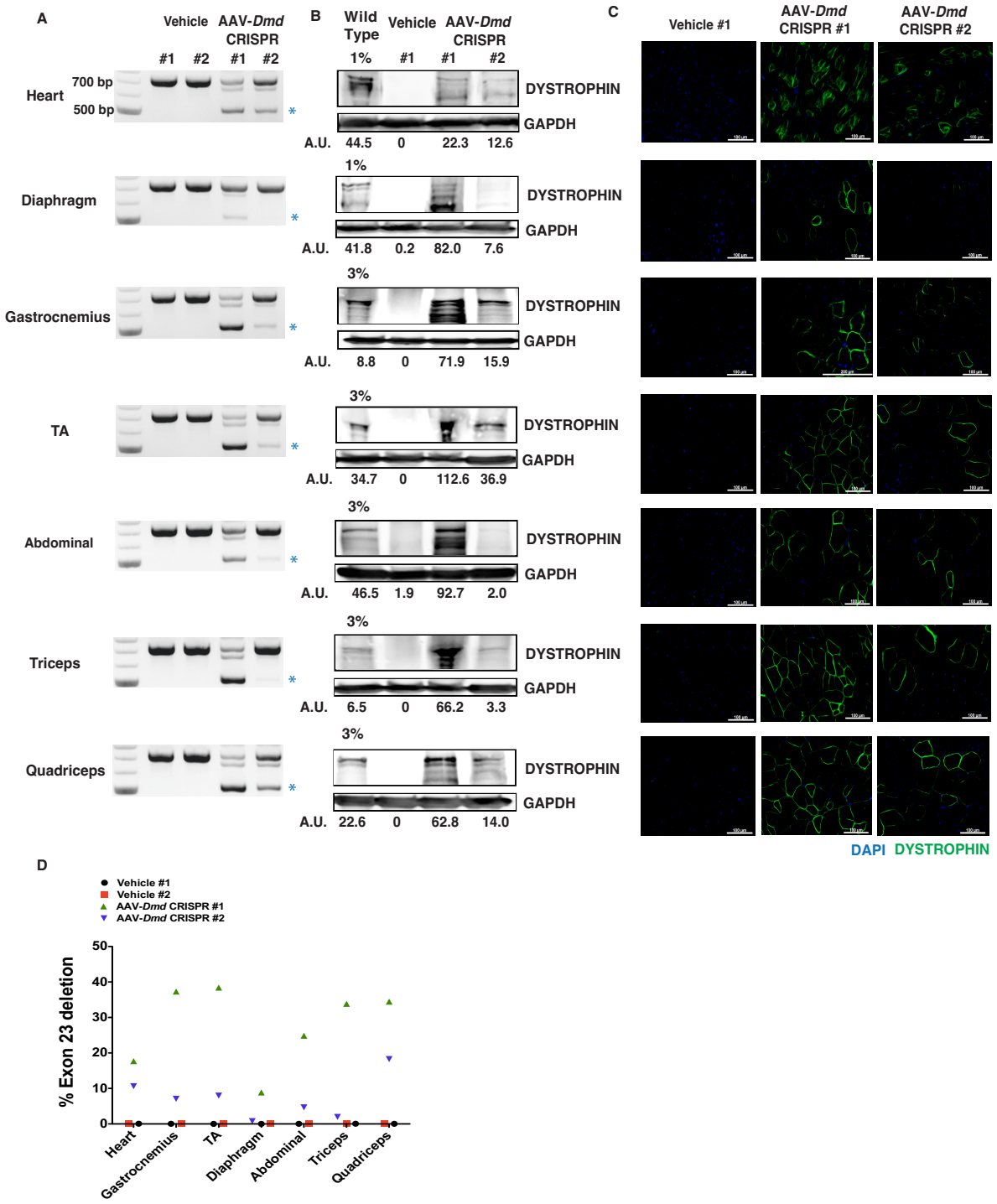

Supplementary figure 7. Systemic delivery of AAV-*Dmd* CRISPR in adult *mdx* mice targets *Dmd* exon23 and restores DYSTROPHIN expression in cardiac and skeletal muscles. Two adult *mdx* mice were injected with 3.6E+13 vg per mouse of AAV-*Dmd* CRISPR at 6 weeks of age. Tissues were harvested for analysis 14 weeks after injection.

Supplementary figure 7 (continued)

Supplementary figure 7_continued. Similar to results obtained following systemic delivery of AAV-*Dmd* CRISPR in neonatal mice, systemic injection of AAV-*Dmd* CRISPR into adult animals results in multi-organ gene targeting with variable efficiencies in different mice and muscle groups, including cardiac and skeletal muscles. (A) Exon23-deleted transcripts are detected by RT-PCR in muscles of adult *mdx;Ai9* mice injected with AAV-*Dmd* CRISPR (right lanes), but not with vehicle (left lanes). Unedited RT- PCR product: 738bp; exon23-deleted product (blue asterisk): 525bp. (B) Detection of DYSTROPHIN and GAPDH (loading control) by Western blot in the indicated muscles of adult *mdx*;Ai9 mice injected intravenously with AAV-*Dmd* CRISPR or vehicle at 6 weeks of age. Third and fourth lanes correspond to muscles from 2 different mice injected with AAV-*Dmd* CRISPR, as compared to a mouse injected with vehicle (second lane). Muscle cell lysate from a wild-type mouse (1% or 3% wild-type proteins) is included for comparison of relative protein levels. Relative signal intensity, determined by densitometry, is given at the bottom. Densitometry for GAPDH in this experiment was performed using a lower exposure blot than that shown here to avoid oversaturation of signal. A.U.: Arbitrary Unit, normalized to GAPDH. Tissue types are indicated at the left side of panel A. (C) Representative images of immunofluorescence staining for DYSTROPHIN in adult *mdx;Ai9* muscles injected with vehicle or AAV-*Dmd* CRISPR (two different animals shown). Green: DYSTROPHIN; Blue: DAPI (nuclei). Scale bar: 100um. Tissue types are indicated at the left side of panel A. (D) Quantification of exon23-deleted transcripts in muscles by Taqman-based real time PCR. Data plotted for individual mice (n=2 receiving AAV-*Dmd* CRISPR (blue and green) and n=2 receiving vehicle (black and red).

Supplementary table 1- Guide RNA target sequences

***Dmd*23 SpCas9 gRNA targets**	
Name	**Sequence**
Sp_Dmd23_L	GAATAATTTCTATTATATTACA
Sp_Dmd23_R	TTCGAAAATTTCAGGTAAGCCG
Ai9 SpCas9 gRNA targets	
Name	**Sequence**
Sp_Ai9_L	AAAGAATTGATTTGATACCG
Sp_Ai9_R	GTATGCTATACGAAGTTATT
***Dmd*23 SaCas9 gRNA targets**	
Name	**Sequence**
Sa_Dmd23_TL2	ATATAATAGAAATTATTCAT
Sa_Dmd23_TL1	TAATATGCCCTGTAATATAA
Sa_Dmd23_BL3	CAGGGCATATTATATTTAGA
Sa_Dmd23_TR6	CAAAAGCCAAATCTATTTCA
Sa_Dmd23_BR8	TGATATCATCAATATCTTTG
Sa_Dmd23_TR8	GCAATTAATTGGAAAATGTG
Sa_Dmd23_L11	CTTTAAGCTTAGGTAAAATCA
Sa_Dmd23_TR7	CAGTAATGTGTCATACCTTC
Ai9 SaCas9 gRNA targets	
Name	**Sequence**
Sa_Ai9_L	CTCTAGAGTCGCAGATCCTC
Sa_Ai9_R	ACGAAGTTATATTAAGGGTT

Supplementary table 2- Primer and Taqman probe sequences

***Dmd*23 Genomic PCR**	
Name	**Sequence**
Genomic_Dmd23_f	AACAGAACAATTTGACCAAAAACA
Genomic_Dmd23_r	TGGCCAACTATGAGAAACACAAC
Genomic_Dmd23_nested_f	GAGAAACTTCTGTGATGTGAGGAC
Genomic_Dmd23_nested_r	GGTAGTGAAAACATATGTCTGCCA
RT-PCR	
Name	**Sequence**
RT_Dmd23_f	GACACTTTACCACCAATGCGCTATCAG
RT_Dmd23_r	CTCTAGATATTCTTCTTCAGCTTGTGTCATC
Taqman assay-DMD exon 4-5	
Name	**Sequence**
E4-5_f	GGCACTGCGGGTCTTACA
E4-5_r	CATCCACTATGTCAGTGCTTCCTAT
E4-5 probe	TTCACTAAATCAACATTATTTTTC
Taqman assay-DMD exon 22-24	
Name	**Sequence**
E2-24_f	CTGAATATGAAATAATGGAGGAGAGACTCG
E22-24_r	CTTCAGCCATCCATTTCTGTAAGGT
E22-24 probe	ATGTGATTCTGTAATTTCC

Supplementary table 3-cloning primers

Name	**Sequence**
EFS_f	aattcgagctcggtacccGGCTCCGGTGCCCGTCAG
EFS_r	ggcagcgctctagaaccggtCCTGTGTTCTGGCGGCAAAC
saCas9_f	ggttctagagcgctgccaccATGAAAAGGAACTACATTC
saCas9_r	ctgcaataaacaagttGAATTCTTAAGCGTAATCTGGAAC
173cmv_f	aattcgagctcggtacccACTCACGGGGATTTCCAAG
gBlock_f	TGACCCTGAAGTTCATCTGC
gBlock_r	CCTTTCGACCTGCATCCATC
pUC19_f	GGGGATCCTCTAGAGTCGAC
pUC19_r	GGGTACCGAGCTCGAATTCAC

Supplementary table 4-gBlock sequences

gBlock1-SV40pA-DmdR7

TGACCCTGAAGTTCATCTGCGAAGACATTTATCGCTTAAGAATTCAACTTGTTT
ATTGCAGCTTATAATGGTTACAAATAAAGCAATAGCATCACAAATTTCACAAATAAAGC
ATTTTTTTCACTGCATTCTAGTTGTGGTTTGTCCAAACTCATCAATGTATCTTAGGTAC
CGAGGGCCTATTTCCCATGATTCCTTCATATTTGCATATACGATACAAGGCTGTTAGA
GAGATAATTAGAATTAATTTGACTGTAAACACAAAGATATTAGTACAAAATACGTGACG
TAGAAAGTAATAATTTCTTGGGTAGTTTGCAGTTTTAAAATTATGTTTTAAAATGGACT
ATCATATGCTTACCGTAACTTGAAAGTATTTCGATTTCTTGGCTTTATATATCTTGTGG
AAAGGACGAAACACCGCAGTAATGTGTCATACCTTCGTTTAAGTACTCTGTGCTGGA
AACAGCACAGAATCTACTTAAACAAGGCAAAATGCCGTGTTTATCTCGTCAACTTGAT
AAATGTCTTCGATGGATGCAGGTCGAAAGG

gBlock2-DmdL2

TGACCCTGAAGTTCATCTGCGAAGACATTTATTGCCGTGTTTATCTCGTCAAC
TTGTTGGCGAGATTTTTTTCCGCGGGAGGGCCTATTTCCCATGATTCCTTCATATTTG
CATATACGATACAAGGCTGTTAGAGAGATAATTAGAATTAATTTGACTGTAAACACAA
AGATATTAGTACAAAATACGTGACGTAGAAAGTAATAATTTCTTGGGTAGTTTGCAGT
TTTAAAATTATGTTTTAAAATGGACTATCATATGCTTACCGTAACTTGAAAGTATTTCG
ATTTCTTGGCTTTATATATCTTGTGGAAAGGACGAAACACCGACGAAGTTATATTAAG
GGTTGTTTAAGTACTCTGTGCTGGAAACAGCACAGAATCTACTTAAACAAGGCAAAAT
GCCGTGTTTATCTCGTCAACTTGTTGGCGAGATTTTTTTGGGGATCCTCTAGAGTCGA
CCTGATAAATGTCTTCGATGGATGCAGGTCGAAAGG

gBlock3-SV40pA-td_L

TGACCCTGAAGTTCATCTGCGAAGACATTTATCGCTTAAGAATTCAACTTGTTT
ATTGCAGCTTATAATGGTTACAAATAAAGCAATAGCATCACAAATTTCACAAATAAAGC
ATTTTTTTCACTGCATTCTAGTTGTGGTTTGTCCAAACTCATCAATGTATCTTAGGTAC
CGAGGGCCTATTTCCCATGATTCCTTCATATTTGCATATACGATACAAGGCTGTTAGA
GAGATAATTAGAATTAATTTGACTGTAAACACAAAGATATTAGTACAAAATACGTGACG
TAGAAAGTAATAATTTCTTGGGTAGTTTGCAGTTTTAAAATTATGTTTTAAAATGGACT
ATCATATGCTTACCGTAACTTGAAAGTATTTCGATTTCTTGGCTTTATATATCTTGTGG
AAAGGACGAAACACCGCTCTAGAGTCGCAGATCCTCGTTTAAGTACTCTGTGCTGGA
AACAGCACAGAATCTACTTAAACAAGGCAAAATGCCGTGTTTATCTCGTCAACTTGAT
AAATGTCTTCGATGGATGCAGGTCGAAAGG

gBlock4-td_R

TGACCCTGAAGTTCATCTGCGAAGACATTTATTGCCGTGTTTATCTCGTCAAC
TTGTTGGCGAGATTTTTTTCCGCGGGAGGGCCTATTTCCCATGATTCCTTCATATTTG
CATATACGATACAAGGCTGTTAGAGAGATAATTAGAATTAATTTGACTGTAAACACAA
AGATATTAGTACAAAATACGTGACGTAGAAAGTAATAATTTCTTGGGTAGTTTGCAGT
TTTAAAATTATGTTTTAAAATGGACTATCATATGCTTACCGTAACTTGAAAGTATTTCG
ATTTCTTGGCTTTATATATCTTGTGGAAAGGACGAAACACCGACGAAGTTATATTAAG
GGTTGTTTAAGTACTCTGTGCTGGAAACAGCACAGAATCTACTTAAACAAGGCAAAAT
GCCGTGTTTATCTCGTCAACTTGTTGGCGAGATTTTTTTGGGGATCCTCTAGAGTCGA
CCTGATAAATGTCTTCGATGGATGCAGGTCGAAAGG

References

1 Tabebordbar, M., Wang, E. T. & Wagers, A. J. Skeletal muscle degenerative diseases and strategies for therapeutic muscle repair. *Annu Rev Pathol* **8**, 441-475, doi:10.1146/annurev-pathol-011811-132450 (2013).

2 Sanes, J. R. The basement membrane/basal lamina of skeletal muscle. *Journal of Biological Chemistry* **278**, 12601-12604, doi:Doi 10.1074/Jbc.R200027200 (2003).

3 Sanger, J. M. & Sanger, J. W. The dynamic Z bands of striated muscle cells. *Science signaling* **1**, pe37, doi:10.1126/scisignal.132pe37 (2008).

4 Ervasti, J. M. & Campbell, K. P. A Role for the Dystrophin-Glycoprotein Complex as a Transmembrane Linker between Laminin and Actin. *Journal of Cell Biology* **122**, 809-823 (1993).

5 Pardo, J. V., Siliciano, J. D. & Craig, S. W. A Vinculin-Containing Cortical Lattice in Skeletal-Muscle - Transverse Lattice Elements (Costameres) Mark Sites of Attachment between Myofibrils and Sarcolemma. *Proceedings of the National Academy of Sciences of the United States of America-Biological Sciences* **80**, 1008-1012 (1983).

6 Mauro, A. Satellite cell of skeletal muscle fibers. *J Biophys Biochem Cytol* **9**, 493-495 (1961).

7 Goldring, K., Partridge, T. & Watt, D. Muscle stem cells. *J Pathol* **197**, 457-467 (2002).

8 Pallafacchina, G. *et al.* An adult tissue-specific stem cell in its niche: a gene profiling analysis of in vivo quiescent and activated muscle satellite cells. *Stem cell research* **4**, 77-91, doi:10.1016/j.scr.2009.10.003 (2010).

9 Jacobs, S. C., Wokke, J. H., Bar, P. R. & Bootsma, A. L. Satellite cell activation after muscle damage in young and adult rats. *The Anatomical record* **242**, 329-336, doi:10.1002/ar.1092420306 (1995).

10 McGeachie, J. K. & Grounds, M. D. Initiation and duration of muscle precursor replication after mild and severe injury to skeletal muscle of mice. An autoradiographic study. *Cell and tissue research* **248**, 125-130 (1987).

11 Ciemerych, M. A., Archacka, K., Grabowska, I. & Przewozniak, M. Cell cycle regulation during proliferation and differentiation of mammalian muscle precursor cells. *Results and problems in cell differentiation* **53**, 473-527, doi:10.1007/978-3-642-19065-0_20 (2011).

12 Litwack, G. Stem cell regulators. Preface. *Vitamins and hormones* **87**, xxi-xxii, doi:10.1016/B978-0-12-386015-6.00046-9 (2011).

13 Taipale, J. & Keski-Oja, J. Growth factors in the extracellular matrix. *The FASEB journal : official publication of the Federation of American Societies for Experimental Biology* **11**, 51-59 (1997).

14 Christov, C. *et al.* Muscle satellite cells and endothelial cells: close neighbors and privileged partners. *Molecular biology of the cell* **18**, 1397-1409, doi:10.1091/mbc.E06-08-0693 (2007).

15 Tidball, J. G. Inflammatory cell response to acute muscle injury. *Med Sci Sports Exerc* **27**, 1022-1032. (1995).

16 Seale, P. *et al.* Pax7 is required for the specification of myogenic satellite cells. *Cell* **102**, 777-786 (2000).

17 Cornelison, D. D., Filla, M. S., Stanley, H. M., Rapraeger, A. C. & Olwin, B. B. Syndecan-3 and syndecan-4 specifically mark skeletal muscle satellite cells and are implicated in satellite cell maintenance and muscle regeneration. *Dev Biol* **239**, 79-94 (2001).

18 Beauchamp, J. R. *et al.* Expression of CD34 and Myf5 defines the majority of quiescent adult skeletal muscle satellite cells. *J Cell Biol* **151**, 1221-1234. (2000).

19 Dhawan, J. & Rando, T. A. Stem cells in postnatal myogenesis: molecular mechanisms of satellite cell quiescence, activation and replenishment. *Trends Cell Biol* (2005).

20 Zammit, P. S. *et al.* Muscle satellite cells adopt divergent fates: a mechanism for self-renewal? *J Cell Biol* **166**, 347-357 (2004).

21 Conboy, I. M. & Rando, T. A. The regulation of Notch signaling controls satellite cell activation and cell fate determination in postnatal myogenesis. *Dev Cell* **3**, 397-409. (2002).

22 Brack, A. S., Conboy, I. M., Conboy, M. J., Shen, J. & Rando, T. A. A temporal switch from notch to Wnt signaling in muscle stem cells is necessary for normal adult myogenesis. *Cell stem cell* **2**, 50-59, doi:10.1016/j.stem.2007.10.006 (2008).

23 Shinin, V., Gayraud-Morel, B., Gomes, D. & Tajbakhsh, S. Asymmetric division and cosegregation of template DNA strands in adult muscle satellite cells. *Nature cell biology* **8**, 677-687, doi:10.1038/ncb1425 (2006).

24 Conboy, M. J., Karasov, A. O. & Rando, T. A. High incidence of non-random template strand segregation and asymmetric fate determination in dividing stem cells and their progeny. *PLoS biology* **5**, e102, doi:10.1371/journal.pbio.0050102 (2007).

25 Rocheteau, P., Gayraud-Morel, B., Siegl-Cachedenier, I., Blasco, M. A. & Tajbakhsh, S. A subpopulation of adult skeletal muscle stem cells retains all template DNA strands after cell division. *Cell* **148**, 112-125, doi:10.1016/j.cell.2011.11.049 (2012).

26 McCroskery, S., Thomas, M., Maxwell, L., Sharma, M. & Kambadur, R. Myostatin negatively regulates satellite cell activation and self-renewal. *J Cell Biol* **162**, 1135-1147 (2003).

27 Pisconti, A. *et al.* Follistatin induction by nitric oxide through cyclic GMP: a tightly regulated signaling pathway that controls myoblast fusion. *The Journal of cell biology* **172**, 233-244, doi:10.1083/jcb.200507083 (2006).

28 Amthor, H. *et al.* Muscle hypertrophy driven by myostatin blockade does not require stem/precursor-cell activity. *Proc Natl Acad Sci U S A* **106**, 7479-7484, doi:0811129106 [pii] 10.1073/pnas.0811129106 (2009).

29 Lescaudron, L. *et al.* Blood borne macrophages are essential for the triggering of muscle regeneration following muscle transplant. *Neuromuscul Disord* **9**, 72-80 (1999).

30 Joe, A. W. *et al.* Muscle injury activates resident fibro/adipogenic progenitors that facilitate myogenesis. *Nat Cell Biol* **12**, 153-163 (2010).

31 Uezumi, A., Fukada, S., Yamamoto, N., Takeda, S. & Tsuchida, K. Mesenchymal progenitors distinct from satellite cells contribute to ectopic fat cell formation in skeletal muscle. *Nat Cell Biol* **12**, 143-152 (2010).

32 Fielding, R. A. *et al.* Acute phase response in exercise. III. Neutrophil and IL-1 beta accumulation in skeletal muscle. *Am J Physiol* **265**, R166-172 (1993).

33 Tidball, J. G. Inflammatory processes in muscle injury and repair. *Am J Physiol Regul Integr Comp Physiol* **288**, R345-353 (2005).

34 Tidball, J. G. & Wehling-Henricks, M. The role of free radicals in the pathophysiology of muscular dystrophy. *J Appl Physiol* **102**, 1677-1686, doi:01145.2006 [pii] 10.1152/japplphysiol.01145.2006 (2007).

35 Mantovani, A., Sica, A. & Locati, M. Macrophage polarization comes of age. *Immunity* **23**, 344-346, doi:S1074-7613(05)00313-4 [pii] 10.1016/j.immuni.2005.10.001 (2005).

36 Merly, F., Lescaudron, L., Rouaud, T., Crossin, F. & Gardahaut, M. F. Macrophages enhance muscle satellite cell proliferation and delay their differentiation. *Muscle & nerve* **22**, 724-732, doi:10.1002/(SICI)1097-4598(199906)22:6<724::AID-MUS9>3.0.CO;2-O [pii] (1999).

37 Cantini, M. *et al.* Macrophages regulate proliferation and differentiation of satellite cells. *Biochem Biophys Res Commun* **202**, 1688-1696, doi:S0006291X84721292 [pii] (1994).

38 Massimino, M. L. *et al.* ED2+ macrophages increase selectively myoblast proliferation in muscle cultures. *Biochem Biophys Res Commun* **235**, 754-759, doi:S0006-291X(97)96823-6 [pii] 10.1006/bbrc.1997.6823 (1997).

39 Sherwood, R. I. *et al.* Isolation of adult mouse myogenic progenitors: functional heterogeneity of cells within and engrafting skeletal muscle. *Cell* **119**, 543-554 (2004).

40 Schulz, T. J. *et al.* Identification of inducible brown adipocyte progenitors residing in skeletal muscle and white fat. *Proc Natl Acad Sci U S A* **108**, 143-148 (2011).

41 Monaco, A. P. *et al.* Isolation of candidate cDNAs for portions of the Duchenne muscular dystrophy gene. *Nature* **323**, 646-650, doi:10.1038/323646a0 (1986).

42 Burghes, A. H. *et al.* A cDNA clone from the Duchenne/Becker muscular dystrophy gene. *Nature* **328**, 434-437, doi:10.1038/328434a0 (1987).

43 Chaturvedi, L. S., Mukherjee, M., Srivastava, S., Mittal, R. D. & Mittal, B. Point mutation and polymorphism in Duchenne/Becker muscular dystrophy (D/BMD) patients. *Experimental & molecular medicine* **33**, 251-256 (2001).

44 Ervasti, J. M. & Campbell, K. P. Membrane organization of the dystrophin-glycoprotein complex. *Cell* **66**, 1121-1131 (1991).

45 Hoffman, E. P., Brown, R. H., Jr. & Kunkel, L. M. Dystrophin: the protein product of the Duchenne muscular dystrophy locus. *Cell* **51**, 919-928 (1987).

46 Straub, V., Bittner, R. E., Leger, J. J. & Voit, T. Direct visualization of the dystrophin network on skeletal muscle fiber membrane. *The Journal of cell biology* **119**, 1183-1191 (1992).

47 Koenig, M. & Kunkel, L. M. Detailed analysis of the repeat domain of dystrophin reveals four potential hinge segments that may confer flexibility. *The Journal of biological chemistry* **265**, 4560-4566 (1990).

48 Ibraghimov-Beskrovnaya, O. *et al.* Primary structure of dystrophin-associated glycoproteins linking dystrophin to the extracellular matrix. *Nature* **355**, 696-702, doi:10.1038/355696a0 (1992).

49 Campbell, K. P. & Kahl, S. D. Association of dystrophin and an integral membrane glycoprotein. *Nature* **338**, 259-262, doi:10.1038/338259a0 (1989).

50 Sacco, A. *et al.* Short telomeres and stem cell exhaustion model Duchenne muscular dystrophy in mdx/mTR mice. *Cell* **143**, 1059-1071 (2010).

51 Cerletti, M. *et al.* Highly efficient, functional engraftment of skeletal muscle stem cells in dystrophic muscles. *Cell* **134**, 37-47 (2008).

52 Dumont, N. A. *et al.* Dystrophin expression in muscle stem cells regulates their polarity and asymmetric division. *Nat Med* **21**, 1455-1463, doi:10.1038/nm.3990 (2015).

53 Wallace, G. Q. & McNally, E. M. Mechanisms of muscle degeneration, regeneration, and repair in the muscular dystrophies. *Annual review of physiology* **71**, 37-57, doi:10.1146/annurev.physiol.010908.163216 (2009).

54 Brenman, J. E. *et al.* Interaction of nitric oxide synthase with the postsynaptic density protein PSD-95 and alpha1-syntrophin mediated by PDZ domains. *Cell* **84**, 757-767 (1996).

55 Sander, M. *et al.* Functional muscle ischemia in neuronal nitric oxide synthase-deficient skeletal muscle of children with Duchenne muscular dystrophy. *Proceedings of the National Academy of Sciences of the United States of America* **97**, 13818-13823, doi:10.1073/pnas.250379497 (2000).

56 Spencer, M. J. & Tidball, J. G. Do immune cells promote the pathology of dystrophin-deficient myopathies? *Neuromuscular disorders : NMD* **11**, 556-564 (2001).

57 Monaco, A. P., Bertelson, C. J., Liechti-Gallati, S., Moser, H. & Kunkel, L. M. An explanation for the phenotypic differences between patients bearing partial deletions of the DMD locus. *Genomics* **2**, 90-95 (1988).

58 Hoffman, E. P. *et al.* Characterization of dystrophin in muscle-biopsy specimens from patients with Duchenne's or Becker's muscular dystrophy. *N Engl J Med* **318**, 1363-1368, doi:10.1056/NEJM198805263182104 (1988).

59 McNally, E. M. & Pytel, P. Muscle diseases: the muscular dystrophies. *Annual review of pathology* **2**, 87-109, doi:10.1146/annurev.pathol.2.010506.091936 (2007).

60 Beggs, A. H. *et al.* Exploring the molecular basis for variability among patients with Becker muscular dystrophy: dystrophin gene and protein studies. *Am J Hum Genet* **49**, 54-67 (1991).

61 Yazaki, M. *et al.* Clinical characteristics of aged Becker muscular dystrophy patients with onset after 30 years. *European neurology* **42**, 145-149 (1999).

62 Muir, L. A. & Chamberlain, J. S. Emerging strategies for cell and gene therapy of the muscular dystrophies. *Expert Rev Mol Med* **11**, e18, doi:S1462399409001100 [pii] 10.1017/S1462399409001100 (2009).

63 Partridge, T. A. Impending therapies for Duchenne muscular dystrophy. *Curr Opin Neurol* **24**, 415-422, doi:10.1097/WCO.0b013e32834aa3f1 (2011).

64 Miller, R. G. *et al.* Myoblast implantation in Duchenne muscular dystrophy: the San Francisco study. *Muscle Nerve* **20**, 469-478. (1997).

65 Tremblay, J. P. & Guerette, B. Myoblast Transplantation: a Brief Review of the Problems and of Some Solutions. *Basic Appl Myol.* **7**, 221-230 (1997).

66 Dellavalle, A. *et al.* Pericytes of human skeletal muscle are myogenic precursors distinct from satellite cells. *Nat Cell Biol* **9**, 255-267 (2007).

67 Cossu, G. & Bianco, P. Mesoangioblasts--vascular progenitors for extravascular mesodermal tissues. *Curr Opin Genet Dev* **13**, 537-542, doi:S0959437X03001126 [pii] (2003).

68 Dellavalle, A. *et al.* Pericytes resident in postnatal skeletal muscle differentiate into muscle fibres and generate satellite cells. *Nat Commun* **2**, 499, doi:ncomms1508 [pii] 10.1038/ncomms1508 (2011).

69 Sampaolesi, M. *et al.* Mesoangioblast stem cells ameliorate muscle function in dystrophic dogs. *Nature* **444**, 574-579 (2006).

70 Negroni, E. *et al.* In vivo myogenic potential of human CD133+ muscle-derived stem cells: a quantitative study. *Mol Ther* **17**, 1771-1778, doi:mt2009167 [pii] 10.1038/mt.2009.167 (2009).

71 Bachrach, E. *et al.* Muscle engraftment of myogenic progenitor cells following intraarterial transplantation. *Muscle Nerve* **34**, 44-52 (2006).

72 Sampaolesi, M. *et al.* Cell therapy of alpha-sarcoglycan null dystrophic mice through intra-arterial delivery of mesoangioblasts. *Science* **301**, 487-492 (2003).

73 Gussoni, E. *et al.* Dystrophin expression in the mdx mouse restored by stem cell transplantation. *Nature* **401**, 390-394. (1999).

74 LaBarge, M. A. & Blau, H. M. Biological progression from adult bone marrow to mononucleate muscle stem cell to multinucleate muscle fiber in response to injury. *Cell* **111**, 589-601. (2002).

75 Sherwood, R. I., Christensen, J. L., Weissman, I. L. & Wagers, A. J. Determinants of skeletal muscle contributions from circulating cells, bone marrow cells, and hematopoietic stem cells. *Stem Cells* **22**, 1292-1304 (2004).

76 Gussoni, E. *et al.* Long-term persistence of donor nuclei in a Duchenne muscular dystrophy patient receiving bone marrow transplantation. *J Clin Invest* **110**, 807-814 (2002).

77 Yu, J. *et al.* Induced pluripotent stem cell lines derived from human somatic cells. *Science* **318**, 1917-1920 (2007).

78 Takahashi, K. *et al.* Induction of pluripotent stem cells from adult human fibroblasts by defined factors. *Cell* **131**, 861-872 (2007).

79 Rashid, S. T. & Vallier, L. Induced pluripotent stem cells--alchemist's tale or clinical reality? *Expert Rev Mol Med* **12**, 25, doi:S1462399410001596 [pii] 10.1017/S1462399410001596 (2010).

80 Darabi, R. *et al.* Engraftment of embryonic stem cell-derived myogenic progenitors in a dominant model of muscular dystrophy. *Exp Neurol* **220**, 212-216 (2009).

81 Darabi, R. *et al.* Functional skeletal muscle regeneration from differentiating embryonic stem cells. *Nat Med* **14**, 134-143 (2008).

82 Darabi, R. *et al.* Functional myogenic engraftment from mouse iPS cells. *Stem Cell Rev* **7**, 948-957, doi:10.1007/s12015-011-9258-2 (2011).

83 Darabi, R. *et al.* Assessment of the myogenic stem cell compartment following transplantation of Pax3/Pax7-induced embryonic stem cell-derived progenitors. *Stem Cells* **29**, 777-790, doi:10.1002/stem.625 (2011).

84 Mizuno, Y. *et al.* Generation of skeletal muscle stem/progenitor cells from murine induced pluripotent stem cells. *Faseb J* **24**, 2245-2253 (2010).

85 Xu, C. *et al.* A zebrafish embryo culture system defines factors that promote vertebrate myogenesis across species. *Cell* **155**, 909-921, doi:10.1016/j.cell.2013.10.023 (2013).

86 Borchin, B., Chen, J. & Barberi, T. Derivation and FACS-mediated purification of PAX3+/PAX7+ skeletal muscle precursors from human pluripotent stem cells. *Stem Cell Reports* **1**, 620-631, doi:10.1016/j.stemcr.2013.10.007 (2013).

87 Chal, J. *et al.* Differentiation of pluripotent stem cells to muscle fiber to model Duchenne muscular dystrophy. *Nat Biotechnol* **33**, 962-969, doi:10.1038/nbt.3297 (2015).

88 Kazuki, Y. *et al.* Complete genetic correction of ips cells from Duchenne muscular dystrophy. *Mol Ther* **18**, 386-393, doi:mt2009274 [pii] 10.1038/mt.2009.274 (2010).

89 Move over ZFNs. *Nat Biotechnol* **29**, 681-684, doi:nbt.1935 [pii] 10.1038/nbt.1935 (2011).

90 Barrangou, R. *et al.* CRISPR provides acquired resistance against viruses in prokaryotes. *Science* **315**, 1709-1712, doi:10.1126/science.1138140 (2007).

91 Mojica, F. J., Diez-Villasenor, C., Garcia-Martinez, J. & Almendros, C. Short motif sequences determine the targets of the prokaryotic CRISPR defence system. *Microbiology* **155**, 733-740, doi:10.1099/mic.0.023960-0 (2009).

92 Wiedenheft, B., Sternberg, S. H. & Doudna, J. A. RNA-guided genetic silencing systems in bacteria and archaea. *Nature* **482**, 331-338, doi:10.1038/nature10886 (2012).

93 Garneau, J. E. *et al.* The CRISPR/Cas bacterial immune system cleaves bacteriophage and plasmid DNA. *Nature* **468**, 67-71, doi:10.1038/nature09523 (2010).

94 Jinek, M. *et al.* A programmable dual-RNA-guided DNA endonuclease in adaptive bacterial immunity. *Science* **337**, 816-821, doi:10.1126/science.1225829 (2012).

95 Mali, P. *et al.* RNA-guided human genome engineering via Cas9. *Science* **339**, 823-826, doi:10.1126/science.1232033 (2013).

96 Cong, L. *et al.* Multiplex genome engineering using CRISPR/Cas systems. *Science* **339**, 819-823, doi:10.1126/science.1231143 (2013).

97 Cho, S. W., Kim, S., Kim, J. M. & Kim, J. S. Targeted genome engineering in human cells with the Cas9 RNA-guided endonuclease. *Nat Biotechnol* **31**, 230-232, doi:10.1038/nbt.2507 (2013).

98 Ding, Q. *et al.* Enhanced efficiency of human pluripotent stem cell genome editing through replacing TALENs with CRISPRs. *Cell Stem Cell* **12**, 393-394, doi:10.1016/j.stem.2013.03.006 (2013).

99 Hwang, W. Y. *et al.* Efficient genome editing in zebrafish using a CRISPR-Cas system. *Nat Biotechnol* **31**, 227-229, doi:10.1038/nbt.2501 (2013).

100 Yang, H. *et al.* One-step generation of mice carrying reporter and conditional alleles by CRISPR/Cas-mediated genome engineering. *Cell* **154**, 1370-1379, doi:10.1016/j.cell.2013.08.022 (2013).

101 Wang, H. *et al.* One-step generation of mice carrying mutations in multiple genes by CRISPR/Cas-mediated genome engineering. *Cell* **153**, 910-918, doi:10.1016/j.cell.2013.04.025 (2013).

102 Xue, W. *et al.* CRISPR-mediated direct mutation of cancer genes in the mouse liver. *Nature* **514**, 380-384, doi:10.1038/nature13589 (2014).

103 Yin, H. *et al.* Genome editing with Cas9 in adult mice corrects a disease mutation and phenotype. *Nat Biotechnol* **32**, 551-553, doi:10.1038/nbt.2884 (2014).

104 Zuris, J. A. *et al.* Cationic lipid-mediated delivery of proteins enables efficient protein-based genome editing in vitro and in vivo. *Nat Biotechnol* **33**, 73-80, doi:10.1038/nbt.3081 (2015).

105 Ran, F. A. *et al.* In vivo genome editing using Staphylococcus aureus Cas9. *Nature* **520**, 186-191, doi:10.1038/nature14299 (2015).

106 Wells, D. J., Ferrer, A. & Wells, K. E. Immunological hurdles in the path to gene therapy for Duchenne muscular dystrophy. *Expert Rev Mol Med* **4**, 1-23, doi:doi:10.1017/S146239940200515X S146239940200515X [pii] (2002).

107 Wilton, S. D. *et al.* Specific removal of the nonsense mutation from the mdx dystrophin mRNA using antisense oligonucleotides. *Neuromuscul Disord* **9**, 330-338, doi:S0960896699000103 [pii] (1999).

108 Lu, Q. L. *et al.* Functional amounts of dystrophin produced by skipping the mutated exon in the mdx dystrophic mouse. *Nat Med* **9**, 1009-1014, doi:10.1038/nm897 (2003).

109 Lu, Q. L. *et al.* Systemic delivery of antisense oligoribonucleotide restores dystrophin expression in body-wide skeletal muscles. *Proceedings of the National Academy of Sciences of the United States of America* **102**, 198-203, doi:10.1073/pnas.0406700102 (2005).

110 van Deutekom, J. C. *et al.* Local dystrophin restoration with antisense oligonucleotide PRO051. *The New England journal of medicine* **357**, 2677-2686, doi:10.1056/NEJMoa073108 (2007).

111 Goemans, N. M. *et al.* T.O.4 A phase I/IIa study on antisense compound PRO051 in patients with Duchenne muscular dystrophy. *Neuromuscul. Disord* **19**, 659–660 (2009).

112 Gebski, B. L., Mann, C. J., Fletcher, S. & Wilton, S. D. Morpholino antisense oligonucleotide induced dystrophin exon 23 skipping in mdx mouse muscle. *Human molecular genetics* **12**, 1801-1811 (2003).

113 Alter, J. *et al.* Systemic delivery of morpholino oligonucleotide restores dystrophin expression bodywide and improves dystrophic pathology. *Nat Med* **12**, 175-177, doi:10.1038/nm1345 (2006).

114 Kinali, M. *et al.* Local restoration of dystrophin expression with the morpholino oligomer AVI-4658 in Duchenne muscular dystrophy: a single-blind, placebo-controlled, dose-escalation, proof-of-concept study. *Lancet neurology* **8**, 918-928, doi:10.1016/S1474-4422(09)70211-X (2009).

115 Escolar, D. M. & Scacheri, C. G. Pharmacologic and genetic therapy for childhood muscular dystrophies. *Current neurology and neuroscience reports* **1**, 168-174 (2001).

116 Manzur, A. Y., Kuntzer, T., Pike, M. & Swan, A. Glucocorticoid corticosteroids for Duchenne muscular dystrophy. *Cochrane database of systematic reviews*, CD003725, doi:10.1002/14651858.CD003725.pub3 (2008).

117 Aartsma-Rus, A., Van Deutekom, J. C., Fokkema, I. F., Van Ommen, G. J. & Den Dunnen, J. T. Entries in the Leiden Duchenne muscular dystrophy mutation database: an overview of mutation types and paradoxical cases that confirm the reading-frame rule. *Muscle & nerve* **34**, 135-144, doi:10.1002/mus.20586 (2006).

118 Manuvakhova, M., Keeling, K. & Bedwell, D. M. Aminoglycoside antibiotics mediate context-dependent suppression of termination codons in a mammalian translation system. *RNA* **6**, 1044-1055 (2000).

119 Barton-Davis, E. R., Cordier, L., Shoturma, D. I., Leland, S. E. & Sweeney, H. L. Aminoglycoside antibiotics restore dystrophin function to skeletal muscles of mdx mice. *The Journal of clinical investigation* **104**, 375-381, doi:10.1172/JCI7866 (1999).

120 Finkel, R. S. Read-through strategies for suppression of nonsense mutations in Duchenne/ Becker muscular dystrophy: aminoglycosides and ataluren (PTC124). *Journal of child neurology* **25**, 1158-1164, doi:10.1177/0883073810371129 (2010).

121 Welch, E. M. *et al.* PTC124 targets genetic disorders caused by nonsense mutations. *Nature* **447**, 87-91, doi:10.1038/nature05756 (2007).

122 Finkel, R. S. *et al.* Phase 2a study of ataluren-mediated dystrophin production in patients with nonsense mutation Duchenne muscular dystrophy. *PLoS One* **8**, e81302, doi:10.1371/journal.pone.0081302 (2013).

123 Tinsley, J. M. *et al.* Daily treatment with SMTC1100, a novel small molecule utrophin upregulator, dramatically reduces the dystrophic symptoms in the mdx mouse. *PloS one* **6**, e19189, doi:10.1371/journal.pone.0019189 (2011).

124 Kawahara, G. *et al.* Drug screening in a zebrafish model of Duchenne muscular dystrophy. *Proceedings of the National Academy of Sciences of the United States of America* **108**, 5331-5336, doi:10.1073/pnas.1102116108 (2011).

125 Essayan, D. M. Cyclic nucleotide phosphodiesterases. *The Journal of allergy and clinical immunology* **108**, 671-680, doi:10.1067/mai.2001.119555 (2001).

126 Adamo, C. M. *et al.* Sildenafil reverses cardiac dysfunction in the mdx mouse model of Duchenne muscular dystrophy. *Proceedings of the National Academy of Sciences of the United States of America* **107**, 19079-19083, doi:10.1073/pnas.1013077107 (2010).

127 Asai, A. *et al.* Primary role of functional ischemia, quantitative evidence for the two-hit mechanism, and phosphodiesterase-5 inhibitor therapy in mouse muscular dystrophy. *PloS one* **2**, e806, doi:10.1371/journal.pone.0000806 (2007).

128 Hathout, Y. *et al.* Large-scale serum protein biomarker discovery in Duchenne muscular dystrophy. *Proc Natl Acad Sci U S A* **112**, 7153-7158, doi:10.1073/pnas.1507719112 (2015).

129 Lu, Q. L., Cirak, S. & Partridge, T. What Can We Learn From Clinical Trials of Exon Skipping for DMD? *Mol Ther Nucleic Acids* **3**, e152, doi:10.1038/mtna.2014.6 (2014).

130 Sacco, A., Doyonnas, R., Kraft, P., Vitorovic, S. & Blau, H. M. Self-renewal and expansion of single transplanted muscle stem cells. *Nature* **456**, 502-506 (2008).

131 Sherwood, R. I. *et al.* Isolation of adult mouse myogenic progenitors: functional heterogeneity of cells within and engrafting skeletal muscle. *Cell* **119**, 543-554 (2004).

132 Tanaka, K. K. *et al.* Syndecan-4-expressing muscle progenitor cells in the SP engraft as satellite cells during muscle regeneration. *Cell Stem Cell* **4**, 217-225 (2009).

133 Chakkalakal, J. V., Jones, K. M., Basson, M. A. & Brack, A. S. The aged niche disrupts muscle stem cell quiescence. *Nature* **490**, 355-360, doi:10.1038/nature11438 (2012).

134 Fukada, S. *et al.* Purification and cell-surface marker characterization of quiescent satellite cells from murine skeletal muscle by a novel monoclonal antibody. *Exp Cell Res* **296**, 245-255 (2004).

135 Montarras, D. *et al.* Direct isolation of satellite cells for skeletal muscle regeneration. *Science* **309**, 2064-2067, doi:10.1126/science.1114758 (2005).

136 Berghella, L. *et al.* Reversible immortalization of human myogenic cells by site-specific excision of a retrovirally transferred oncogene. *Hum Gene Ther* **10**, 1607-1617, doi:10.1089/10430349950017617 (1999).

137 Roy, R. *et al.* Antibody formation after myoblast transplantation in Duchenne-dystrophic patients, donor HLA compatible. *Transplant Proc* **25**, 995-997 (1993).

138 Huard, J. *et al.* Human myoblast transplantation between immunohistocompatible donors and recipients produces immune reactions. *Transplant Proc* **24**, 3049-3051 (1992).

139 Weinberg, E. S. *et al.* Developmental regulation of zebrafish MyoD in wild-type, no tail and spadetail embryos. *Development* **122**, 271-280 (1996).

140 Hinits, Y., Osborn, D. P. & Hughes, S. M. ifferential requirements for myogenic regulatory factors distinguish medial and lateral somitic, cranial and fin muscle fibre populations. *Development* **136**, 403-414 (2009).

141 Ju, B. *et al.* Recapitulation of fast skeletal muscle development in zebrafish by transgenic expression of GFP under the mylz2 promoter. *Dev Dyn.* **227**, 14-26 (2003).

142 Thisse, B. *et al.* Expression of the zebrafish genome during embryogenesis (NIH R01 RR15402). *ZFIN Direct Data Submission (*http://zfin.org). (2001).

143 Fan, L. & Collodi, P. Zebrafish embryonic stem cells. *Methods Enzymol.* **418**, 64-77 (2006).

144 Draper, B. W., Stock, D. W. & Kimmel, C. B. Zebrafish fgf24 functions with fgf8 to promote posterior mesodermal development. *Development* **130**, 4639-4654 (2003).

145 Fisher, M. E., Isaacs, H. V. & Pownall, M. E. eFGF is required for activation of XmyoD expression in the myogenic cell lineage of Xenopus laevis. *Development* **129**, 1307-1301 (2002).

146 Sicinski, P. *et al.* The molecular basis of muscular dystrophy in the mdx mouse: a point mutation. *Science* **244**, 1578-1580 (1989).

147 Seamon, K. B., Padgett, W. & Daly, J. W. Forskolin: unique diterpene activator of adenylate cyclase in membranes and in intact cells. *Proceedings of the National Academy of Sciences of the United States of America* **78**, 3363-3367 (1981).

148 Metzger, H. & Lindner, E. The positive inotropic-acting forskolin, a potent adenylate cyclase activator. *Arzneimittel-Forschung* **31**, 1248-1250 (1981).

149 Cerletti, M., Jang, Y. C., Finley, L. W., Haigis, M. C. & Wagers, A. J. Short-term calorie restriction enhances skeletal muscle stem cell function. *Cell Stem Cell* **10**, 515-519, doi:10.1016/j.stem.2012.04.002 (2012).

150 Wright, D. E. *et al.* Cyclophosphamide/granulocyte colony-stimulating factor causes selective mobilization of bone marrow hematopoietic stem cells into the blood after M phase of the cell cycle. *Blood* **97**, 2278-2285 (2001).

151 Madisen, L. *et al.* A robust and high-throughput Cre reporting and characterization system for the whole mouse brain. *Nat Neurosci* **13**, 133-140, doi:10.1038/nn.2467 (2010).

152 Goyenvalle, A. *et al.* Functional correction in mouse models of muscular dystrophy using exon-skipping tricyclo-DNA oligomers. *Nat Med* **21**, 270-275, doi:10.1038/nm.3765 (2015).

153 Stewart, R., Flechner, L., Montminy, M. & Berdeaux, R. CREB is activated by muscle injury and promotes muscle regeneration. *PloS one* **6**, e24714, doi:10.1371/journal.pone.0024714 (2011).

154 Rodriguez, G., Ross, J. A., Nagy, Z. S. & Kirken, R. A. Forskolin-inducible cAMP pathway negatively regulates T-cell proliferation by uncoupling the interleukin-2 receptor complex. *J Biol Chem* **288**, 7137-7146, doi:M112.408765 [pii] 10.1074/jbc.M112.408765 (2013).

155 Yano, Y. *et al.* Growth suppression of thyroid cancer cells by adenylcyclase activator. *Oncol Rep* **18**, 441-445 (2007).

156 Ousterout, D. G. *et al.* Multiplex CRISPR/Cas9-based genome editing for correction of dystrophin mutations that cause Duchenne muscular dystrophy. *Nat Commun* **6**, 6244, doi:10.1038/ncomms7244 (2015).

157 Li, H. L. *et al.* Precise correction of the dystrophin gene in duchenne muscular dystrophy patient induced pluripotent stem cells by TALEN and CRISPR-Cas9. *Stem Cell Reports* **4**, 143-154, doi:10.1016/j.stemcr.2014.10.013 (2015).

158 Nakamura, A. *et al.* Follow-up of three patients with a large in-frame deletion of exons 45-55 in the Duchenne muscular dystrophy (DMD) gene. *J Clin Neurosci* **15**, 757-763, doi:10.1016/j.jocn.2006.12.012 (2008).

159 Taglia, A. *et al.* Clinical features of patients with dystrophinopathy sharing the 45-55 exon deletion of DMD gene. *Acta Myol* **34**, 9-13 (2015).

160 Echigoya, Y. *et al.* Long-term efficacy of systemic multiexon skipping targeting dystrophin exons 45-55 with a cocktail of vivo-morpholinos in mdx52 mice. *Mol Ther Nucleic Acids* **4**, e225, doi:10.1038/mtna.2014.76 (2015).

161 van Deutekom, J. C. *et al.* Local dystrophin restoration with antisense oligonucleotide PRO051. *N Engl J Med* **357**, 2677-2686, doi:10.1056/NEJMoa073108 (2007).

162 Kinali, M. *et al.* Local restoration of dystrophin expression with the morpholino oligomer AVI-4658 in Duchenne muscular dystrophy: a single-blind, placebo-controlled, dose-escalation, proof-of-concept study. *Lancet Neurol* **8**, 918-928, doi:10.1016/S1474-4422(09)70211-X (2009).

163 Yin, H. *et al.* Pip5 transduction peptides direct high efficiency oligonucleotide-mediated dystrophin exon skipping in heart and phenotypic correction in mdx mice. *Mol Ther* **19**, 1295-1303, doi:10.1038/mt.2011.79 (2011).

164 Vila, M. C. *et al.* Elusive sources of variability of dystrophin rescue by exon skipping. *Skelet Muscle* **5**, 44, doi:10.1186/s13395-015-0070-6 (2015).

165 Le Hir, M. *et al.* AAV genome loss from dystrophic mouse muscles during AAV-U7 snRNA-mediated exon-skipping therapy. *Mol Ther* **21**, 1551-1558, doi:10.1038/mt.2013.121 (2013).

166 Kotterman, M. A. & Schaffer, D. V. Engineering adeno-associated viruses for clinical gene therapy. *Nat Rev Genet* **15**, 445-451, doi:10.1038/nrg3742 (2014).

167 Mingozzi, F. & High, K. A. Therapeutic in vivo gene transfer for genetic disease using AAV: progress and challenges. *Nat Rev Genet* **12**, 341-355, doi:10.1038/nrg2988 (2011).

168 Flanigan, K. M. *et al.* Mutational spectrum of DMD mutations in dystrophinopathy patients: application of modern diagnostic techniques to a large cohort. *Hum Mutat* **30**, 1657-1666, doi:10.1002/humu.21114 (2009).

169 Beroud, C. *et al.* Multiexon skipping leading to an artificial DMD protein lacking amino acids from exons 45 through 55 could rescue up to 63% of patients with Duchenne muscular dystrophy. *Hum Mutat* **28**, 196-202, doi:10.1002/humu.20428 (2007).

170 Wu, Z., Yang, H. & Colosi, P. Effect of genome size on AAV vector packaging. *Mol Ther* **18**, 80-86, doi:10.1038/mt.2009.255 (2010).

171 Dong, J. Y., Fan, P. D. & Frizzell, R. A. Quantitative analysis of the packaging capacity of recombinant adeno-associated virus. *Hum Gene Ther* **7**, 2101-2112, doi:10.1089/hum.1996.7.17-2101 (1996).

172 Nielsen, S., Yuzenkova, Y. & Zenkin, N. Mechanism of eukaryotic RNA polymerase III transcription termination. *Science* **340**, 1577-1580, doi:10.1126/science.1237934 (2013).

173 Chen, B. *et al.* Dynamic imaging of genomic loci in living human cells by an optimized CRISPR/Cas system. *Cell* **155**, 1479-1491, doi:10.1016/j.cell.2013.12.001 (2013).

174 Ostedgaard, L. S. *et al.* A shortened adeno-associated virus expression cassette for CFTR gene transfer to cystic fibrosis airway epithelia. *Proc Natl Acad Sci U S A* **102**, 2952-2957, doi:10.1073/pnas.0409845102 (2005).

175 Shalem, O. *et al.* Genome-scale CRISPR-Cas9 knockout screening in human cells. *Science* **343**, 84-87, doi:10.1126/science.1247005 (2014).

176 Zincarelli, C., Soltys, S., Rengo, G. & Rabinowitz, J. E. Analysis of AAV serotypes 1-9 mediated gene expression and tropism in mice after systemic injection. *Mol Ther* **16**, 1073-1080, doi:10.1038/mt.2008.76 (2008).

177 Lu, Q. L. *et al.* Massive idiosyncratic exon skipping corrects the nonsense mutation in dystrophic mouse muscle and produces functional revertant fibers by clonal expansion. *J Cell Biol* **148**, 985-996 (2000).

178 Bosnakovski, D. *et al.* Prospective isolation of skeletal muscle stem cells with a Pax7 reporter. *Stem Cells* **26**, 3194-3204, doi:10.1634/stemcells.2007-1017 (2008).

179 van Putten, M. *et al.* Low dystrophin levels in heart can delay heart failure in mdx mice. *J Mol Cell Cardiol* **69**, 17-23, doi:10.1016/j.yjmcc.2014.01.009 (2014).

180 van Putten, M. *et al.* Low dystrophin levels increase survival and improve muscle pathology and function in dystrophin/utrophin double-knockout mice. *FASEB J* **27**, 2484-2495, doi:10.1096/fj.12-224170 (2013).

181 van Putten, M. *et al.* The effects of low levels of dystrophin on mouse muscle function and pathology. *PLoS One* **7**, e31937, doi:10.1371/journal.pone.0031937 (2012).

182 Long, C. *et al.* Prevention of muscular dystrophy in mice by CRISPR/Cas9-mediated editing of germline DNA. *Science* **345**, 1184-1188, doi:10.1126/science.1254445 (2014).

183 Neri, M. *et al.* Dystrophin levels as low as 30% are sufficient to avoid muscular dystrophy in the human. *Neuromuscul Disord* **17**, 913-918, doi:10.1016/j.nmd.2007.07.005 (2007).

184 Arnett, A. L. *et al.* Adeno-associated viral (AAV) vectors do not efficiently target muscle satellite cells. *Mol Ther Methods Clin Dev* **1**, doi:10.1038/mtm.2014.38 (2014).

185 Lu, Q. L. *et al.* Systemic delivery of antisense oligoribonucleotide restores dystrophin expression in body-wide skeletal muscles. *Proc Natl Acad Sci U S A* **102**, 198-203, doi:10.1073/pnas.0406700102 (2005).

186 Wang, D. *et al.* Adenovirus-Mediated Somatic Genome Editing of Pten by CRISPR/Cas9 in Mouse Liver in Spite of Cas9-Specific Immune Responses. *Hum Gene Ther* **26**, 432-442, doi:10.1089/hum.2015.087 (2015).

187 Xu, L. *et al.* CRISPR-mediated Genome Editing Restores Dystrophin Expression and Function in mdx Mice. *Mol Ther*, doi:10.1038/mt.2015.192 (2015).

188 Slaymaker, I. M. *et al.* Rationally engineered Cas9 nucleases with improved specificity. *Science* **351**, 84-88, doi:10.1126/science.aad5227 (2016).

189 Kleinstiver, B. P. *et al.* High-fidelity CRISPR-Cas9 nucleases with no detectable genome-wide off-target effects. *Nature*, doi:10.1038/nature16526 (2016).

190 van Deutekom, J. C. *et al.* Antisense-induced exon skipping restores dystrophin expression in DMD patient derived muscle cells. *Human molecular genetics* **10**, 1547-1554 (2001).

191 von Maltzahn, J., Jones, A. E., Parks, R. J. & Rudnicki, M. A. Pax7 is critical for the normal function of satellite cells in adult skeletal muscle. *Proc Natl Acad Sci U S A* **110**, 16474-16479, doi:10.1073/pnas.1307680110 (2013).

192 Konermann, S. *et al.* Genome-scale transcriptional activation by an engineered CRISPR-Cas9 complex. *Nature* **517**, 583-588, doi:10.1038/nature14136 (2015).

193 Gilbert, L. A. *et al.* Genome-Scale CRISPR-Mediated Control of Gene Repression and Activation. *Cell* **159**, 647-661, doi:10.1016/j.cell.2014.09.029 (2014).

194 Yokota, T. *et al.* Expansion of revertant fibers in dystrophic mdx muscles reflects activity of muscle precursor cells and serves as an index of muscle regeneration. *J Cell Sci* **119**, 2679-2687, doi:10.1242/jcs.03000 (2006).

195 Lisowski, L. *et al.* Selection and evaluation of clinically relevant AAV variants in a xenograft liver model. *Nature* **506**, 382-386, doi:10.1038/nature12875 (2014).

196 Dalkara, D. *et al.* In vivo-directed evolution of a new adeno-associated virus for therapeutic outer retinal gene delivery from the vitreous. *Sci Transl Med* **5**, 189ra176, doi:10.1126/scitranslmed.3005708 (2013).

197 Matera, A. G., Terns, R. M. & Terns, M. P. Non-coding RNAs: lessons from the small nuclear and small nucleolar RNAs. *Nat Rev Mol Cell Biol* **8**, 209-220, doi:10.1038/nrm2124 (2007).

198 Fu, Y. *et al.* High-frequency off-target mutagenesis induced by CRISPR-Cas nucleases in human cells. *Nat Biotechnol* **31**, 822-826, doi:10.1038/nbt.2623 (2013).

199 Hsu, P. D. *et al.* DNA targeting specificity of RNA-guided Cas9 nucleases. *Nat Biotechnol* **31**, 827-832, doi:10.1038/nbt.2647 (2013).

200 Ran, F. A. *et al.* Double nicking by RNA-guided CRISPR Cas9 for enhanced genome editing specificity. *Cell* **154**, 1380-1389, doi:10.1016/j.cell.2013.08.021 (2013).

201 Fu, Y., Sander, J. D., Reyon, D., Cascio, V. M. & Joung, J. K. Improving CRISPR-Cas nuclease specificity using truncated guide RNAs. *Nat Biotechnol* **32**, 279-284, doi:10.1038/nbt.2808 (2014).

202 Zangi, L. *et al.* Modified mRNA directs the fate of heart progenitor cells and induces vascular regeneration after myocardial infarction. *Nat Biotechnol* **31**, 898-907, doi:10.1038/nbt.2682 (2013).

203 Kim, S., Kim, D., Cho, S. W., Kim, J. & Kim, J. S. Highly efficient RNA-guided genome editing in human cells via delivery of purified Cas9 ribonucleoproteins. *Genome Res* **24**, 1012-1019, doi:10.1101/gr.171322.113 (2014).

204 Nelson, C. E. *et al.* In vivo genome editing improves muscle function in a mouse model of Duchenne muscular dystrophy. *Science*, doi:10.1126/science.aad5143 (2015).

205 Long, C. *et al.* Postnatal genome editing partially restores dystrophin expression in a mouse model of muscular dystrophy. *Science*, doi:10.1126/science.aad5725 (2015).

206 Kornegay, J. N. *et al.* Canine models of Duchenne muscular dystrophy and their use in therapeutic strategies. *Mamm Genome* **23**, 85-108, doi:10.1007/s00335-011-9382-y (2012).

207 Zhang, Y. *et al.* Human skeletal muscle xenograft as a new preclinical model for muscle disorders. *Hum Mol Genet* **23**, 3180-3188, doi:10.1093/hmg/ddu028 (2014).

208 Picconi, J. L. *et al.* Kidney-specific expression of GFP by in-utero delivery of pseudotyped adeno-associated virus 9. *Mol Ther Methods Clin Dev* **1**, 14014, doi:10.1038/mtm.2014.14 (2014).

209 Anderson, L. V. & Davison, K. Multiplex Western blotting system for the analysis of muscular dystrophy proteins. *Am J Pathol* **154**, 1017-1022, doi:10.1016/S0002-9440(10)65354-0 (1999).

210 Burkholder, T. J., Fingado, B., Baron, S. & Lieber, R. L. Relationship between muscle fiber types and sizes and muscle architectural properties in the mouse hindlimb. *J Morphol* **221**, 177-190, doi:10.1002/jmor.1052210207 (1994).

211 Mendez J, K. A. Density and composition of mamalian miscle. *Metabolism* **9**, 184-188.